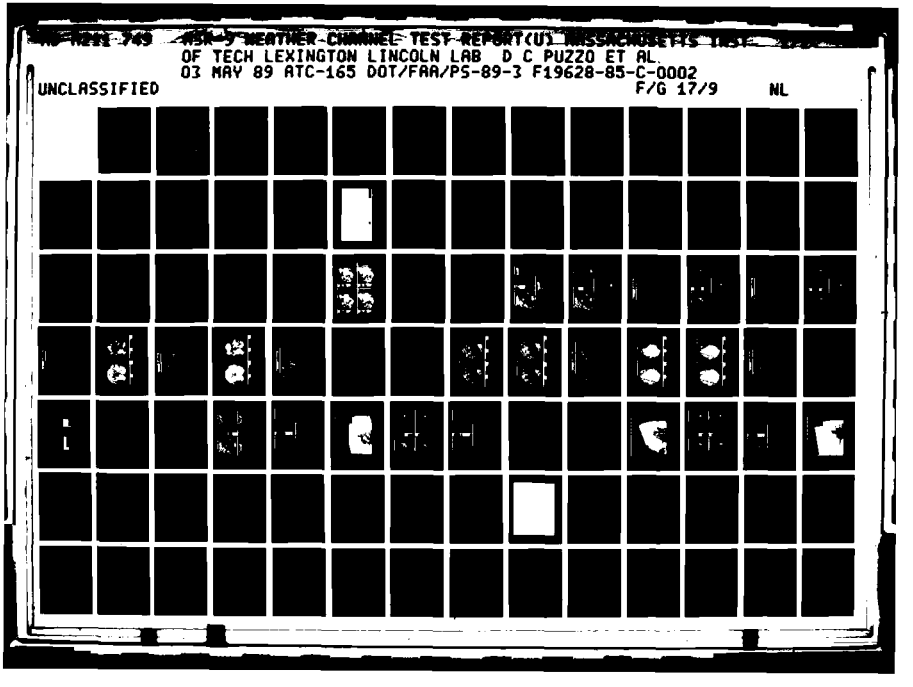
AD-A221 749 ASR-9 WEATHER CHANNEL TEST REPORT(U) MASSACHUSETTS INST
OF TECH LEXINGTON LINCOLN LAB D C PUZZO ET AL
03 MAY 89 ATC-165 DOT/FAA/PS-89-3 F19628-85-C-0002
UNCLASSIFIED F/G 17/9 NL

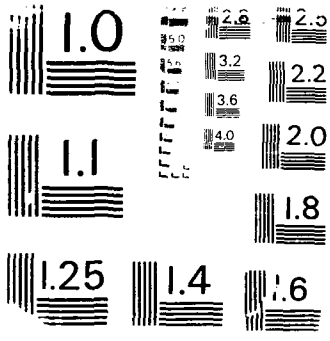
1.0
1.1
1.25
1.4
1.6
1.8
2.0
2.2
2.5
3.2
3.6
4.0

Report No. DOT FAA PS-89 3

(2)

Project Report
ATC-165

ASR-9 Weather Channel Test Report

D.C. Puzzo
S.W. Troxel
M.A. Meister
M.E. Weber
J.V. Pieronek

3 May 1989

Lincoln Laboratory

MASSACHUSETTS INSTITUTE OF TECHNOLOGY

LEXINGTON, MASSACHUSETTS

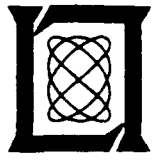

Prepared for the Federal Aviation Administration.

TECHNICAL REPORT STANDARD TITLE PAGE

1. Report No.	2. Government Accession No.	3. Recipient's Catalog No.
DOT/FAA/PS-89/3		

4. Title and Subtitle	5. Report Date
ASR-9 Weather Channel Test Report	3 May 1989
	6. Performing Organization Code

7. Author(s)	8. Performing Organization Report No.
Dean C. Puzzo, Seth W. Troxel, Mark A. Meister, Mark E. Weber, and James V. Pieronek	ATC-165

9. Performing Organization Name and Address	10. Work Unit No. (TRAIS)
Lincoln Laboratory, MIT P.O. Box 73 Lexington, MA 02173-0073	11. Contract or Grant No. DT-FA01-80-Y-10546
	13. Type of Report and Period Covered
12. Sponsoring Agency Name and Address Department of Transportation Federal Aviation Administration Systems Research and Development Service Washington, DC 20591	Project Report
	14. Sponsoring Agency Code

15. Supplementary Notes

The work reported in this document was performed at Lincoln Laboratory, a center for research operated by Massachusetts Institute of Technology under Air Force Contract F19628-85-C-0002.

16. Abstract

The ASR-9, the next generation airport surveillance radar, will be deployed by the FAA at over 100 locations throughout the United States. The system includes a weather channel designed to provide ATC personnel with timely and accurate weather reflectivity information as a supplement to normal aircraft information. This report presents results of an assessment of the ASR-9 weather channel performance. Two issues addressed are: (1) whether the ASR-9 weather channel performs according to FAA specifications, and (2) whether the ASR-9 weather channel adequately represents weather reflectivity for ATC purposes. These assessment results are intended to support the FAA in developing the operational use of ASR-9 weather information.

Comparisons between data from an ASR-9 in Huntsville, Alabama, recorded during design qualification and testing, and data from two other "reference" radars, were used as the basis for the assessment. Several storm cases were analyzed, comprised of stratiform rain, isolated convective storms, squall lines, and cold fronts containing multiple simultaneous convective storms. Results suggest that, with the exception of an apparent 3 dB discrepancy between the weather products of the ASR-9 and the "reference" radars, the ASR-9 weather channel seems to perform according to FAA specifications. Although the ASR-9 products give a reasonable representation of the extent and severity of potentially hazardous weather in Huntsville, the results suggest that the static storm model used to determine beamfill corrections for the ASR-9 should be optimized for the particular climatic region in which an ASR-9 will be operated.

17. Key Words		18. Distribution Statement
ASR-9	beamfilling compensations	Document is available to the public through the National Technical Information Service, Springfield, VA 22161.
fan-beam radar	computer simulation	
ground clutter	pencil-beam radar	
weather channel	precipitation reflectivity	
airport surveillance radar	reflectivity estimate accuracy	
anomalous propagation	spatial and temporal smoothing	

19. Security Classif. (of this report)	20. Security Classif. (of this page)	21. No. of Pages	22. Price
Unclassified	Unclassified	186	

FORM DOT F 1700.7 (8-72) Reproduction of completed page authorized

ABSTRACT

The ASR-9, the next generation airport surveillance radar, will be deployed by the FAA at over 100 locations throughout the United States. The system includes a weather channel designed to provide ATC personnel with timely and accurate weather reflectivity information as a supplement to normal aircraft information. This report presents results of an assessment of the ASR-9 weather channel performance. Two issues addressed are: (1) whether the ASR-9 weather channel performs according to FAA specifications, and (2) whether the ASR-9 weather channel adequately represents weather reflectivity for ATC purposes. These assessment results are intended to support the FAA in developing the operational use of ASR-9 weather information.

Comparisons between data from an ASR-9 in Huntsville, Alabama, recorded during design qualification and testing, and data from two other "reference" radars, were used as the basis for the assessment. Several storm cases were analyzed, comprised of stratiform rain, isolated convective storms, squall lines, and cold fronts containing multiple simultaneous convective storms. Results suggest that, with the exception of an apparent 3 dB discrepancy between the weather products of the ASR-9 and the "reference" radars, the ASR-9 weather channel seems to perform according to FAA specifications. Although the ASR-9 products give a reasonable representation of the extent and severity of potentially hazardous weather in Huntsville, the results suggest that the static storm model used to determine beamfill corrections for the ASR-9 should be optimized for the particular climatic region in which an ASR-9 will be operated.

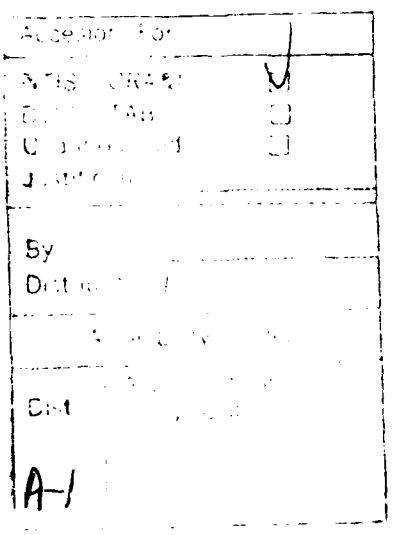

Original contains color plates: All DTIC reproductions will be in black and white

CONTENTS

ILLUSTRATIONS

TABLES

ACRONYMS AND SYMBOLS

AFC	Automatic Frequency Control
AP	Anomalous Propagation
ASR	Airport Surveillance Radar
ATC	Air Traffic Control
CFT	Common Format Tape
COHO	Coherent Oscillator
CP	Circular Polarization
CPI	Coherent Processing Interval
FAA	Federal Aviation Administration
FFT	Fast Fourier Transform
FIR	Finite Impulse Response
HP	Horizontal Polarization
LEC	Local Environmental Check
LP	Linear Polarization
LSB	Least Significant Bit
MTI	Moving Target Indicator
NEXRAD	Next Generation Weather Radar
NSSL	National Severe Storms Laboratory
NWS	National Weather Service
PPI	Plan Position Indicator
PRF	Pulse Repetition Frequency
STC	Sensitivity Time Control
TDWR	Terminal Doppler Weather Radar
VP	Vertical Polarization
Z	Reflectivity factor

SECTION 1

INTRODUCTION

The ASR-9 is a next generation Airport Surveillance Radar, to be deployed by the Federal Aviation Agency (FAA) at over 100 locations throughout the United States. In contrast to earlier FAA radars, the ASR-9 will provide air traffic controllers with quantitative precipitation reflectivity information without the biases introduced by moving target indicator (MTI) circuits or circular polarization. It features robust ground clutter suppression algorithms, spatial and temporal smoothing of the weather maps and range dependent compensation for reflectivity biases introduced by the broad, cosecant-squared elevation antenna pattern of ASRs.

Field Testing and Evaluation of the first production ASR-9 was conducted in Huntsville, Alabama by the FAA and the primary contractor, Westinghouse Electric Corporation. These tests are intended to measure the operational performance of the radar and to verify that the system meets FAA specifications. Verification of the ASR-9's weather channel hardware was conducted by the FAA, previous to the field tests, using a controllable, target simulator while monitoring the weather channel output. As an adjunct to the Field Test and Evaluation program, Lincoln Laboratory collected data to verify the performance of the ASR-9 weather channel against "live weather".

Two independent radar systems were operated from a site located about 1 nmi from the ASR-9. A calibrated, pencil-beam Doppler weather radar and a modified ASR-8 provide respectively volumetric weather reflectivity data and a reflectivity measurement from a calibrated radar with beam shape almost identical to that of the ASR-9. The resulting data allow for analysis leading to confirmation that the ASR-9 weather channel is operating in conformance with the FAA specification. In addition, the volumetric weather reflectivity data facilitates determination as to whether the ASR-9 weather channel adequately conveys the information pertinent for air traffic control.

During the summer and fall of 1988, weather data were collected on the three radar systems. Data from the pencil beam weather radar, herein referred to as the MIT radar, were integrated over elevation angle with appropriate weighting so as to simulate the ASR-9 weather reflectivity measurement. In addition, signals from Lincoln Laboratory's ASR-8, herein referred to as the FL-3 radar, were processed with the algorithms employed by the six-level reflectivity channel to "emulate" the ASR-9 report. These products were then compared to the corresponding data from the ASR-9. For all data collected after August 1988, a 3 dB difference was observed between the reflectivity levels measured by the Lincoln Laboratory radars and the ASR-9. The most likely explanation is a simple calibration difference. Even with the 3 dB difference, the ASR-9 weather products were generally within one NWS level of the MIT radar based simulation and the FL-3 radar based emulation.

To provide data pertinent to operational interpretation of weather maps from the fan-beamed ASR, measurements from the pencil beam weather radar were used to calculate various two-dimensional representations of the three dimensional reflectivity field. Examples are:

(i) "layer-average" reflectivity -- one of the reflectivity products from the Next Generation Weather Radar (NEXRAD);

(ii) horizon scan reflectivity -- equivalent to the PPI measurement from current National Weather Service (NWS) radars;

(iii) maximum reflectivity (over elevation angle or height) for each range-azimuth resolution cell. This represents the most conservative two dimensional representation of precipitation intensity.

Comparison of the resulting fields with the ASR-9 weather reports showed varying degrees of correlation. For storms with strong precipitation cores aloft, the ASR-9 reports resembled most closely the layer average and horizon-scan reflectivity field. When the cores of storms were near the ground, the ASR-9 data agreed closely with the maximum scan reflectivity, suggesting that the ASR-9's beamfill correction storm model (see Section 1.2) was implemented as originally specified by Westinghouse. While the ASR-9 reports were generally within one level of the average, maximum, and horizon scan reflectivity metrics, the variability from case to case suggests a need determine if there is a static storm model that better characterizes the average storm which occurs in Huntsville.

The remainder of this section discusses the ASR-9 weather channel characteristics and issues relating to ASR-9 weather channel performance. Section 2 describes the methods used to collect, process, and compare the data from the radars employed for the field measurements in Huntsville. Section 3 contains detailed results and provides both visual and computer-based comparisons that substantiate the validity of the ASR-9 weather channel. Sections 4 and 5 summarize conclusions and recommendations, respectively.

1.1 BACKGROUND

Current ASRs do not give a quantitative indication of weather intensity. Accurate calibration of current ASRs for weather reflectivity measurement is limited by several factors including the wide fan-beam antenna, MTI circuits, high antenna scan rate, and use of circular polarization during periods of extensive rain. Appendix A provides a more detailed discussion of the problems with ASR-8 and earlier ASR models.

In the 1970s, the FAA initiated studies designed to investigate the feasibility of modifying existing FAA ATC radars to improve the radar weather display available to air traffic controllers. *Pell* [1] found that valuable quantitative reflectivity measurements could be obtained from a broad-beam S-band radar. This was supported by *Dobson et al* [2] in a study that investigated the use of existing FAA terminal and enroute radars for providing weather information. In fact, a later study by *Wilk and Dooley* [3] found that the wide vertical beam and high scan rate of FAA radars may often be more beneficial than narrow beam counterparts for the early detection of rain developing aloft. However, the effects of variations in the storm's vertical profile and in the characteristics of receivers designed for optimum aircraft detection remained a problem.

Based on the results of various studies on the performance of FAA radars for hazardous weather detection, *Hopson and Coonley* [4] concluded that ASRs as currently operated could not provide accurately calibrated weather reflectivity measurements. Their recommendation was to incorporate a separate weather receiver and processor that would alleviate the problems associated with earlier ASRs. These recommendations were adopted in the specification for the ASR-9 weather channel.

1.2 ASR-9 WEATHER CHANNEL DESCRIPTION

The ASR-9 weather channel is designed to provide ATC personnel with an accurate, quantized, clutter-free representation of the precipitation field. Its weather products are generated by either a two-level or six-level weather processor. Because the two-level processor is similar to and intended as a back-up to the six-level processor, this section is limited to the description of the six-level processor. The ASR-9 weather channel allows ATC personnel to select and display any two of the six National Weather Service (NWS) levels. The levels are defined in terms of reflectivity in dBZ[1] as follows:

LEVEL	REFLECTIVITY	PRECIPITATION RATE
1	18 - 30 dBZ	Light (Mist)
2	30 - 41 dBZ	Moderate
3	41 - 46 dBZ	Heavy
4	46 - 50 dBZ	Very Heavy
5	50 - 57 dBZ	Intense
6	57– dBZ	Extreme (Hail)

Figure 1-1a shows a typical ASR-9 PPI weather display with the selected levels indicated by light and dark intensities. In this particular case, Levels 2 and 4 are chosen and displayed in the "discrete" mode where only those two levels chosen are indicated. Note, however, that areas of Level 3, and Level 5 and above, can be inferred from the Level 2 and 4 contours. Figure 1-1b shows the same storm but with the "summation" mode selected; here the levels between the two chosen are indicated by the lighter color contour and the levels above the highest chosen level are indicated by the darker color contour.

As is the case for previous terminal radars, many ASR-9 system features (frequency, pulse width, peak power, pulse repetition frequency, and clutter rejection) make it well suited for weather observations. System features adverse for weather measurement in previous ASRs, have been either changed or compensated for in the ASR-9 weather channel. The following paragraphs outline features of the ASR-9 that facilitate weather reflectivity measurement. Refer to Table 2-1 for a summary of the parameters of the ASR-9 transmitter, receiver, and antenna.

[1] Z is proportional to volume reflectivity (e.g., m^2/m^3) with the wavelength dependence (λ^4) for Rayleigh scatterers removed. Conventionally, Z is expressed in units of mm^6/m^3.

Previous ASRs receive both weather and target information from the same channel. However, when these radars operate with circular polarization (CP), the weather echo power return is decreased by as much as 18 dB to improve target detection. This reduction of weather echo power in the target channel is caused by the reversal of polarization sense when the transmitted signal is reflected by spherical rain drops. To allow the simultaneous optimum detection of both aircraft targets and weather, the ASR-9 has a receiver channel for weather reflectivity measurement and another receiver channel for aircraft detection (see Figure 1-2). The weather channel receives orthogonal sense polarization when the radar is operated in CP to match to the polarization of the weather signal. It receives same sense polarization from the target channel when the radar is operated in linear polarization (LP).

The ASR-9 antenna rotates at 12.5 RPM and utilizes range-azimuth selectable dual receiving beams ("high" and "low"). The angular extent of the 3 dB elevation beamwidth is approximately 6 degrees for both beams, with the high beam displaced by 3.5 degrees with respect to the low beam. The peak of the lower antenna beam is typically placed at 2.0 degrees above the horizon, which places its lower -3 dB edge on the horizon. The upper beam is selected for near ranges (typically less than 18 nmi) in order to reduce the impact of ground clutter with the low beam selected thereafter. The wide elevation beamwidth and rapid scan rate are dictated by the ASR-9's primary function of detecting and resolving rapidly-moving aircraft at altitudes up to 35,000 feet, over a 60 nautical mile radius. This configuration allows a large volume to be sampled while providing a sufficiently rapid update rate (approximately 5 seconds for aircraft targets). Radar echoes are sampled at 1/16 nmi [115.8 m] range intervals over 60 nmi [111.1 km]. There are two coherent processing intervals (CPIs) per azimuthal beamwidth (1.4 degrees) for a total of 256 azimuth intervals. The two CPIs consist of one set of 8 pulses at one pulse repetition frequency (PRF) and one set of 10 pulses at a higher PRF. The weather processor takes advantage of the alternating PRF strategy to filter second-trip echos by comparing the reflectivity estimate from 8 and 10 pulse CPI then choosing the lowest reflectivity estimate for that CPI pair (this assumes that second-trip weather will not be detected for both PRFs).

Figure 1-2 is a simplified block diagram of the ASR-9 weather channel processor. The weather processor incorporates coherent ground clutter suppression using four clutter filters that produce clutter attenuation of zero to 49 dB. One of the four filters is chosen for each range-azimuth cell based on the weather reflectivity and a stored clear-day clutter map. This allows for sufficient signal to clutter ratio, while minimizing the degradation of the weather reflectivity estimate due to filter attenuation.

After passing through the clutter filters, data are converted to equivalent NWS six-level intensities through the use of a memory-resident thresholding map. The map contains thresholds as a function of range, polarization, receiving beam, and sensitivity time constant (STC). Storm reflectivity cores of limited vertical extent may not fill the entire ASR-9 fan-beam; reflectivities of these storms may therefore be underestimated. To correct this bias, the weather processor thresholds are adjusted with range based on a predetermined storm reflectivity model. The threshold adjustments may be changed, although not in real time, to accommodate other storm models. The storm model used by the contractor for the Huntsville climate assumes a storm of constant reflectivity from the ground up to 4 km in elevation, then decreasing 3 dB per km above 4 km.

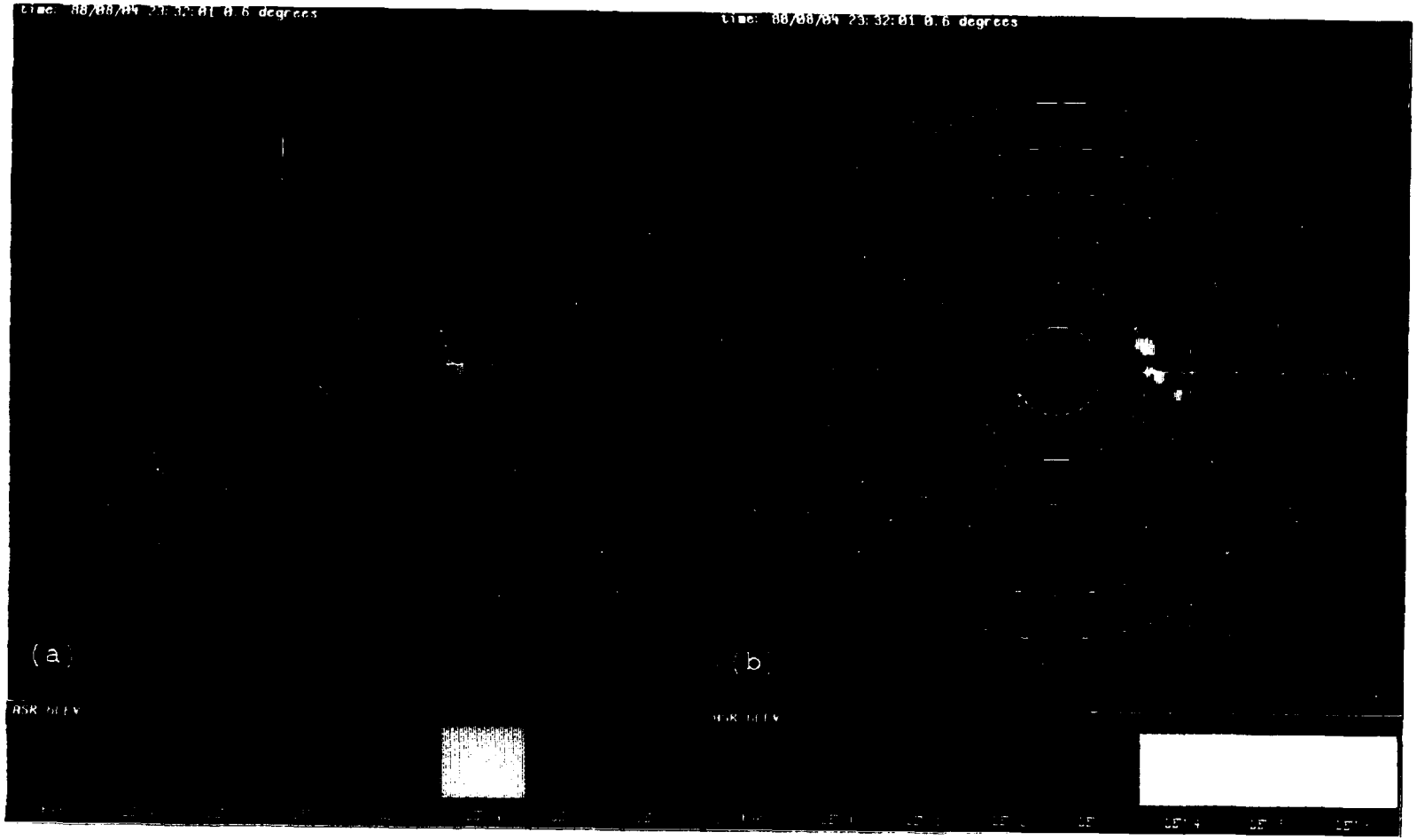

Figure 1-1. Simulation of ASR-9 weather channel display in (a) continuous mode and (b) discrete mode. (Weather event 4 August 1988)

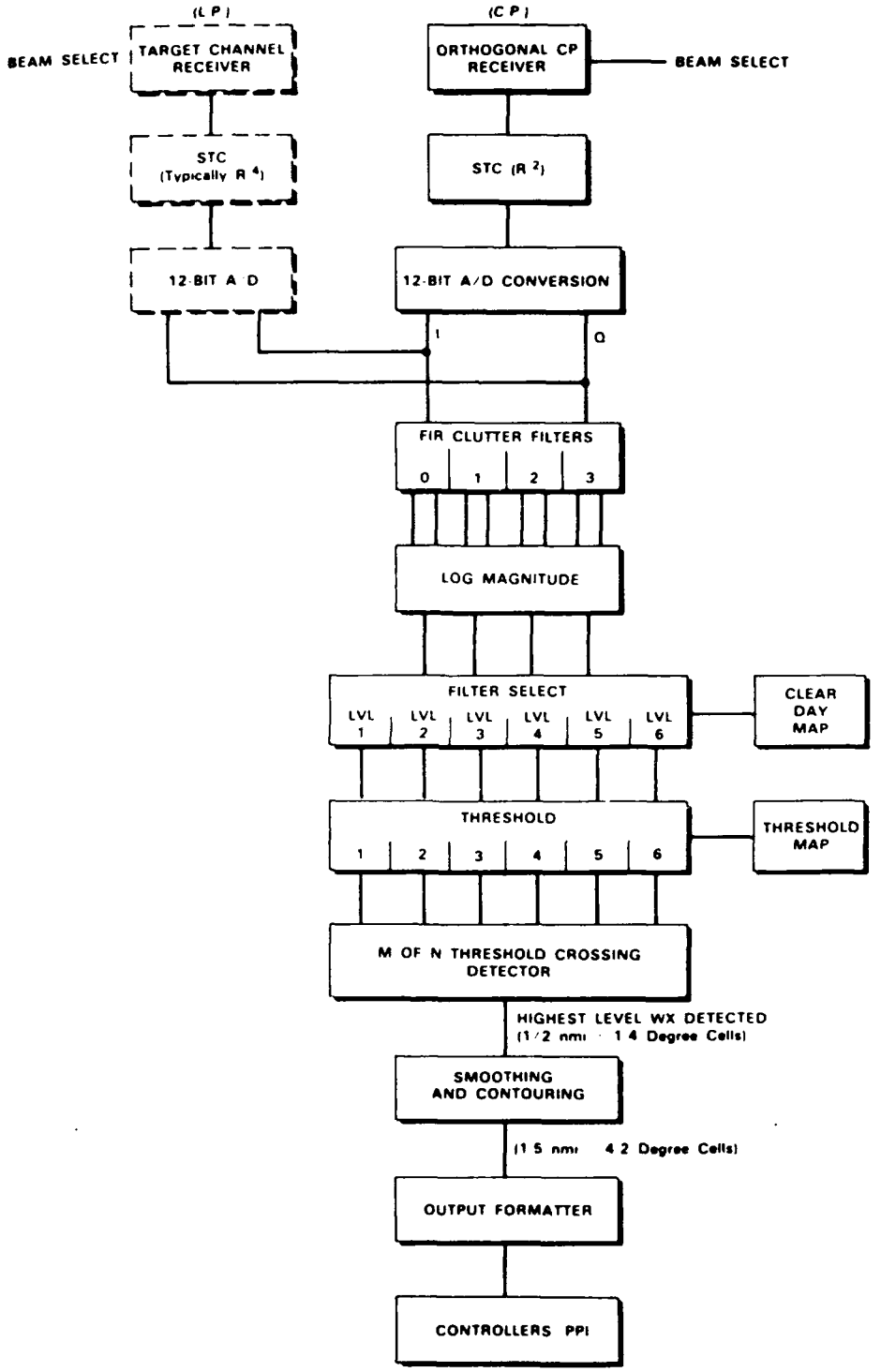

Figure 1-2. ASR-9 Weather Channel Processor Block Diagram.

To overcome the inherent noisiness of the reflectivity estimates, a sequence of spatial and temporal smoothing filters is employed. First, the data are smoothed in range over 1 nmi intervals by passing the data through a median filter. This filter selects the highest level exceeded in at least 8 out of 16 range gates, and is repeated at 0.5 nmi increments. Then, the data are passed through a three-stage smoothing and contouring processor. The stages of smoothing are as follows; 1) the median level from three consecutive scans is computed for each range-azimuth cell, 2) the highest level found in at least "WWW" (an adjustable parameter typically equal to 5) of a nine-cell cluster centered about the weather cell is computed for each range-azimuth cell, 3) the highest level of the nine-cell cluster centered about the weather cell is assigned to that cell. The spatial filters have the added benefit of reducing the impact of clutter-censored cells and enlarging regions of the higher reflectivity weather.

The weather channel output consists of cells 1.4 degrees in azimuth by 0.5 nmi in range (256 azimuths by 120 range samples per azimuth, for a total of 30,720 cells per plan view), generated by processing echoes received over a 2 nmi range and a 4.2 degree azimuth interval. Reference [5] gives a more complete description of the ASR-9 weather channel and presents a simulation analysis of its performance.

1.3 PERFORMANCE ISSUES

The following four features of the ASR-9 weather channel need to be considered with respect to their impact on the accuracy of the product displayed to air traffic controllers.

(i) Clutter filtering
(ii) Beamfill corrections
(iii) Spatial and temporal smoothing
(iv) Polarization matching

Brief descriptions of these issues drawn largely from reference [6] follow. More detailed discussions are contained in the appendices referenced.

Clutter Filtering: Appendix B contains an excerpt from [5] addressing the impact of ground clutter on the ASR-9 weather channel. This report showed that the adaptive clutter filters, together with the spatial and temporal smoothing should result in accurate precipitation reflectivity measurements even in the presence of intense ground clutter at short range. Results contained herein generally support those findings.

In Huntsville, significant ground-clutter break-through was occasionally observed during the night and early morning hours on the ASR-9's weather display where no weather was present. This problem has been attributed to anomalous propagation (AP). A problem common to ground-based radars, AP occurs under certain climatic conditions where radio waves are bent down toward the earth causing ground echoes to appear on the radar display in regions which are usually free of ground echoes. The ASR-9 ground clutter suppression technique, based on a fixed, clear-day clutter map, does not generally suppress AP-based ground clutter returns.

The AP problem may be treated operationally by simply turning off the weather display during occurrences of AP. This would not compromise safety since the conditions leading to AP are not conducive to thunderstorm generation. However, two methods were considered for removing AP clutter from the ASR-9 weather channel products; 1) identification of clutter break-through based on spatial characteristics of ground clutter, and 2) identification of clutter break-through based on spectral characteristics. Both methods would require changes to the weather channel's processing algorithms. These methods are discussed in detail in Appendix I where FL-3 radar based emulation is used to assess the effects of both methods on weather and AP clutter. Results suggest that clutter identification based on its spectral characteristics may significantly reduce AP based clutter break-through while having a minimal effect on weather reflectivity estimates.

Beamfill Corrections: The static storm model used for calculation of the ASR-9 beamfill corrections will produce errors when the actual storm vertical reflectivity profile deviates from that of the model. There are two major factors that govern the effectiveness of beam fill correction algorithms: (1) the particular phase of the storm's life cycle during which it is observed; and (2) the climatology governing the vertical reflectivity distribution in the storm. Figure 1-3 shows vertical reflectivity cross sections of storms of increasing severity over time. One can see that a single storm model will not accurately characterize the actual storm over its entire life cycle, although it may during one particular phase.

The issue of ASR-9 weather channel beamfill corrections was also addressed in [5]. Appendix B contains an excerpt from Weber's report in which he used relatively small data sets from eastern Massachusetts and Oklahoma to conclude that relative errors between corrected and uncorrected ASR reports would generally be no larger than 2 to 3 dB, corresponding to at most one NWS level.

Optimal performance from the beamfill correction can only be obtained if the static storm model accurately characterizes the ensemble of storms that the ASR-9 is likely to encounter in its region. Therefore, it would be appropriate to develop storm reflectivity models for regions of the United States which have similar climatology. Regions may be chosen based on similarity of environmental factors governing the height and vertical reflectivity structure of storms which occur in each region. Seasonal models would have to be developed for those regions which exhibit large seasonal changes in storm characteristics. Regional and seasonal storm models would also have to be verified by comparing these models against site-specific models computed from actual radar data recorded at several locations within each region. Refinement of the storm model will be processed.

Smoothing and Contouring: The smoothing algorithms used in the ASR-9 weather processor are intended to minimize statistical fluctuations of the weather maps. The issues of ASR-9 weather channel smoothing and contouring were previously addressed in [5]. Appendix B contains an excerpt from that report in which it was concludes that, after smoothing, statistical fluctuations of the weather reports are insignificant.

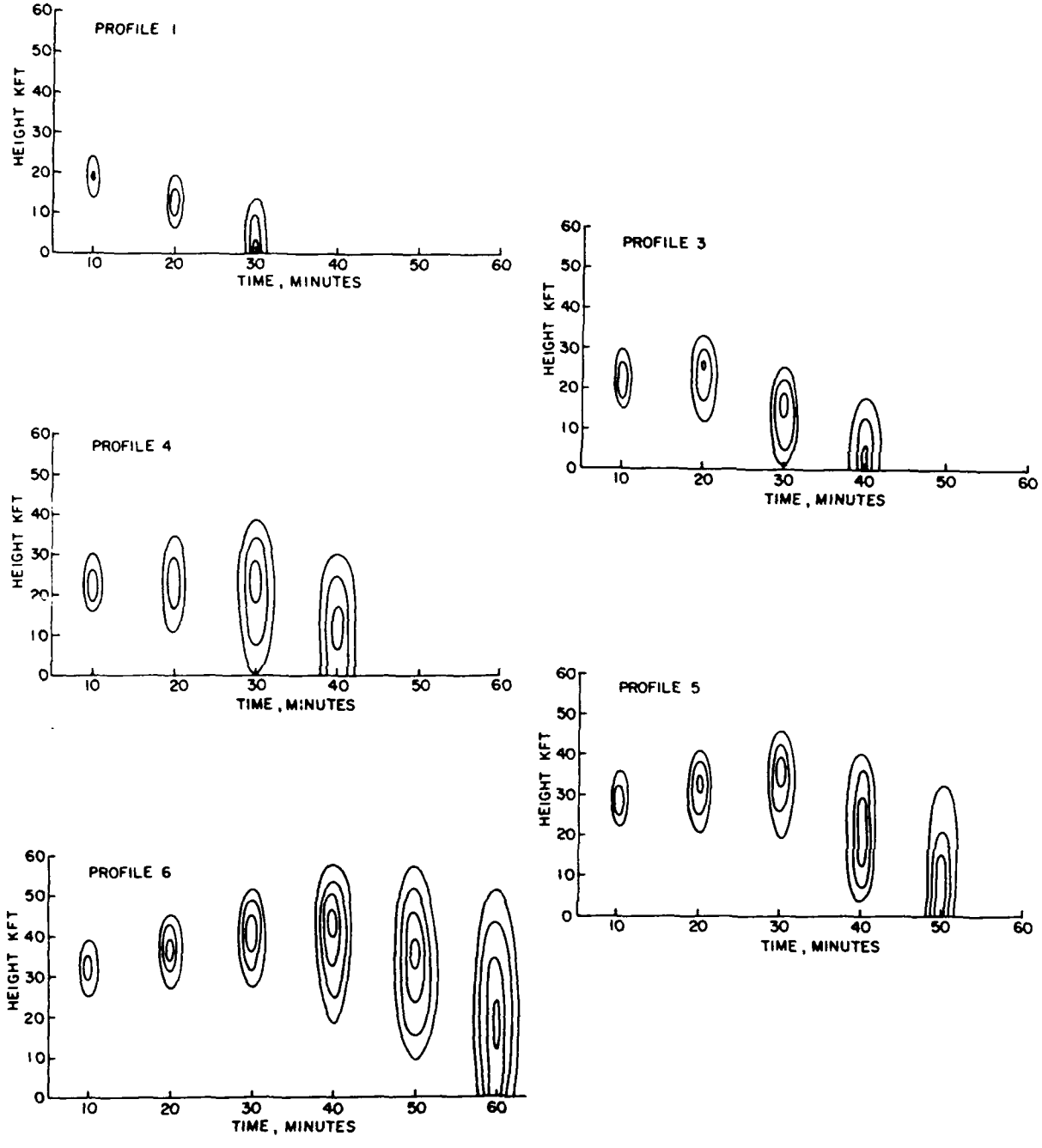

Figure 1-3. Vertical reflectivity cross sections representing initial echo growth in storms of increasing severity [4]. The ASR-9's static storm model and variations in the storm's vertical reflectivity structure over time, cause errors in ASR-9 weather reports.

Polarization Matching: Normally, the ASR-9 transmits and receives vertical polarization (VP). However, when there is reflectivity greater than Level 3 covering a large area, the ASR-9 transmits and receives circularly polarized (CP) signals through its target channel to reduce the interference from rain echoes, and receives the opposite sense CP in the weather channel and the same sense in the target channel. Rain scatterers are generally spherical and, in CP, the reflected signal is opposite sense polarized relative to the transmitted signal. Thus, right-hand (left-hand) CP signals are reflected in left-hand (right-hand) CP. However, as the individual scatterers increase in size, i.e. the reflectivity increases, they become oblate resulting in an elliptically polarized signal reflected back to the weather channel and a subsequent loss in measured power. Appendix H contains an analysis of polarization loss in a CP/VP receiver assuming the sense (right or left hand) of the received signal is matched to the receiver. The analysis indicates that polarization loss in a CP receiver should be less than 3 dB. However, polarization loss in a VP receiver may be greater than 3 dB because the reduced vertical dimension of the rain drops do to their asymmetry at higher reflectivity levels. Comparison of level differences between the ASR-9 and FL-3 emulation weather reports, when the ASR-9 was operating using CP and VP, give no noticeable indication of polarization loss in the ASR-9 weather channel when operating in CP. However, the relatively few weather events including ASR-9 CP data, does not allow a definitive statement to be made on this issue.

Polarization loss may also occur if the sense (right hand or left hand) of the incoming signal is not the same as that of the receiving antenna. Zrnic [6] has shown that for a CP receiver, during intense storms, the difference in the propagation phase constants between the vertical and horizontal components of the CP signal through precipitation results in significant depolarization attenuation (over 1 dB) at a 10 cm wavelength over relatively short propagation paths (10 km). Furthermore, he shows that the depolarization attenuation becomes worse with increasing storm intensities and spatial extent. The potential problem with the ASR-9 is that it is likely to operate in CP during spatially extensive and high reflectivity precipitation, the conditions under which this type of polarization loss occurs. The results of this assessment, as stated above, give no indication of underestimation of reflectivity by the ASR-9 weather channel. However, the conditions under which these losses are expected may not have been represented in the data sets used. This issue, therefore, warrants further investigation, especially in the case of a radial line storm.

SECTION 2

METHOD OF ANALYSIS

Figure 2-1 shows the geographical location of the sensors used to collect data at the FAA designated Huntsville test site. Although NWS radar data were recorded for possible reference, the typical horizon-scan mode, lack of ground clutter rejection, and low update rate make its data unsuitable for assessment of ASR-9 weather channel performance. (see Appendix G). The ASR-9, MIT radar, and FL-3 radar recorded data simultaneously during occurrences of precipitation. Table 2-1 contains general information related to these radar systems.

Table 2-2 is a list of the weather events used in the assessment. Data were collected on several different types of storms as indicated in the "TYPE" column of the table. The following are brief definitions of each of these storm types:

Air Mass: Sometimes referred to as convective storms, thunderstorms of this type occur in warm, moist air masses as a result of summertime surface heating (convection). They are the most random and have a life cycle on the order of 1 hour. Because of their association with surface heating, they usually reach maximum intensity and frequency during middle and late afternoon. Air mass thunderstorms tend to remain isolated and disorganized, but may occasionally organize into squall lines and can sometimes reach severe intensity.

Frontal: This classification refers to thunderstorm events which are triggered by the passage of a large-scale weather front, usually a cold front. The lifting produced by the low-level cold air wedge on the leading edge of the front provides the forcing mechanism for development of thunderstorms which may be imbedded in the more widespread precipitation regions of the front.

Squall line: A squall line is an any non-frontal organized line of active thunderstorms. These sometimes form as a result of organization of a group of isolated air mass thunderstorms or in advance of vigorous cold fronts. Squall lines may have lateral extents of hundreds of miles, but are usally less than 50 miles wide. Individual thunderstorms may be severe.

Stratiform: This type of weather event is characterized by widespread precipitation which is usually of light to moderate intensity (NWS levels 1 and 2) and is of limited vertical extent; cloud tops are generally less than 25,000 feet. Horizontal precipitation intensity gradients tend to be weak, and the resulting echoes seen on a weather radar display appear amorphous.

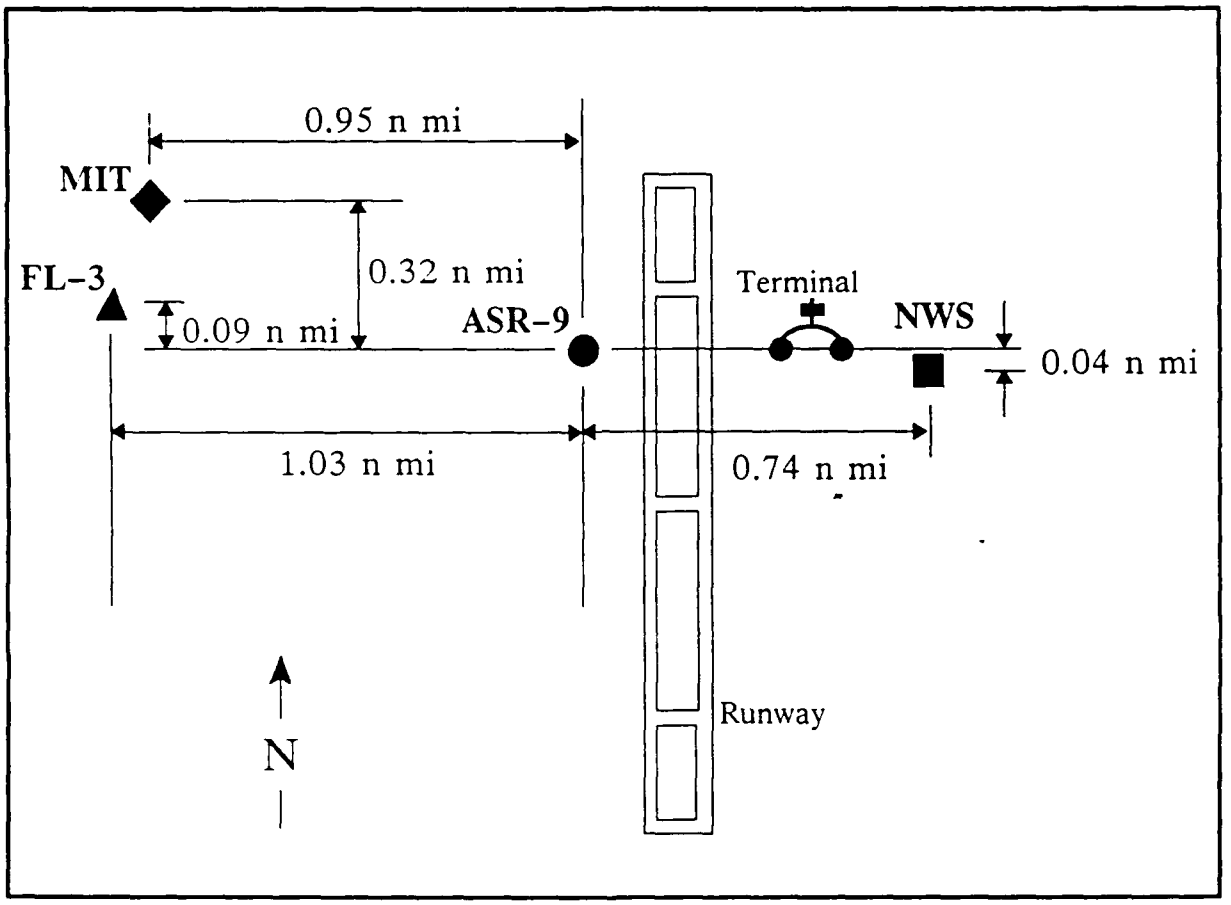

Figure 2-1. Sensor locations at the Huntsville, Alabama airport.

TABLE 2-1

OPERATING CHARACTERISTICS OF THE ASR-9, FL-3, MIT, AND NWS RADAR SYSTEMS

PARAMETER	ASR-9	FL-3	NWS	MIT
Frequency (MHz)	2884	2730	5620	5590
Transmitter Type	Klystron	Klystron	Magnetron	Magnetron
Peak Power (kW)	1100	1100	200	160
Pulse Width (us)	1.0	0.65	0.5, 2, 3, 4	0.5, 1
Range Sample (m)	120	120	250	250
PRF (Hz) (typical)	(1)	(1)	164 - 545	924
Max Range (nmi)	60	60	243	122
Reflectivity	Six-level	(2)	Six level	dBZ
Clutter Rej. (dB)	45	45	NONE	30 (max)
Noise Figure (dB)	6	6		6
Sensitivity (dBm)	-108	-107		-106
Beamwidth (deg)				
Elevation	6.0*	5.8*	2.0	1.4
Azimuth	1.3	1.35	2.0	1.4
Polarization	VP CP	VP	HP	HP
Antenna Gain (dB)	34	34	40	41
Scan Rate (rpm)	12.5	12.5	3	3

* Cosecant squared in elevation

(1) PRF block stagger mode; typical PRF pair is 8 pulses of 940; 10 pulses of 1200, 1000 average.

(2) dBZ or Six-Level

HP: Horizontal Polarization

VP: Vertical Polarization

CP: Circular Polarization

TABLE 2-2

WEATHER EVENTS USED IN ASSESSMENT

CASE*	DATE	TIME	TYPE	WEATHER CHANNEL	ASR-9 POLARIZATION
1	2 Aug 88	21:01:19	Air mass	Two-level	Unknown
1	2 Aug 88	21:07:47	Air mass	Two-level	Unknown
2	4 Aug 88	23:32:01	Air mass	Six-level	Unknown
3	8 Aug 88	19:55:00	Air mass	Six-level	Unknown
	16 Sept 88	17:50:00	Stratiform	Six-level	Unknown
4	16 Sept 88	20:49:34	Stratiform	Six-level	Unknown
	18 Oct 88	22:13:00	Squall line	Six-level	LP
	18 Oct 88	22:28:54	Squall line	Six-level	LP
	20 Oct 88	21:48:00	Air mass	Six-level	Unknown
	4 Nov 88	16:52:00	Frontal**	Six-level	LP
	4 Nov 88	16:56:11	Frontal**	Six-level	LP
	4 Nov 88	22:34:21	Frontal**	Six-level	LP
	4 Nov 88	22:38:00	Frontal**	Six-level	LP
	4 Nov 88	23:13:28	Frontal**	Six-level	CP
5	4 Nov 88	23:17:12	Frontal**	Six-level	CP
	4 Nov 88	23:21:22	Frontal**	Six-level	CP
	4 Nov 88	23:54:28	Frontal**	Six-level	CP
6	26 Nov 88	22:16:23	Squall line	Six-level	LP
	26 Nov 88	23:34:39	Squall line	Six-level	LP

* Cases which are detailed in Section 3.

** Day on which tornado was reported northwest of airport

ASR-9 weather data were obtained prior to FAA acceptance of the system, while the contractor was performing field test and evaluations. Prior to October 1988, no record was available indicating the polarization of the ASR-9 during data collection. Nonetheless, all ASR-9 data used in this assessment appear valid. For each weather event, a set of data was generated, comprised of:

(i) Observed ASR-9 weather data
(ii) FL-3 radar based emulation of the ASR-9 weather channel
(iii) MIT radar based simulation of the ASR-9 weather channel
(iv) MIT radar based maximum reflectivity data
(v) MIT radar based layer average reflectivity data
(vi) MIT radar based horizon-scan data (NWS equivalent)

In October of 1988, the MIT pencil-beam radar was dismantled so that the MIT Department of Earth, Atmosphere, and Planetary Sciences (EAPS) could fulfill a prior commitment to the National Science Foundation (NSF) to take measurements in Australia. The delayed ASR-9 schedule, which resulted in shipment of equipment to Huntsville in January of 1988, resulted in the absence of pencil beam data during October and November. However, the FL-3 radar continued to operate and collect data throughout the period, allowing events recorded during those months to be used in the assessment.

2.1 DATA COLLECTION AND PROCESSING

Following storm observations, the associated tapes containing data recorded by each of the four radars were appropriately marked and sent to Lincoln Laboratory for processing and analysis. Processing accounted for differences in the radar systems (e.g., differences in location and data resolution). Processed data sets consisted of six-level reflectivity cells in Cartesian form, with resolution that matched the output of the ASR-9 weather channel processor. Data were stored in separate files for subsequent computer and visual comparison. The following paragraphs briefly describe each radar sensor, the recorded data, and any post-processing involved.

ASR-9 data ASR-9 weather channel data (either six or two level) were recorded from the output of the surveillance and communications interface processor (SCIP) transmitter via dedicated telephone line at the FL-3 Huntsville facility. ASR-9 weather channel data were reformatted, time-tagged every minute with 1 second accuracy, and stored on 6250 bpi tape.

Pencil-beam data To provide pencil-beam radar data, Lincoln Laboratory contracted with the MIT Weather Radar Laboratory of the EAPS to operate a C-band Doppler weather radar and record volume scan data simultaneously with the ASR-9. The MIT radar is similar to the NWS radar at Huntsville in terms of its operating frequency, antenna beamwidth, and sensitivity. The radar was operated in a volume scan mode to maximize storm volume coverage. Three-dimensional (range, azimuth, elevation) estimates of storm reflectivity and velocity were produced. Reflectivity was measured in units of dBZ and the velocity was measured in meters per second. The update rate was limited only by data sampling considerations and the antenna scan rate (21 seconds per 360 degree azimuth scan). The pencil-beam radar has 30 dB maximum clutter rejection; it was thus able to produce volume weather reflectivity data in the critical near-airport areas where the NWS radar could not. A more detailed discussion of the MIT radar system is contained in Appendix E.

During weather observations, the MIT weather radar operator executed scan sequences based on the range, azimuth, and height of the storm of interest, i.e. volume coverage was chosen just large enough to cover the storm volume. Reflectivity and velocity data were reported every 1.4 degrees in azimuth and in range sampling intervals of either 0.5 or 1 km, depending on the range of the storm. The 0.5 km range samples were chosen for storms within 80 km (43 nmi) while 1 km range samples were chosen for storms beyond 80 km. PPI scans were implemented at discrete elevation angles starting with 0.7 and 1.4 degrees (required for clutter censoring purposes) and stepping in increments of a minimum of 1.4 degrees and a maximum of 2.4 degrees, depending on the height of the storm. These data were used to produce two-dimensional parameterizations (i.e. "truth") of the actual three-dimensional weather field and to simulate the ASR-9 weather channel output.

Pencil-beam volume reflectivity and velocity data were input to a computer program that simulates the beam shape and signal processing of the ASR-9 weather channel. The data products were in the same format as those output by the ASR-9 weather channel. A detailed description of the simulation program is given in Appendix C.

Three separate two-dimensional parameterizations of the reflectivity field were generated based on the maximum, average, and horizon-scan reflectivity. Each version has its advantages and disadvantages in terms of being used to represent what is of importance to ATC. For example, horizon-scan reflectivity is directly relevant to near-airport weather where aircraft on approach and departure paths are close to the ground. Even though the vertical beam width of the ASR-9 is 4 to 5 times that of the MIT radar, at close ranges the absolute difference in their vertical coverages may be negligible. However, horizon-scan data will not be so useful beyond 10 nmi where aircraft will be at higher altitudes. Maximum reflectivity can be interpreted as an important measure of weather because it covers the full elevation volume of the ASR-9 fan-beam antenna pattern and yields the most intense reflectivity that could be encountered by an aircraft at

any altitude. However, the maximum reflectivity is insensitive to variations in the percentage of the storm's vertical structure that is made up of the maximum value. Average reflectivity also covers the full elevation volume of the ASR-9 fan-beam antenna pattern. Unlike the maximum criteria, average reflectivity does have some sensitivity to variations in the depth of the reflectivity core in a storm.

Fan-beam data To provide an additional source of truth, Lincoln Laboratory employed the FAA-Lincoln Laboratory ASR-9 emulation radar system (FL-3). The primary function of the FL-3 radar is to serve as a surrogate for the ASR-9 in developing wind-shear sensoring techniques. The FL-3 radar is a modified ASR-8 S-band system (Table 2-1) with transmitter and antenna characteristics nearly identical to that of an ASR-9. FL-3 transmits and receives vertical polarization (VP). FL-3 upper and lower beam time-series video data were recorded on high-density tape and subsequently transcribed on 6250 bpi tape. The resolution of the FL-3 radar is 120 meters in range by 1.4 degrees in azimuth. A more detailed discussion of the FL-3 emulation radar system is contained in Appendix F. Data were input to a computer program emulating the signal processing of the ASR-9 weather channel. A detailed description of this program is given in Appendix D.

2.2 DATA ANALYSIS AND EVALUATION CRITERIA

Lincoln Laboratory's "live weather" assessment of the ASR-9 weather channel involved both visual- and computer-based analyses. Visual-based analyses resulted in qualitative characterizations of the ASR-9 weather products. The computer-based analyses resulted in quantitative characterizations of the accuracy and probability of false and missed detections of the ASR-9 weather channel. Computer comparisons were used to generate two forms of information: color plots of the difference reflectivity levels between any two PPIs and tables of difference reflectivity statistics.

Certain features of the C-Band pencil beam radar were expected to produce occasional discrepancies relative to the ASR-9 and FL-3 data. The C-Band radar has relatively slow volume coverage resulting in data being collected over a few minutes compared to 30 seconds for the ASR-9 and FL-3 radars. Furthermore, the C-Band radar operates at roughly double the ASR-9 and FL-3 radar frequency, resulting in the the possibility that C-Band signals will be attenuated by precipitation more than the S-Band signals. In contrast, FL-3 and the ASR-9 have similar transmit frequencies and antenna scan rates. FL-3 data are, therefore, considered more reliable for direct comparison with ASR-9 data. Even so, minor spatial and level discrepancies were expected among all three radar data sets due to radars calibration errors and the coarsely partitioned NWS levels. An example of the effects of a simple calibration offset on final data products is shown in Figure 2-2. This figure shows the simulation output for a weather event with the preprocessed reflectivities offset by -2, -1, +1, and +2 dB. Note that offsets of 1 dB can have a significant impact on the resulting weather contours, with the higher levels being more sensitive to variances. This is to be expected because the higher levels represent a smaller range of reflectivity compared to the lower NWS levels. i.e., higher levels are more apt to transition to an adjacent level for a small change in reflectivity. To partially compensate for this potential problem, a 1 nmi acceptance window around each resolution cell was employed when performing computer comparison and statistics generation.

The difference reflectivity plots where generated by simply subtracting six-level reflectivity values on a cell by cell basis. Table 2-3 shows a sample of the format in which the statistics associated with the plot are presented. The table contains difference reflectivity level probabilities as a function of the reflectivity level of the ASR-9. The table includes difference level probability information based on input data over all ranges and azimuths. There are seven rows representing six reflectivity levels plus a Level 0, designating those reflectivities below Level 1. For a given ASR-9 reported reflectivity level, the information in each column represents the probability that the corresponding level reported by FL-3 or MIT radar is, starting with the X-2 column, from left to right, two levels below, one level below, equal to, one level above, or two levels above the reference level. NA (not applicable) entries indicate where a particular condition cannot exist.

The probabilities were calculated by taking the number of occurrences associated with the particular condition and dividing by the total number of cells that contain the reference level of interest. Probability of false alarm and missed detection can be calculated as a function of reflectivity level by simply adding the probabilities to the right or left of the reference level in column X, respectively.

TABLE 2-3

SAMPLE TABLE CONTAINING PROBABILITY THAT AN INDICATED CONDITION WILL OCCUR AS A FUNCTION OF REFERENCE LEVEL

Range Interval	ASR-9 Level	X - 3	X - 2	X - 1	X	X + 1	X + 2	X + 3
0 to 60 nmi	x = 0	NA	NA	NA				
	x = 1	NA	NA					
	x = 2	NA						
	x = 3							
	x = 4							NA
	x = 5						NA	NA
	x = 6					NA	NA	NA

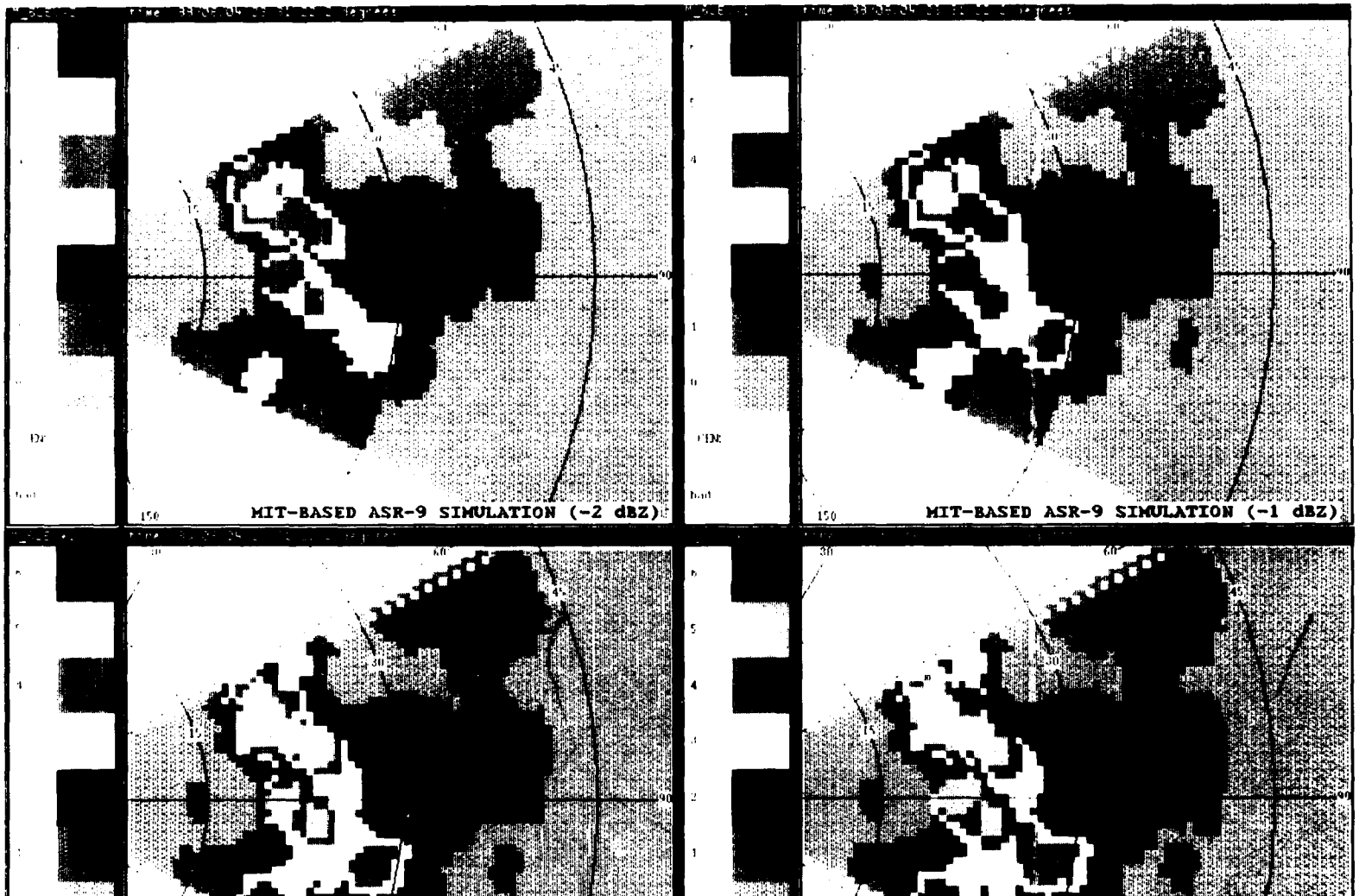

Figure 2-2. Simulation output for convective storm, 4 August 1988 (event 1) for reflectivities offset by (a) -2, (b) -1, (c) +1, and (d) +2 dB. Relatively small reflectivity offsets can have a significant impact on the spatial extent of weather contours reported.

SECTION 3

RESULTS OF ANALYSIS

3.1 ASR-9 WEATHER CHANNEL PRODUCTS COMPARED WITH SIMULATION AND EMULATION DATA

This section uses data from the ASR-9 weather channel, pencil-beam based simulation, and FL-3 based emulation to assess the Huntsville ASR-9 weather channel. In the first part of this section, six cases are detailed, each based on data recorded during the occurrence of a particular type of weather (see Table 2-1). All cases include both ASR-9 and FL-3 emulation data, while only the first three cases include MIT pencil-beam simulation data. The title following each case header includes the date, storm type, which processor the ASR-9 was using (e.g. two-level or six-level), and polarization. Where the polarization is not indicated, the polarization was not known. However, because the ASR-9 normally operates with vertical polarization, it may be assumed that the ASR-9 was most likely operating using vertical polarization for those cases. In the second part of this section, all weather data listed in Table 2-2 are used to generate overall performance statistics quantizing the degree of agreement between ASR-9 products and FL-3 based emulation products.

3.1.1 CASE STUDIES

Case 1 2 August 1988 - Two-Level Processor; Convective Storm

Figures 3-1 and 3-2 show the output of the ASR-9 two-level weather channel, the FL-3 based emulation, and the MIT radar based simulation programs for two separate convective storms which both occurred in the mid-afternoon on 2 August 1988. The Two-level processor of the ASR-9 was configured to report levels 2 and 4. Both figures show good agreement among the three data products. Figure 3-3 shows the resulting difference reflectivity plots between the ASR-9 and emulation outputs for the two storms, tabulated below each plot are associated statistics. The difference plots regions represent areas where the ASR-9 reported one or more levels higher or lower than the emulation data, according to the color-bar. Areas of white represent areas where the two data products reported the same level. Both the difference plots and associated statistics indicate good agreement among the three radars.

Case 2 4 August 1988 - Six-Level Processor; Convective Storm

Figure 3-4 shows the output of the ASR-9 six-level weather channel, the FL-3 based emulation, and the C-band radar based simulation programs based on data recorded during an isolated convective storm which occurred in the late afternoon on 4 August 1988. This event shows excellent agreement among the three data products, with the best agreement between the ASR-9 and FL-3 data. The simulation data shows minor discrepancies as compared to the ASR-9 and emulation data. Specifically, the simulation data underestimated a Level 3 contour at about 80 degrees, 30 nmi and two Level 2 contours at about 70 degrees, 40 nmi. Factors possibly contributing to these discrepancies are MIT scan time and C-band signal attenuation through precipitation, coupled with the coarse quantization of the six NWS weather levels (see Section 2.2). Figure 3-5 shows

the resulting difference reflectivity plot between the ASR-9 and FL-3 based emulation products, and associated statistics. The statistics show that the difference is always one level or less, with the probability of the ASR-9 reports being the same as the emulation data never less than 89 %.

Case 3 8 August 1988 - Six-Level Processor; Convective Storm

Figure 3-6 shows the output of the ASR-9 six-level weather channel, FL-3 based emulation, and C-band radar based simulation programs based on data recorded during an isolated convective storm which occurred in the early afternoon on 8 August 1988. This event, shows excellent agreement among the three data products. Figure 3-7 shows the resulting difference reflectivity plot between the ASR-9 and emulation outputs, and associated statistics, indicating that the difference is generally one level or less. Examination of Figure 3-7 shows that the ASR-9 Level 4 regions are displaced spatially from those in the emulation data by more than the 1 nmi acceptance window. Accordingly, the statistic table indicates only 41 % of the Level 4 ASR-9 cells overlap with Level 4 emulation data, while the remaining 59 % overlap with Level 3 emulation data. However, this is to be expected because of the relatively small amount of Level 4 weather displayed, i.e. spatial differences between the reported centers of two equal-level and spatially small contours will result in a significant fraction of those areas not overlapping.

Case 4 16 September 1988 - Six-Level Processor; Stratiform Rain

Figure 3-8 shows the output of the ASR-9 six-level weather channel and emulation program during stratiform rain in the mid afternoon on 16 September 1988. The MIT radar recorded only horizon-scan data during this event, so MIT based simulation data were unavailable. Figure 3-9 shows the resulting difference reflectivity plots between the ASR-9 and emulation outputs and associated statistics for both events. Both the visual and computer comparisons indicate that the ASR-9 is reporting significantly more area for each level as well as higher levels than the emulation data. We observed that an approximately 3 dB reduction in the weather level thresholds used for the FL-3 emulation was required to produce good agreement. This was found to be true for all cases using data collected during and after September 1988. This discrepancy seems to be independent of range and weather intensity, suggesting a simple difference in calibrations between the two radars. The ongoing testing of the ASR-9 during this time precluded any intensive investigation of the problem. Accordingly, Figure 3-10 shows the output of the ASR-9 six-level weather channel and emulation program with the emulation data biased higher by 3 dB. This comparison shows much better agreement between the two data products. The large spatial difference between the two products for Level 1 weather is assumed to be due to a difference in sensitivity between the two radars and threshold settings. Since stratiform rain tends to have weaker reflectivity gradients than for convective type weather, the weather contours tend to be more amorphous and less likely to agree. Figure 3-11 shows the resulting difference reflectivity plots between the ASR-9 and emulation outputs and associated statistics corresponding to the PPIs of figure 3-10, indicating that the difference is generally within one level.

Case 5 4 November 1988 - Six-Level Processor (CP); Cold Front

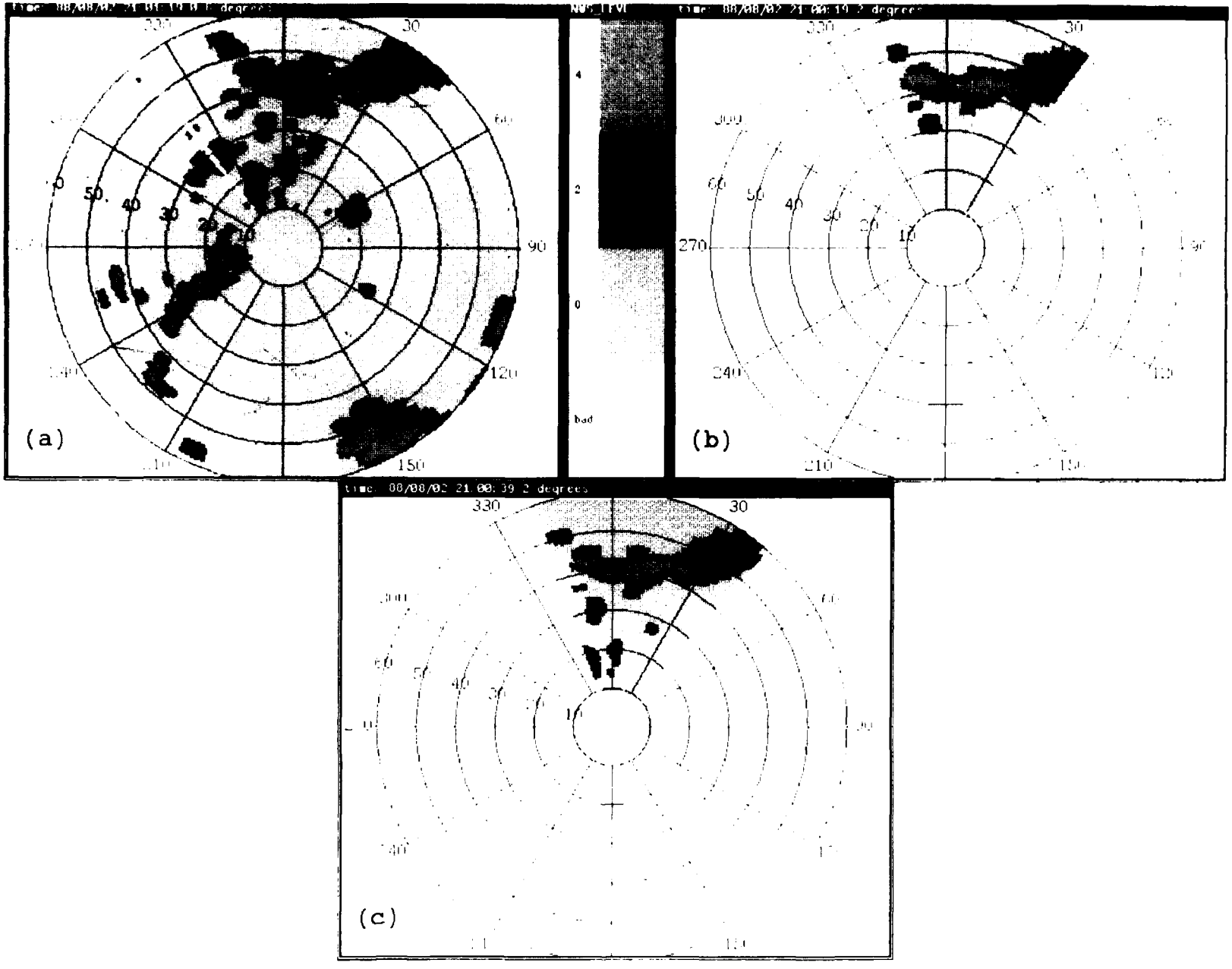

Figure 3-1. Comparison between (a) ASR-9 two-level, (b) simulation, and (c) emulation data, convective storm, 2 August 1988. Inspection indicates good agreement among the three data products.

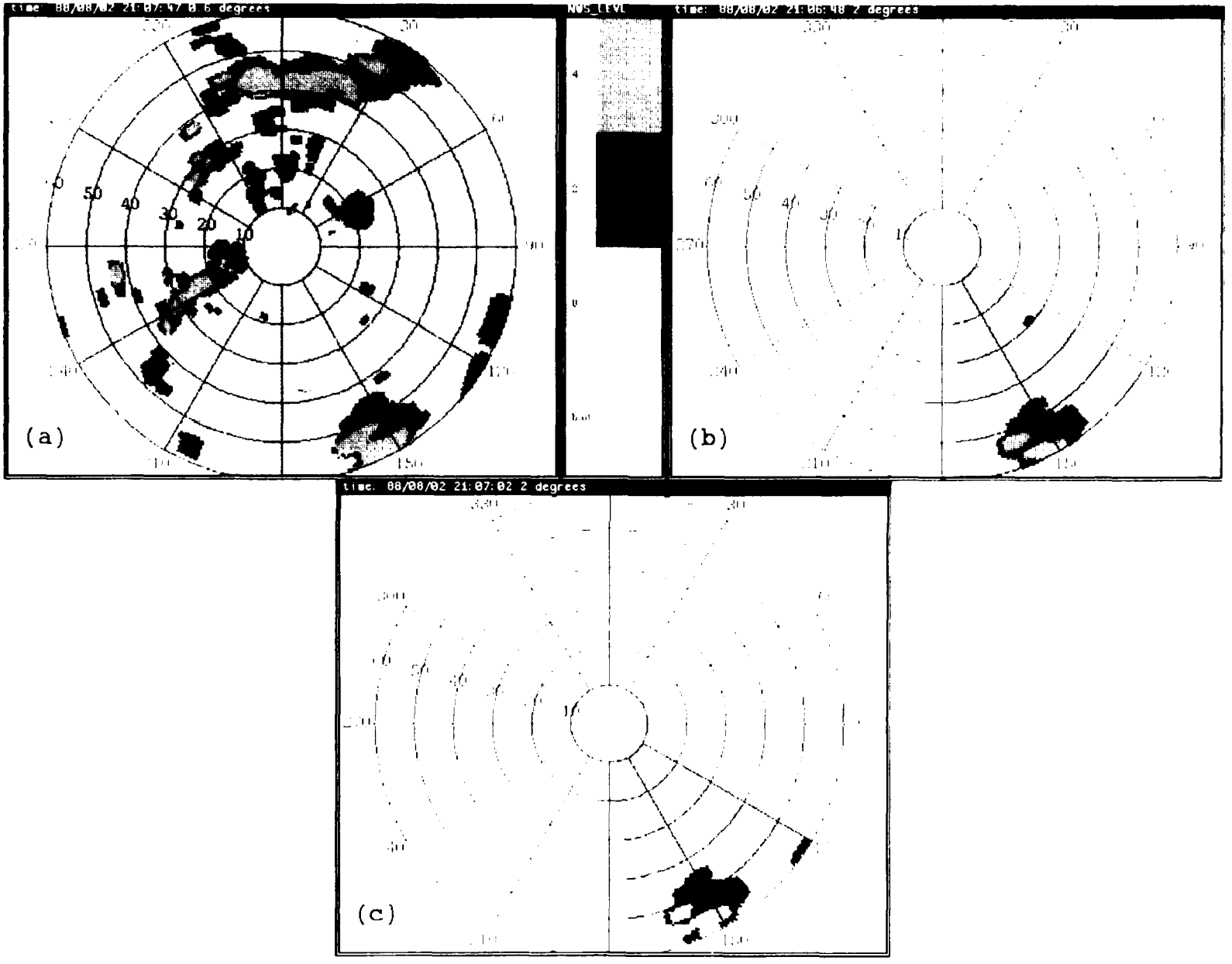

Figure 3-2. Comparison between (a) ASR-9 two-level, (b) simulation, and (c) emulation data, convective storm, 2 August 1988. Inspection indicates good agreement among the three data products.

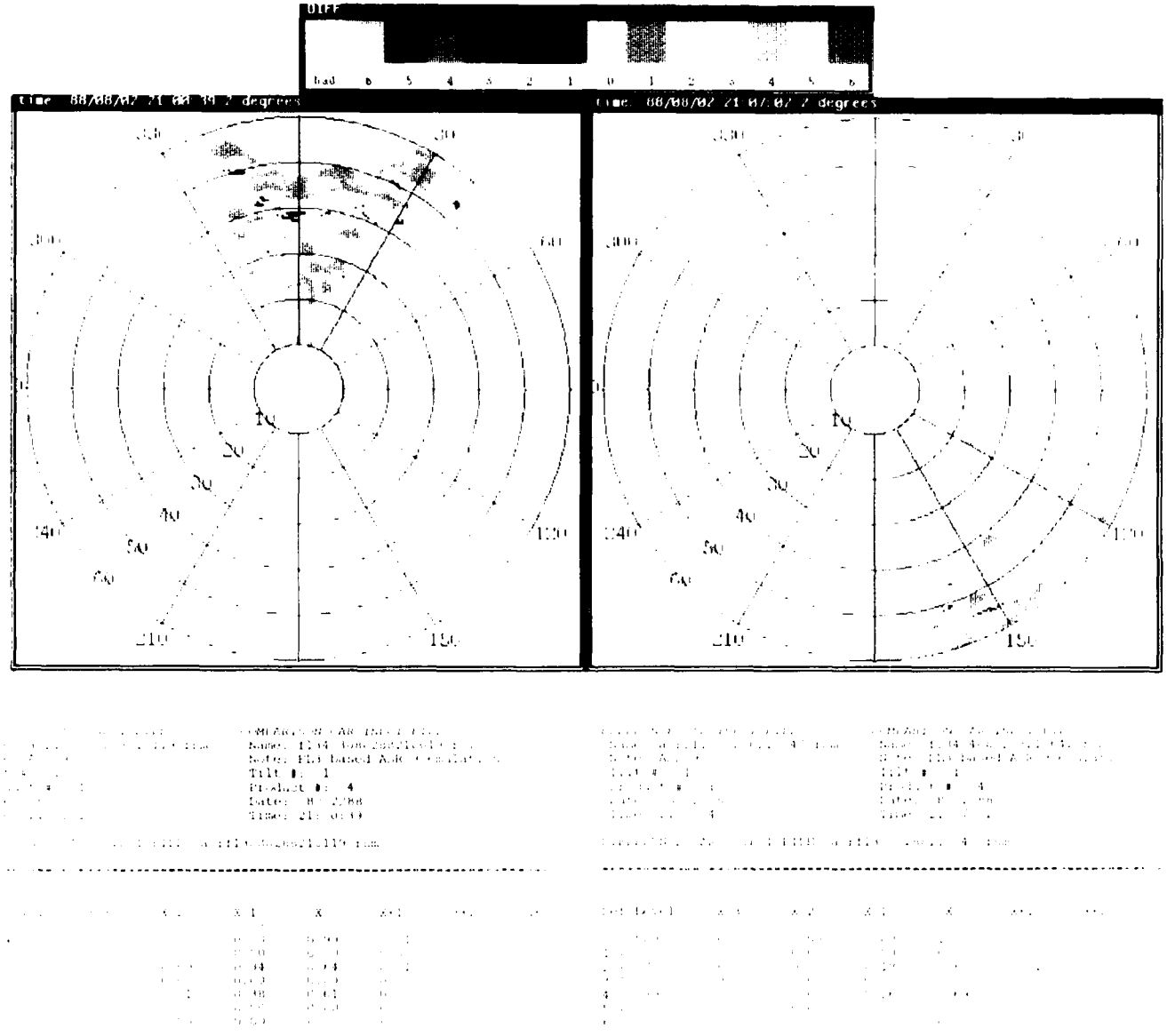

Figure 3-3. Reflectivity difference between ASR-9 two-level and emulation data, two convective storms, 2 August 1988. Both the difference plots and associated statistics indicate good agreement among the three radars.

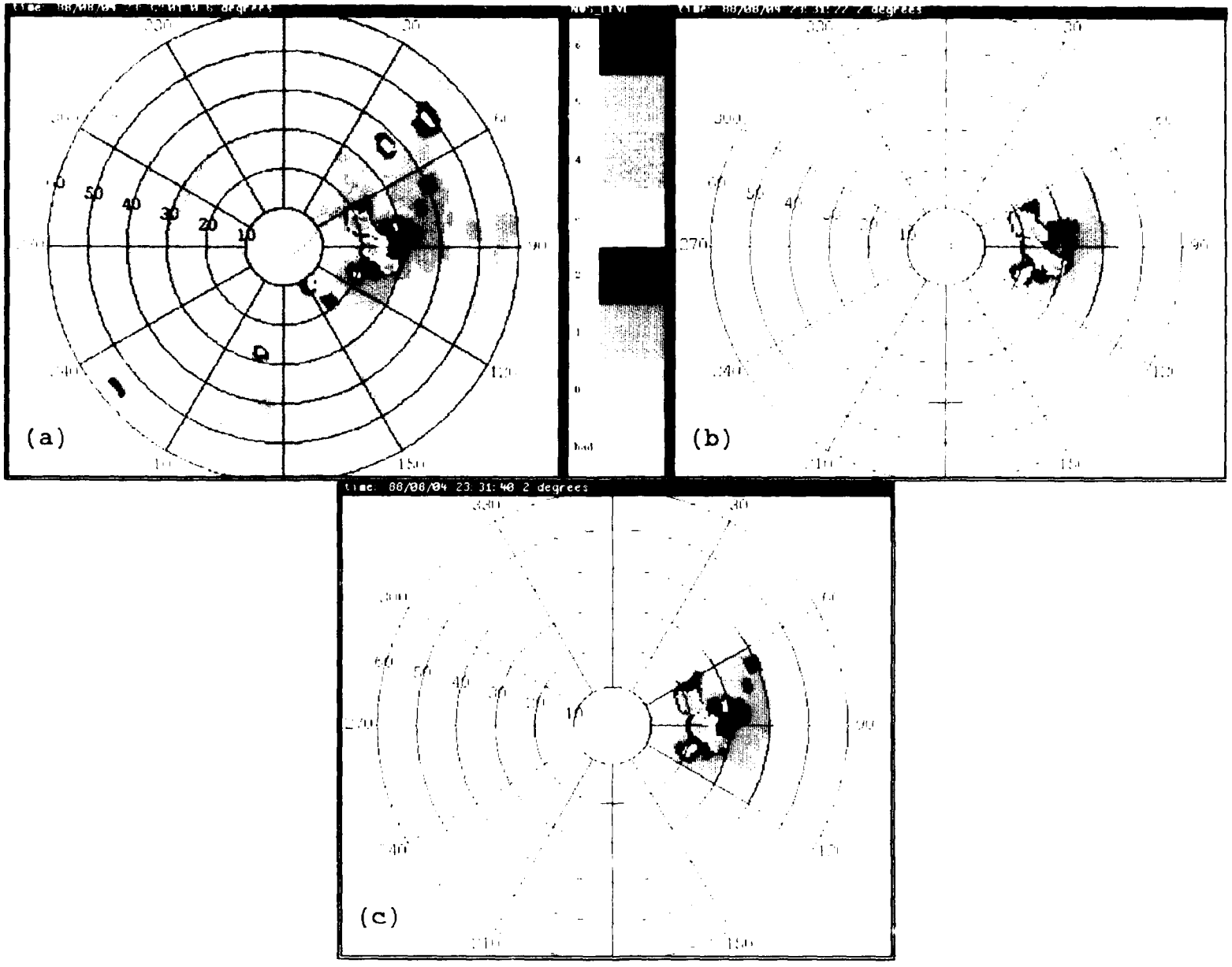

Figure 3-4. Comparison between (a) ASR-9 six-level, (b) simulation, and (c) emulation data, convective storm, 4 August 1988. Inspection indicates excellent agreement among the three data products, with the best agreement between the ASR-9 and TL-3 emulation data.

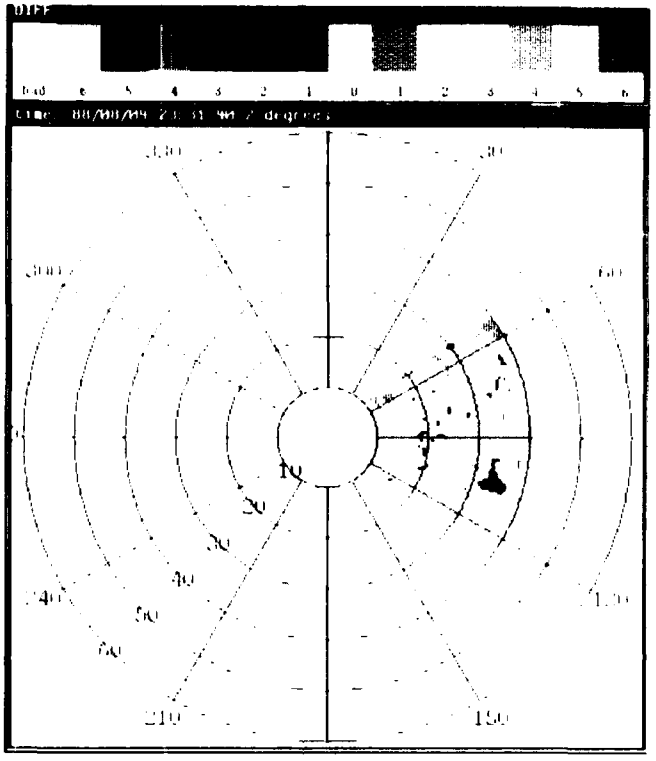

Figure 3-5. Reflectivity difference between ASR-9 six-level and emulation data, convective storm, 4 August 1988. The statistics show that the difference is always one level or less.

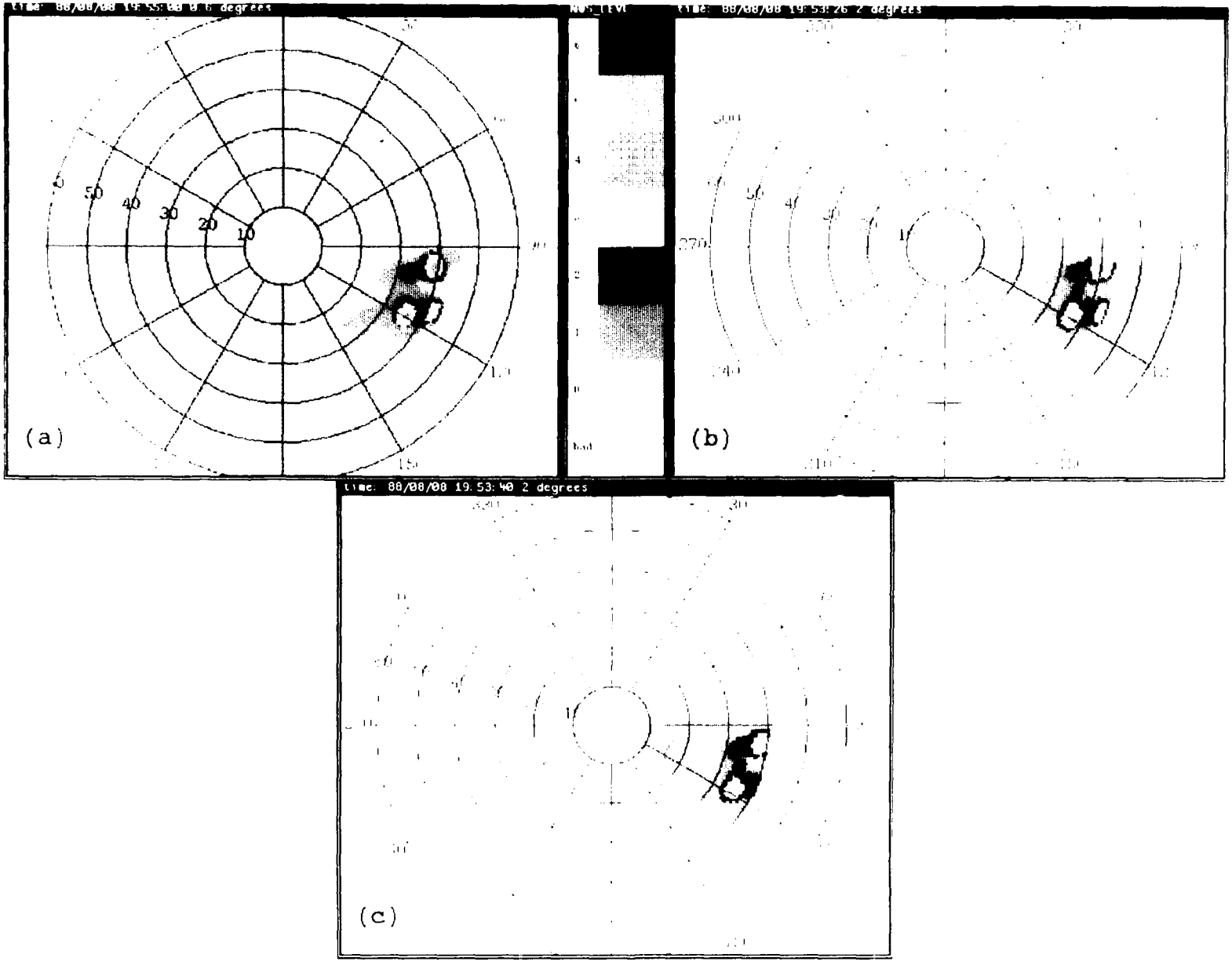

Figure 3-6. Comparison between (a) ASR-9 six-level, (b) simulation, and (c) emulation data, convective storm, 8 August 1988. Inspection indicates excellent agreement among the three data products.

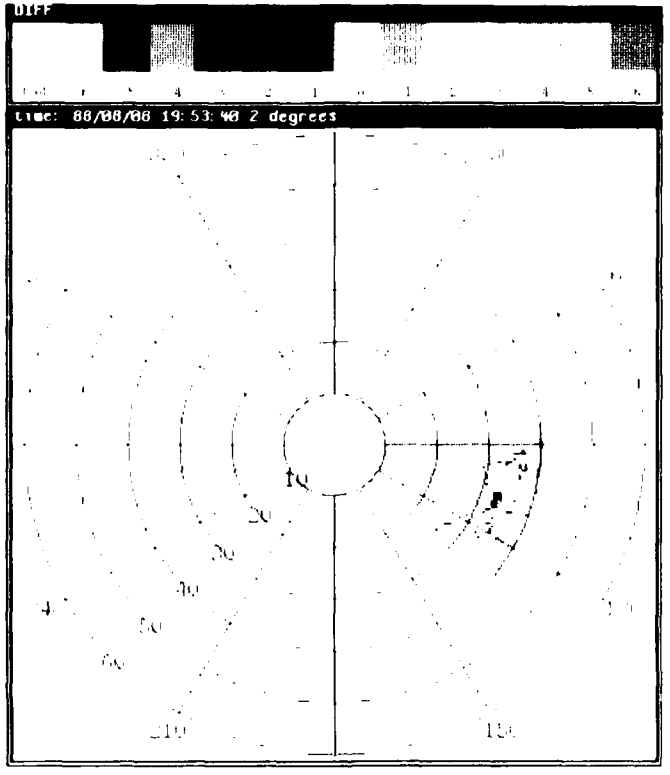

Figure 3-7. Reflectivity difference between ASR-9 six-level and emulation data, convective storm, 8 August 1988. The statistics show that the difference is generally one level or less.

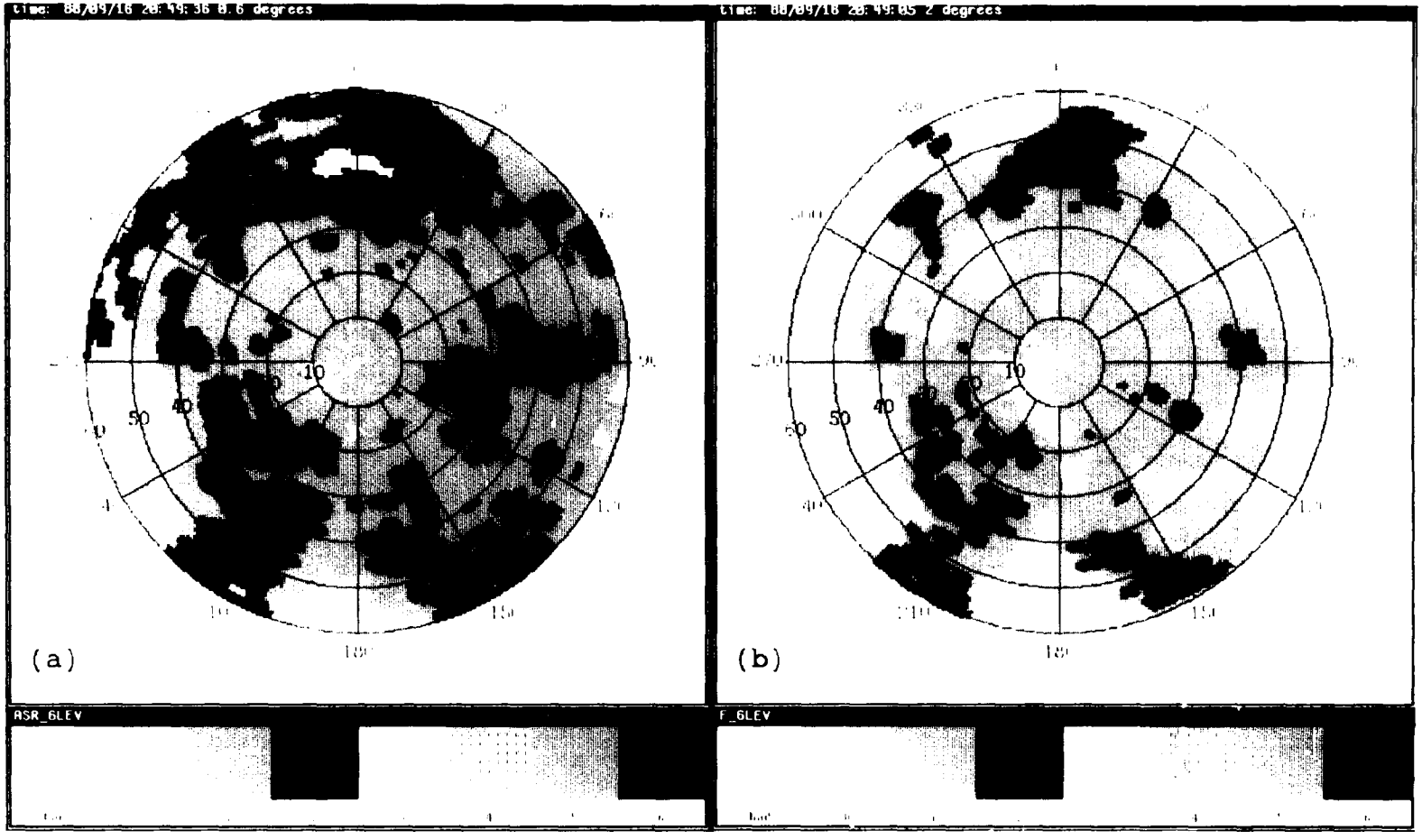

Figure 3-8. Comparison between ASR-9 six-level and emulation data, stratiform rain, 16 September 1988. Inspection indicates that the ASR-9 is reporting significantly more area for each level as well as higher levels than the FL-3 emulation data.

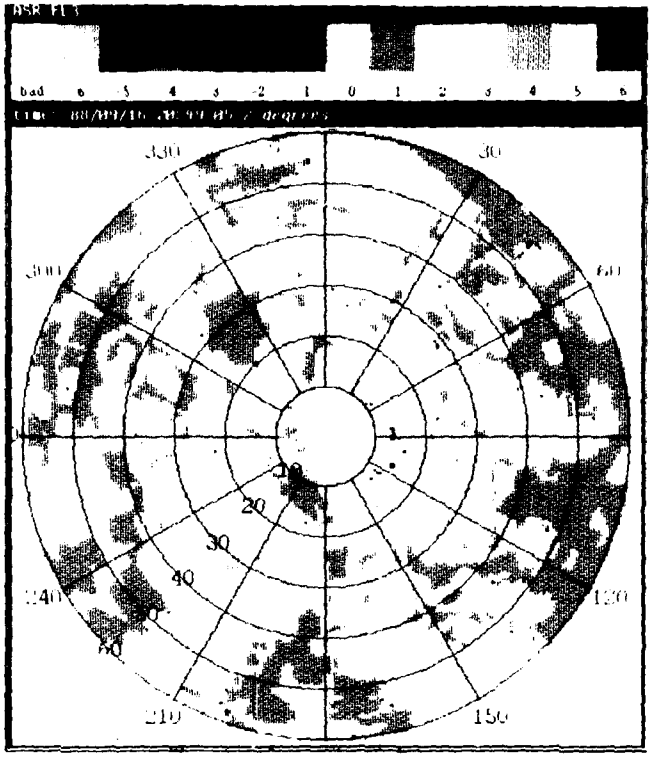

Figure 3-9. Reflectivity difference between ASR-9 six-level and emulation data, stratiform rain, 16 September 1988. Statistics show that the ASR-9 is reporting significantly more area for each level as well as higher levels than the FL-3 emulation data.

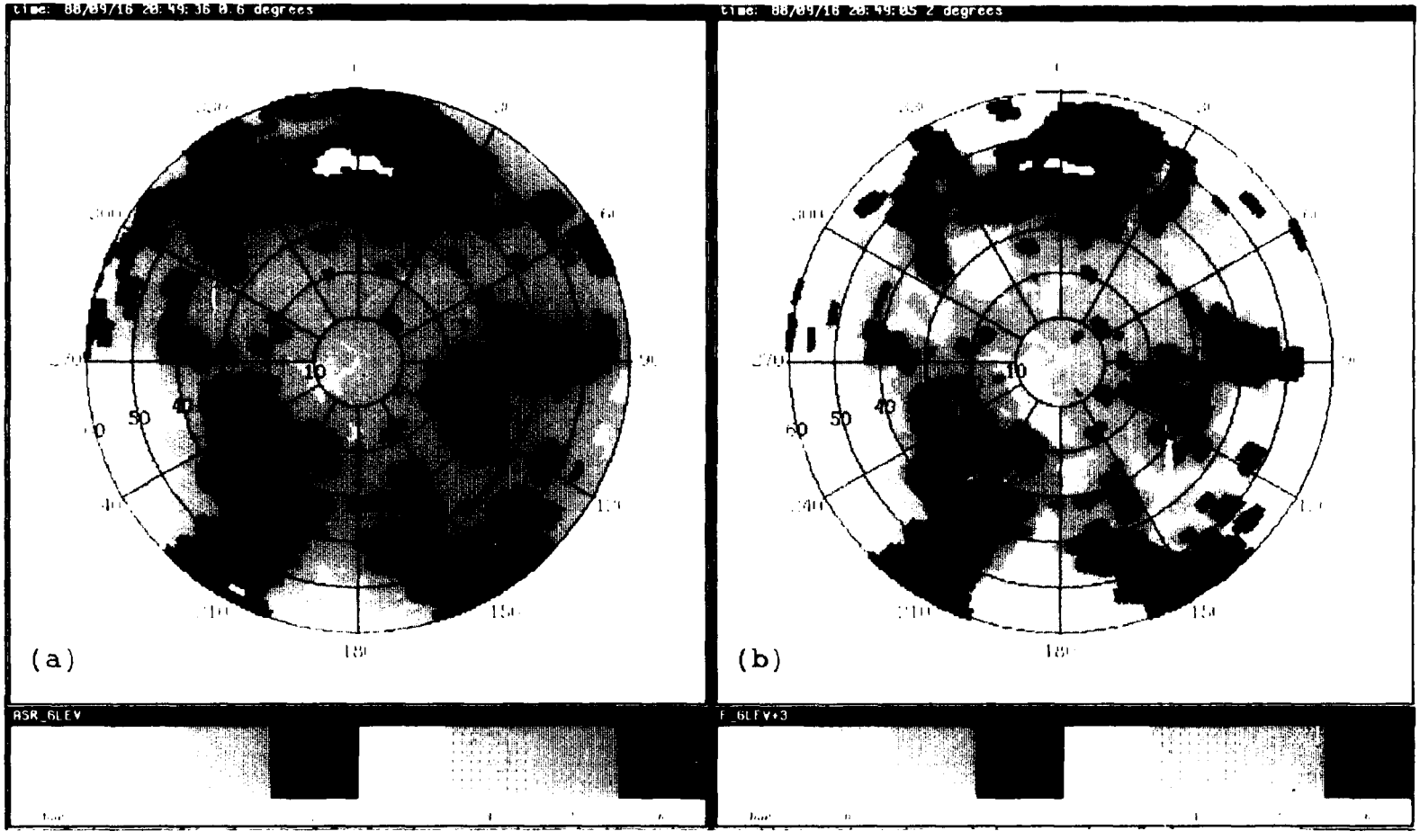

Figure 3-10. Comparison between (a) ASR-9 six-level and (b) emulation data increased by 3 dB, stratiform rain, 16 September 1988. Inspection indicates much better agreement between the two data products as was found without the 3 dB increase. The remaining discrepancy between Level 1 weather produced by both radars is assumed to be due to a difference in sensitivity between the two radars and threshold settings.

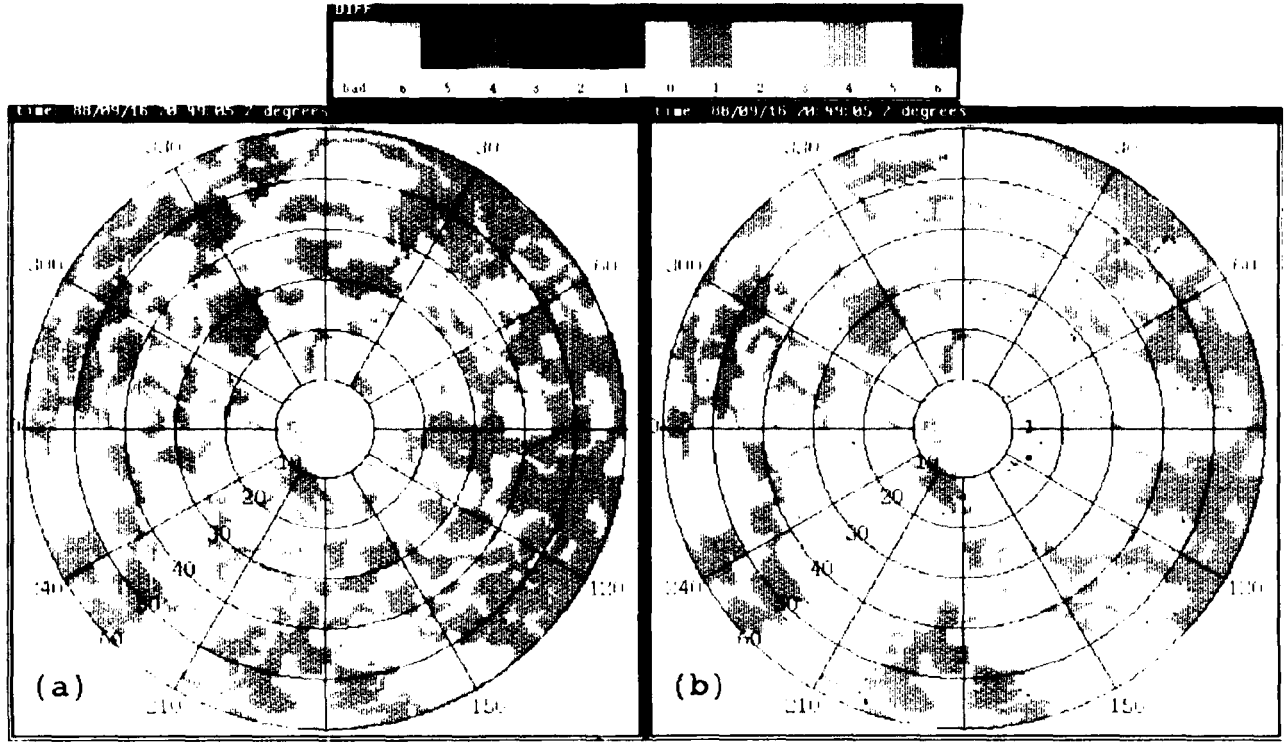

Figure 3-11. Reflectivity difference between ASR-9 six-level and emulation data increased by (a) 0 and (b) 3 dB, stratiform rain, 16 September 1988. Statistics show much better agreement between the two data products as was found without the 3 dB increase. The remaining discrepency between Level 1 weather produced by both radars is assumed to be due to a difference in sensitivity between the two radars and threshold settings.

Figure 3-12 shows the output of the ASR-9 six-level weather channel and FL-3 emulation products recorded during a cold front passage on 4 November 1988. A multitude of embedded thunderstorm cells were triggered in the warm air ahead of the front. A tornado was reported about 41 nmi north-west of the airport during the time these data were recorded. Although the PPIs show good spatial agreement, several of the ASR-9 weather contours are one level higher than the emulation data. Figure 3-13 repeats the comparison with the emulation data biased higher by 3 dB, showing much better agreement. Resulting difference reflectivity plots and associated statistics with and without the 3 dB corrections are shown in Figure 3-14. The probability tables indicate that, when the emulation data is increased by 3 dB, there is a significant decrease in the probability of differences of two levels (see column X-2) and the two PPIs are generally within one level. Note from the difference reflectivity plots that, when the emulation data is increased by 3 dB, the area where the ASR-9 is reporting one level higher than the emulation radar is roughly equal to the area where it is reporting one level lower than the emulation radar. This suggests that the 3 dB offset was an appropriate amount to add to the emulation reflectivity data.

Note the narrow regions of Level 1 and 2 second-trip weather located at approximately 210 degrees in the FL-3 emulation data. Although the ASR-9 successfully filtered almost all of the second-trip returns, FL-3 data taken during this weather event was recorded with a constant PRF, making second-trip filtering impossible. When FL-3 data taken several minutes later in staggered PRF mode was processed with second-trip filtering, the suspected second-trip weather contours vanished confirming that the ASR-9 processor was filtering second-trip weather appropriately.

Case 6 26 November 1988 - Six-Level Processor (LP): Squall Line

Figures 3-15 and 3-16 show the output of the ASR-9 six-level weather channel and FL-3 based emulation products with and without the 3 dB correction recorded during a squall line passage on 26 November 1988. As before, the ASR-9 six-level weather channel and emulation program show much better agreement when the emulation data is increased 3 dB. Figure 3-17 shows the resulting difference reflectivity plots and associated statistics. The probability tables indicate that, when the emulation data is increased by 3 dB, there is a significant decrease in the probability of two-level differences (see column X-2) and one-level differences (see column X-1), while the two PPIs are generally within one level. It is interesting to note that there is a much lower probability of there being more than one level difference between the ASR-9 and FL-3 data compared to the previous case. A possible explanation for this is the lower reflectivity gradient associated with this case than in the previous case.

3.1.2 INTERPRETATION OF COMPARISONS

Table 3-1 contains probabilities of agreement between the ASR-9 and emulation data, as a function of reflectivity level for all cases listed in Table 2-2. Table 3-2 contains the same probabilities with the emulation reflectivity data increased by 3 dB. Table 3-1 indicates a bias between the emulation and ASR-9 weather products; for weather Level 3 and higher, the ASR-9 is most likely to report one level higher than the emulation radar. With the 3 dB added and independent of weather level, the ASR-9 and FL-3 emulation products are more likely to report the same level. Table 3-2 indicates slight bias toward the X-1 side, suggesting that slightly more than the 3 dB would

TABLE 3-1

Ensemble Of Probabilities Resulting From Computer Comparisons Between ASR-9 And FL-3 Emulation Data For All Cases Listed In Table 2-2.

ENSEMBLE STATISTICS - WITHOUT FL3 CALIBRATION ADJUSTMENT
(August, 1988 Data Excluded)

Ref	-3	-2	-1	0	+1	+2	+3
0	0.000	0.000	0.000	0.983	0.016	0.000	0.000
1	0.000	0.000	0.359	0.632	0.009	0.000	0.000
2	0.000	0.042	0.287	0.669	0.001	0.000	0.000
3	0.003	0.006	0.648	0.338	0.006	0.000	0.000
4	0.002	0.125	0.614	0.250	0.005	0.000	0.000
5	0.024	0.191	0.508	0.273	0.000	0.000	0.000
6	0.008	0.060	0.722	0.206	0.000	0.000	0.000

TABLE 3-2

Ensemble Of Probabilities Resulting From Computer Comparisons Between ASR-9 And FL-3 Emulation Data Increased By 3 dB For All Cases Listed In Table 2-2.

ENSEMBLE STATISTICS - WITH +3 DBZ FL3 CALIBRATION ADJUSTMENT
(August, 1988 Data Included)

Ref	-3	-2	-1	0	+1	+2	+3
0	0.000	0.000	0.000	0.982	0.013	0.007	0.000
1	0.000	0.000	0.362	0.559	0.075	0.001	0.000
2	0.000	0.040	0.044	0.902	0.010	0.000	0.000
3	0.003	0.001	0.197	0.766	0.030	0.003	0.000
4	0.000	0.018	0.182	0.758	0.041	0.000	0.000
5	0.008	0.022	0.149	0.808	0.013	0.000	0.000
6	0.000	0.009	0.229	0.744	0.009	0.000	0.000

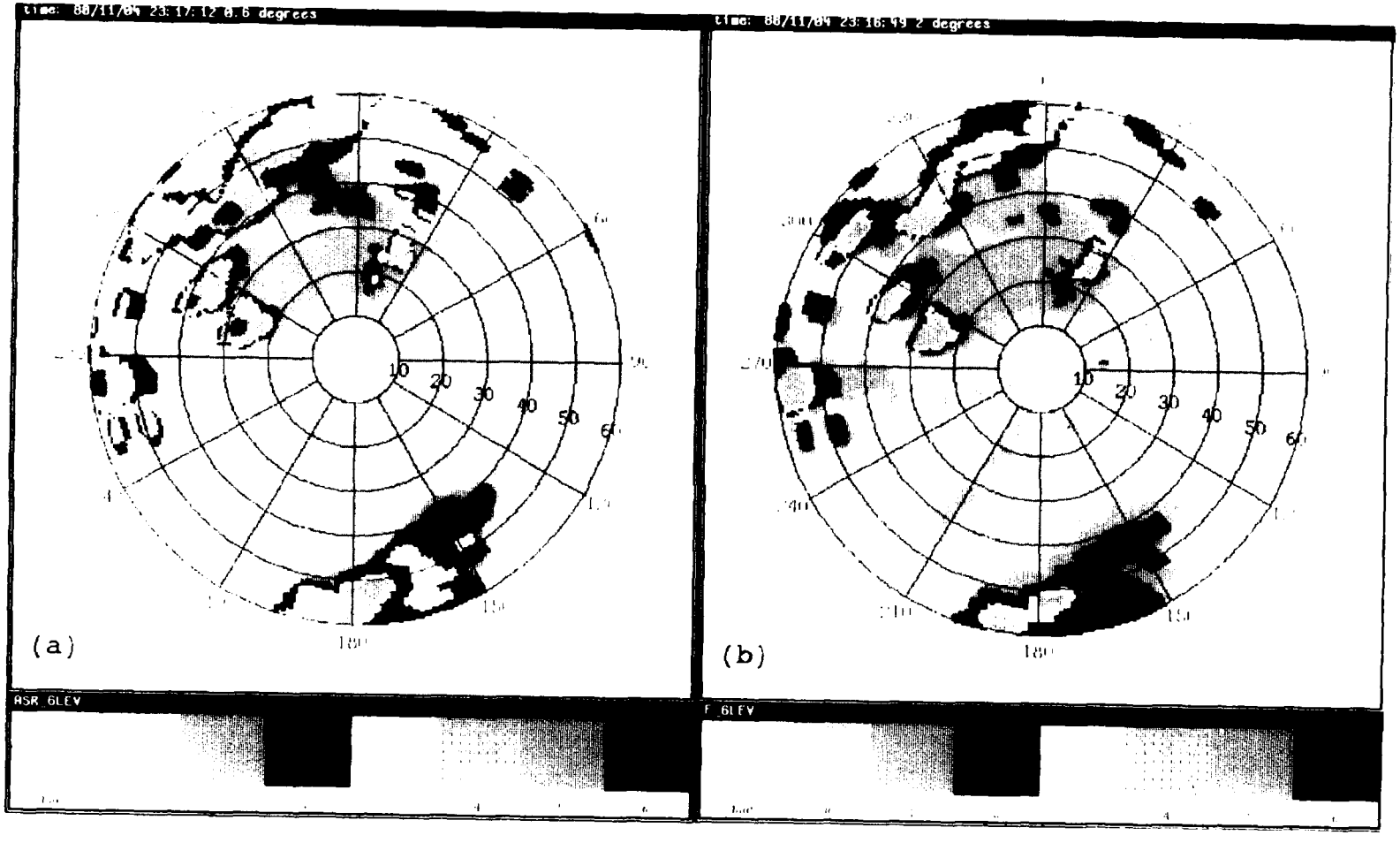

Figure 3-12. Comparison between (a) ASR-9 six-level CP and (b) emulation data, cold front, 4 November 1988. Although the PPIs show good spatial agreement, several of the ASR-9 weather contours are one level higher than the emulation data.

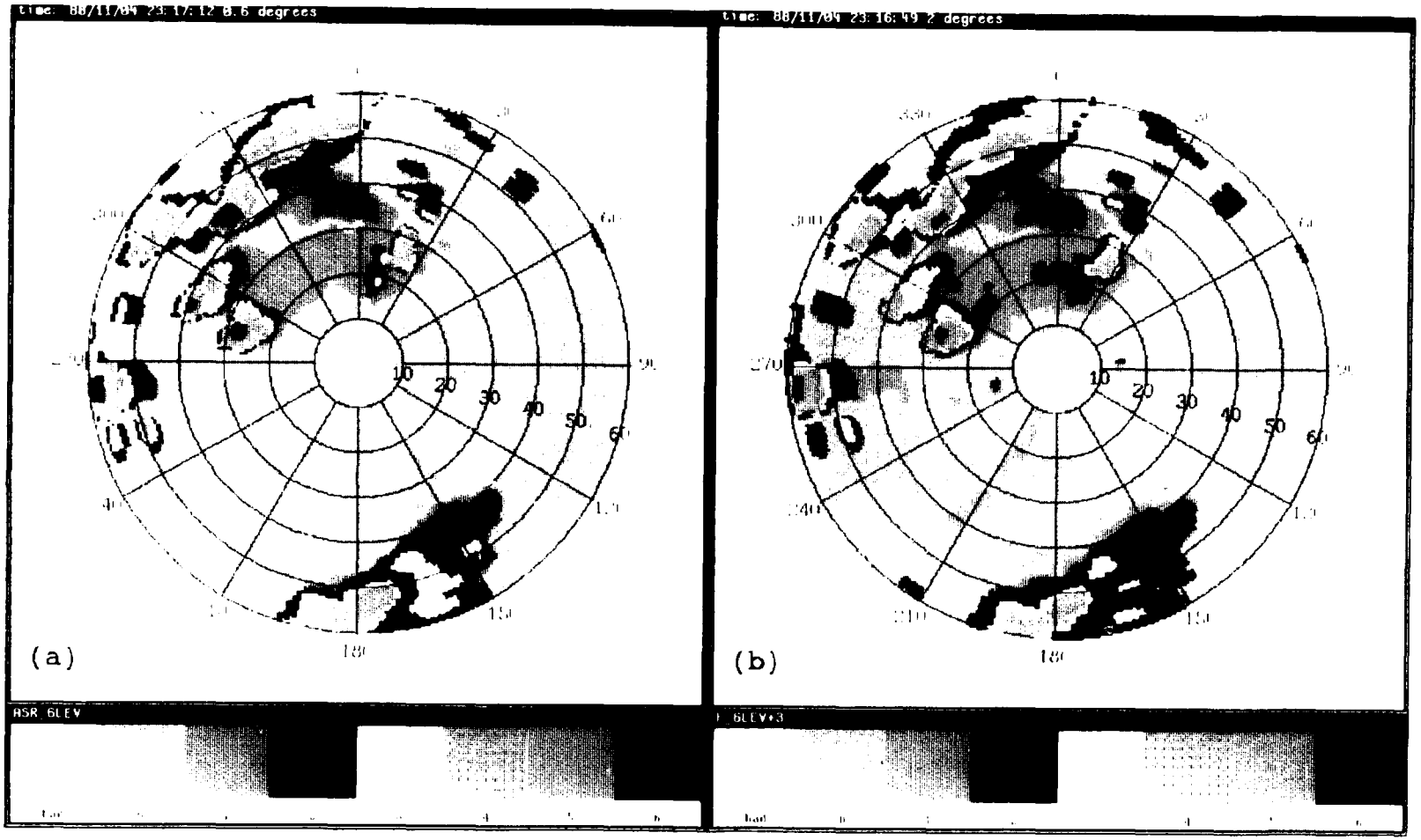

Figure 3-13. Comparison between (a) ASR-9 six-level CP and (b) emulation data increased by 3 dB, cold front, 4 November 1988. Inspection indicates much better agreement between the two radars when emulation data is increased by 3 dB.

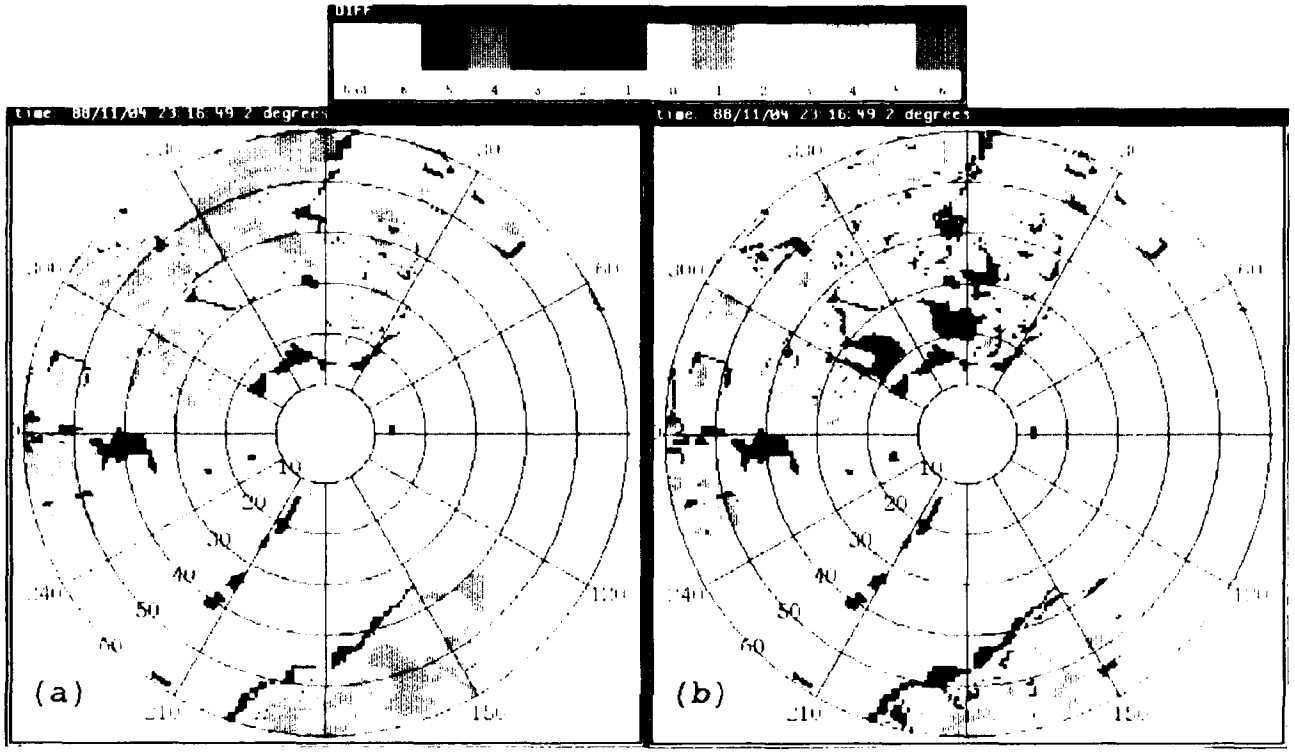

Figure 3-14. Reflectivity difference between ASR-9 six-level CP and emulation data increased by (a) 0 and (b) 3 dB, cold front, 4 November 1988. Statistics show, when the emulation data is increased by 3 dB, there is a significant decrease in the probability of differences of two levels (see column X-2) and the two radars are generally within one NWS level.

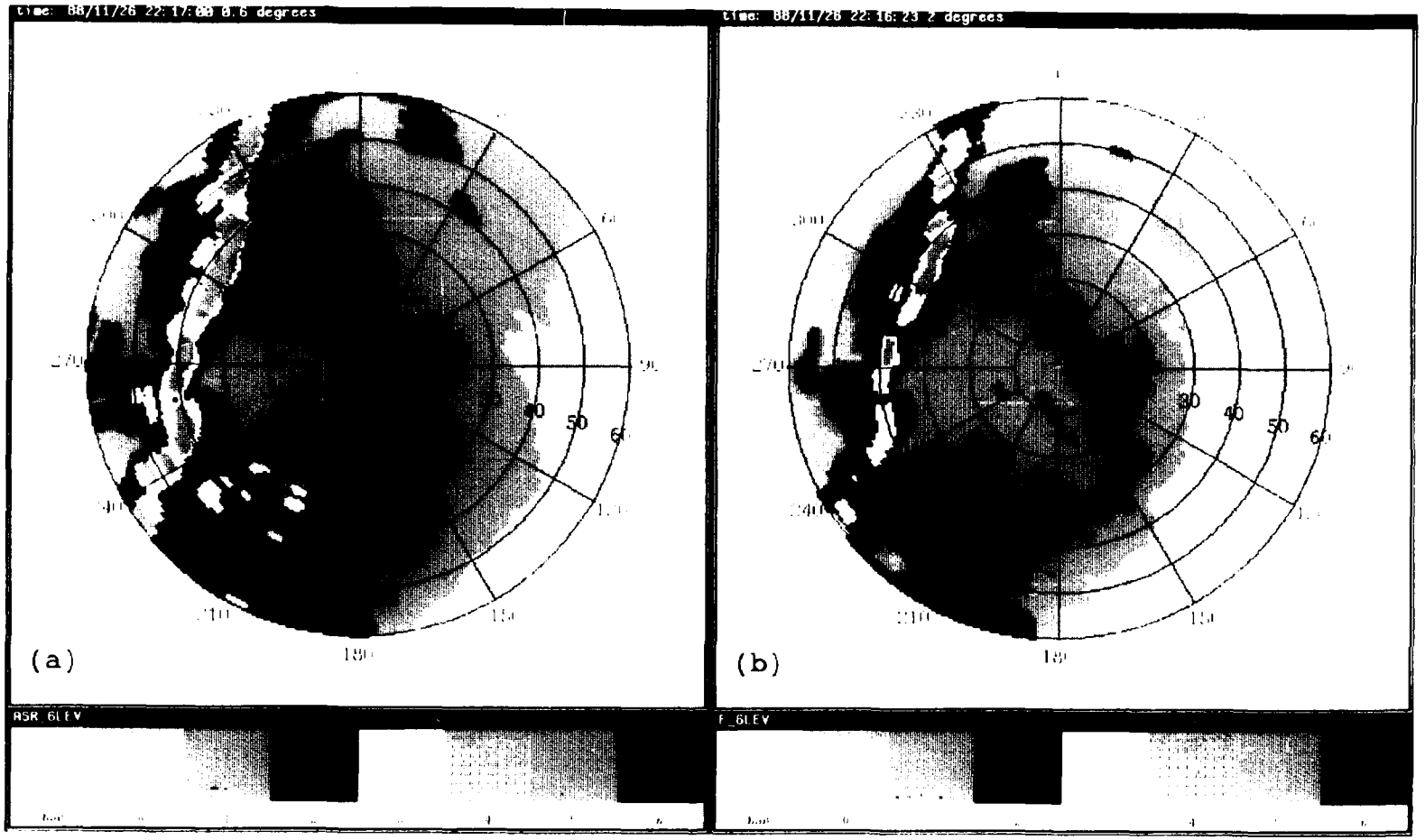

Figure 3-15. Comparison between (a) ASR-9 six-level LP and (b) emulation data, squall line, 26 November 1988. Although the PPIs show good spatial agreement, several of the ASR-9 weather contours are one level higher than the emulation data.

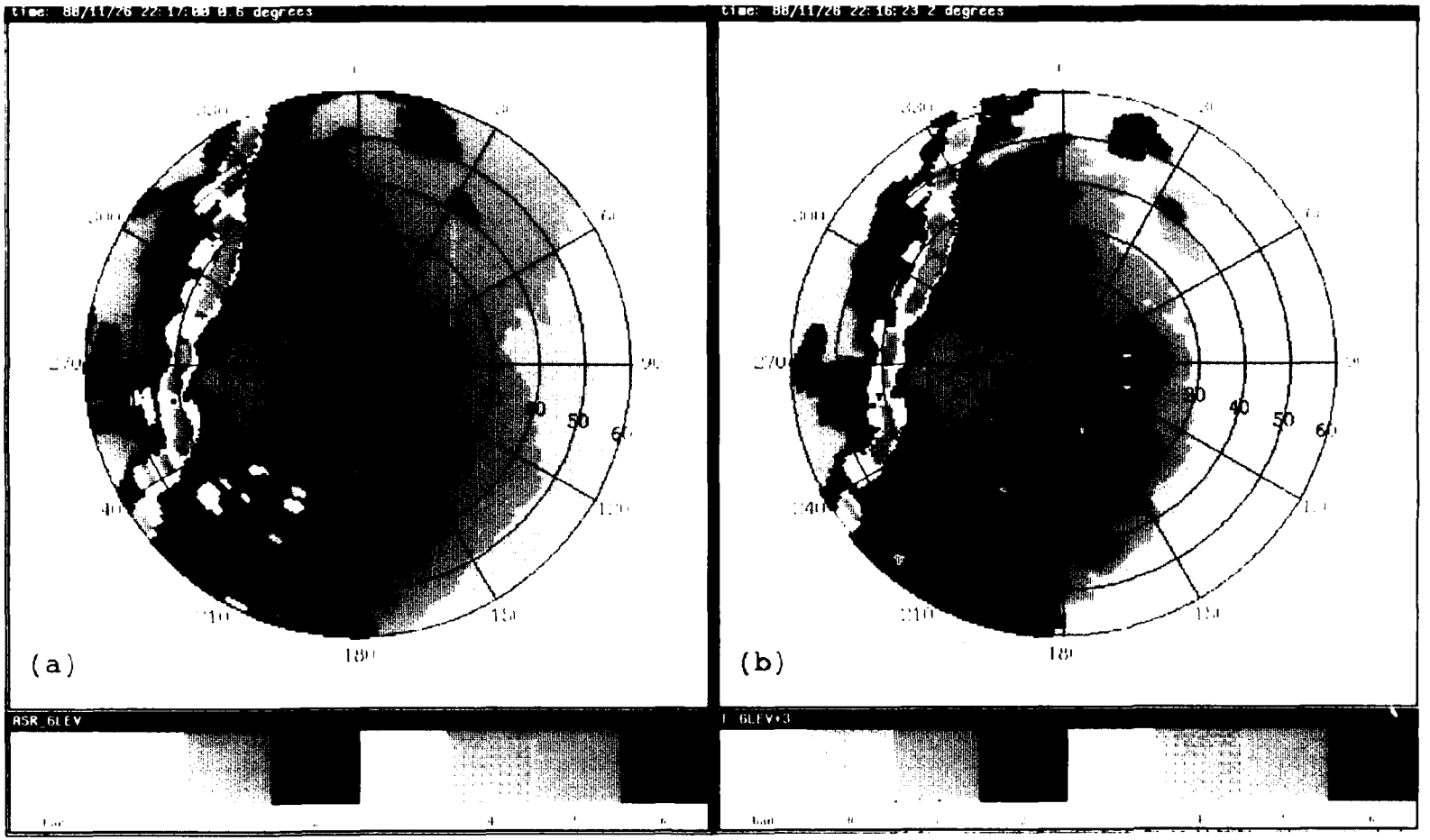

Figure 3-16. Comparison between (a) ASR-9 six-level LP and (b) emulation data increased by 3 dB, squall line, 26 November 1988. Inspection indicates much better agreement between the two radars when emulation data is increased by 3 dB.

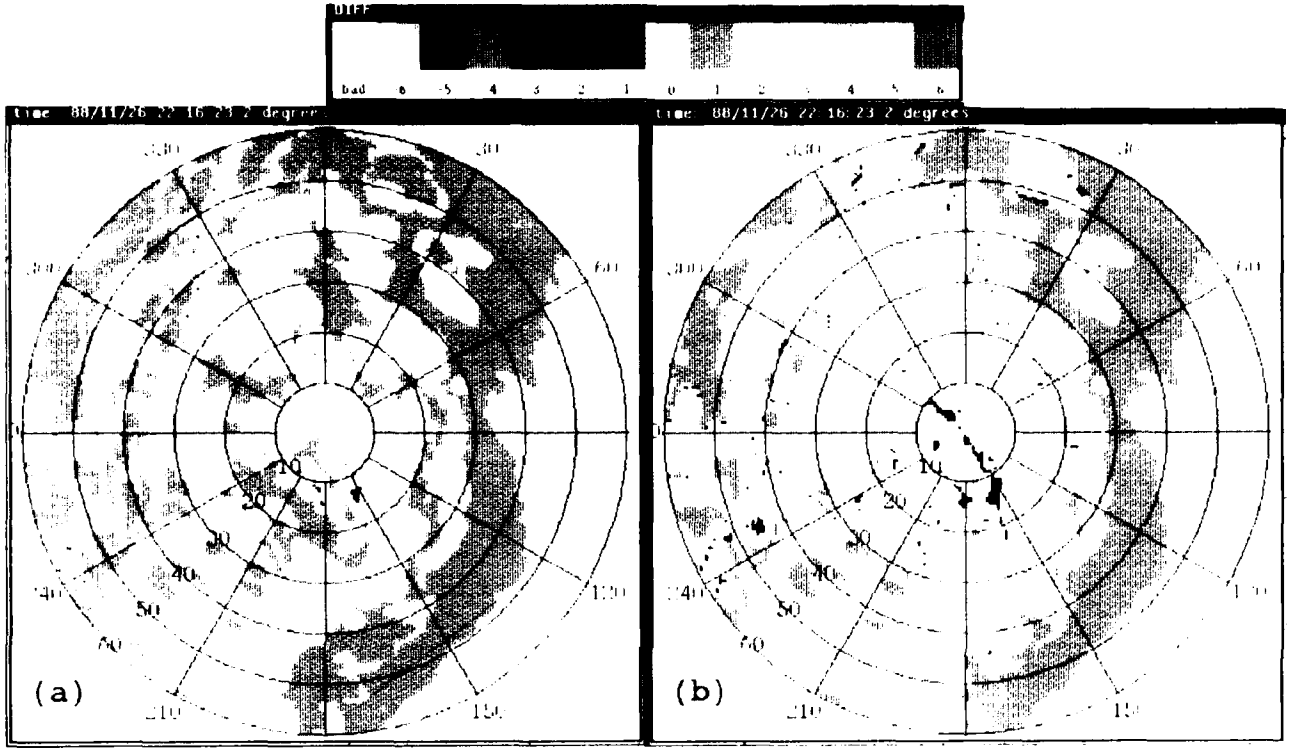

Figure 3-17. Reflectivity difference between ASR-9 six-level LP and emulation data increased by (a) 0 and (b) 3 dB, squall line, 26 November 1988. Statistics show that when the emulation data is increased by 3 dB, there is a significant decrease in the probability of two-level and one-level differences, while the two radars are generally within one NWS level.

need to be added to all emulation data to result in better agreement between the two products.

Spatial and level discrepancies between the ASR-9 and FL-3 radar due to radar calibration errors together with the coarsely partitioned NWS levels have a significant effect on agreement between their reflectivity outputs. It was shown (see Figure 2-2) that a 1 dB offset in the reflectivity estimate can have a significant impact on the resulting weather contour, with the higher levels being most affected. Even with the absence of mean calibration differences, the ASR-9 and FL-3 emulation products will not always be in perfect agreement. Therefore, is reasonable to expect that the ASR-9 and FL-3 data agree very well to within one NWS level. Accordingly, Table 3-3 below lists the probabilities of agreement between the ASR-9 and FL-3 emulation data, with the acceptance band set to one NWS level, for emulation data as recorded and offset 3 dB. This information was calculated from Table 3-1 and 3-2 by summing the probabilities in the -1, 0, and +1 columns for each reference level. Table 3-3 indicates that, without increasing the FL-3 emulation reflectivities by 3 dB, the worst agreement, 78.2 %, occurs for Level 5 data. The agreement at this weather level increases to 97 % when 3 dB is added to the emulation data.

TABLE 3-3

Ensemble Probabilities That The ASR-9 And FL-3 Based Emulation Products Agree To Within One NWS Level, For Emulation Reflectivities Increased By 0 And 3 dB

Reference Level	Emulation data as reported	Emulation data increased 3 dB
0	.999	.995
1	.999	.996
2	.957	.956
3	.992	.993
4	.872	.981
5	.782	.970
6	.928	.982

Figure 3-18 shows a graphical representation of the probability of agreement between the ASR-9 and FL-3 emulation data offset by 0 and 3 dB for all NWS levels. Clearly, without compensation for the suspected 3 dB calibration difference, the distributions show an obvious bias, while with compensation, report differences decrease and the distribution becomes more symmetric about zero. The +1 probability being higher than the -1 probability suggests a bias slightly greater than 3 dB. Based on the assumption that the 3 dB bias between the two weather products is caused by a simple calibration offset, the agreement between ASR-9 and FL-3 based emulation data offset by 3 dB indicates that the ASR-9 is operating as expected and provide an operationally useful representation of the weather.

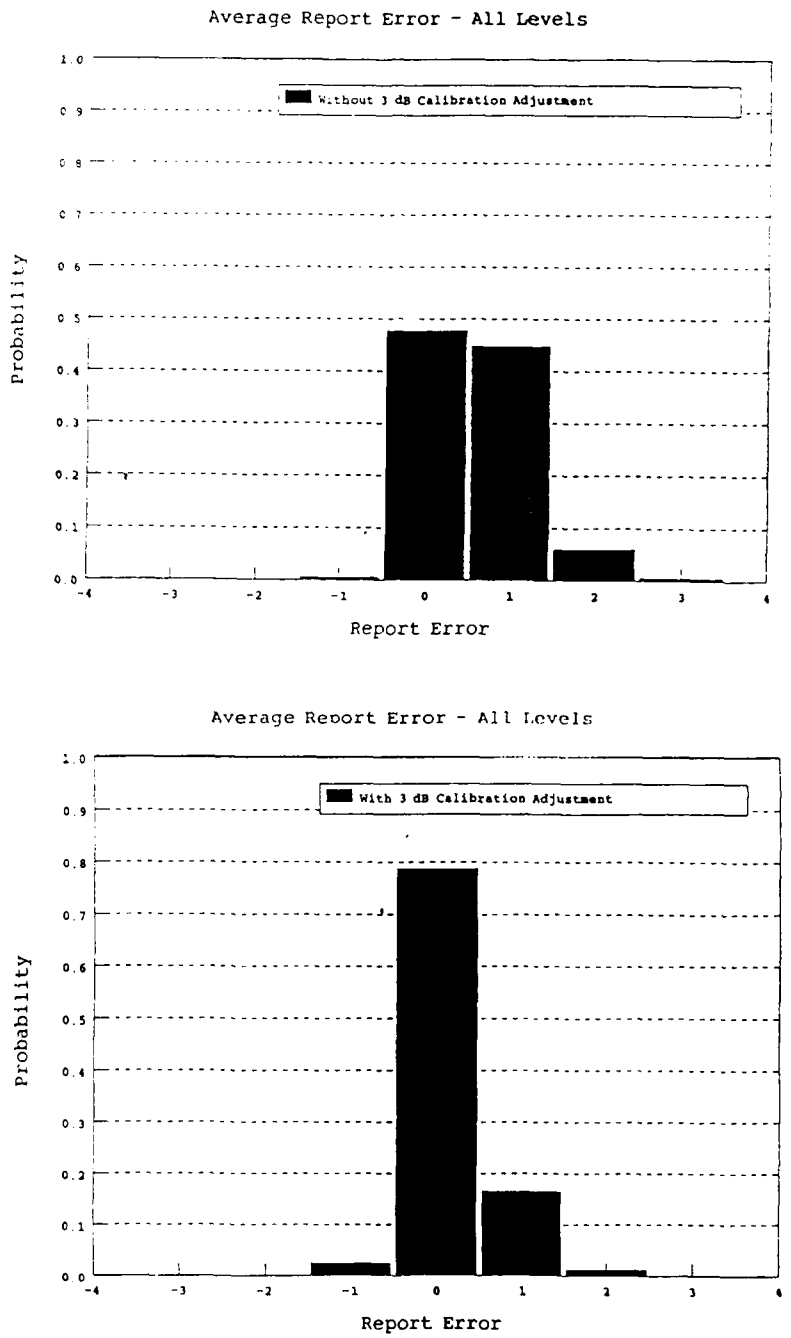

Figure 3-18. Graphical representation of the probability of agreement between the ASR-9 and FL-3 emulation data offset by 0 and 3 dB for all NWS levels. Without compensation for a suspected 3 dB calibration difference, the agreement distributions show an obvious bias, while with compensation, report differences decrease (distribution becomes more symmetric about zero).

3.2 ASR-9 WEATHER CHANNEL PRODUCTS COMPARED WITH PENCIL-BEAM REFLECTIVITY DATA

The following analyses are comparisons based on actual ASR-9 weather channel data and maximum, average, and horizon-scan (equivalent to the NWS radar) reflectivity data derived from the MIT pencil-beam radar data. Three cases are presented, during which MIT volume data were available. Because the ASR-9 data are spatially smoothed in a manner that increases the area of the weather contours (see Section 1.2), the three representations of pencil-beam data used in this section were spatially smoothed using the same algorithms.

The title following each case header includes the date, storm type, and whether the six or two-level ASR-9 weather processor was used. The polarization is not known for these cases. However, because the ASR-9 normally operates with vertical polarization, it was assumed that the ASR-9 was operating using vertical polarization for these cases.

3.2.1 CASE STUDIES

Case 1 2 August 1988 Two-Level Processor; Convective Storm

Figure 3-19 shows the output of the ASR-9 two-level weather channel and the maximum, average, and horizon-scan reflectivity data recorded during a convective storm events on 2 August 1988 (same event as in Figure 3-1). Based on visual comparison, the ASR-9 data is in best agreement with the maximum reflectivity data, with less agreement with the horizon-scan, and the average reflectivity data. Figure 3-20 shows the plots of *difference reflectivity between the ASR-9 and maximum, average,* and horizon scan data, where Table 3-4 shows the associated probabilities. Areas of white shown in the difference reflectivity plot indicate areas where the two particular data sets agree. Both the difference plot and statistics indicate that the ASR-9 agrees best with the maximum data.

The contractor's storm model assumes that a storm will be concentrated just above the ground and decreases in intensity above 4 km. Figure 3-21 shows a range-height indicator (RHI) generated from MIT PPI data at several elevations at 10 degrees in azimuth. This figure shows the vertical reflectivity profile of the storm with its core extending from the ground up to about 3.5 km (11,480 ft.). The ASR-9 beamfill correction based on this model appears to be appropriate for this storm event.

Case 2 4 August 1988 Six-Level Processor; Convective Storm

Figure 3-22 shows the output of the ASR-9 six-level weather channel and the maximum, average, and horizon-scan reflectivity data recorded during the convective storm on 4 August 1988 (same weather event as in Figure 3-4). The highest NWS level reported by the ASR-9 was Level 5. Based on visual comparisons, pencil-beam data processed to reflect the average reflectivity seems to agree best with ASR-9 data, followed closely by the horizon scan data, then the maximum reflectivity data. Figure 3-23 shows the plots of difference reflectivity between the ASR-9 and maximum, average, and horizon scan data, while Table 3-5 shows the associated probabilities of the same. Both the difference plot and statistics indicated that the ASR-9 agrees with both average and

TABLE 3-4

Probabilities Of Differences Between ASR-9 Two-Level And MIT Based Maximum, Average, And Horizon-Scan Data, Convective Storm, 2 August 1988

REFERENCE CAR INPUT FILE
Name: asr197080288210119.rsm
Note: ASR-9
Tilt #: 1
Product #: 1
Date: 8/ 2/88
Time: 21: 1:19

COMPARISON CAR INPUT FILE
Name: mittru080288210019_smooth.r
Note: MIT max projection
Tilt #: 1
Product #: 4
Date: 8/ 2/88
Time: 21: 0:19

DIFFERENCE CAR OUTPUT FILE: asrmax080288210119.rsm

Ref Level	X-3	X-2	X-1	X	X+1	X+2	X+3
0 (3583)	0.00	0.00	0.00	0.99	0.01	0.00	0.00
1 (0)	0.00	0.00	0.00	0.00	0.00	0.00	0.00
2 (1750)	0.00	0.00	0.30	0.69	0.01	0.00	0.00
3 (0)	0.00	0.00	0.00	0.00	0.00	0.00	0.00
4 (750)	0.00	0.02	0.10	0.88	0.00	0.00	0.00
5 (0)	0.00	0.00	0.00	0.00	0.00	0.00	0.00
6 (0)	0.00	0.00	0.00	0.00	0.00	0.00	0.00

REFERENCE CAR INPUT FILE
Name: asr197080288210119.rsm
Note: ASR-9
Tilt #: 1
Product #: 1
Date: 8/ 2/88
Time: 21: 1:19

COMPARISON CAR INPUT FILE
Name: mittru080288210019_smooth.r
Note: MIT avg projection
Tilt #: 1
Product #: 3
Date: 8/ 2/88
Time: 21: 0:19

DIFFERENCE CAR OUTPUT FILE: asravg080288210119.rsm

Ref Level	X-3	X-2	X-1	X	X+1	X+2	X+3
0 (3583)	0.00	0.00	0.00	1.00	0.00	0.00	0.00
1 (0)	0.00	0.00	0.00	0.00	0.00	0.00	0.00
2 (1750)	0.00	0.00	0.41	0.59	0.00	0.00	0.00
3 (0)	0.00	0.00	0.00	0.00	0.00	0.00	0.00
4 (750)	0.00	0.02	0.43	0.55	0.00	0.00	0.00
5 (0)	0.00	0.00	0.00	0.00	0.00	0.00	0.00
6 (0)	0.00	0.00	0.00	0.00	0.00	0.00	0.00

REFERENCE CAR INPUT FILE
Name: asr197080288210119.rsm
Note: ASR-9
Tilt #: 1
Product #: 1
Date: 8/ 2/88
Time: 21: 1:19

COMPARISON CAR INPUT FILE
Name: mittru080288210019_smooth.r
Note: MIT-based horizon scan
Tilt #: 1
Product #: 5
Date: 8/ 2/88
Time: 21: 0:19

DIFFERENCE CAR OUTPUT FILE: asrlow080288210119.rsm

Ref Level	X-3	X-2	X-1	X	X+1	X+2	X+3
0 (3583)	0.00	0.00	0.00	1.00	0.00	0.00	0.00
1 (0)	0.00	0.00	0.00	0.00	0.00	0.00	0.00
2 (1750)	0.00	0.00	0.35	0.65	0.00	0.00	0.00
3 (0)	0.00	0.00	0.00	0.00	0.00	0.00	0.00
4 (750)	0.00	0.02	0.24	0.74	0.00	0.00	0.00
5 (0)	0.00	0.00	0.00	0.00	0.00	0.00	0.00
6 (0)	0.00	0.00	0.00	0.00	0.00	0.00	0.00

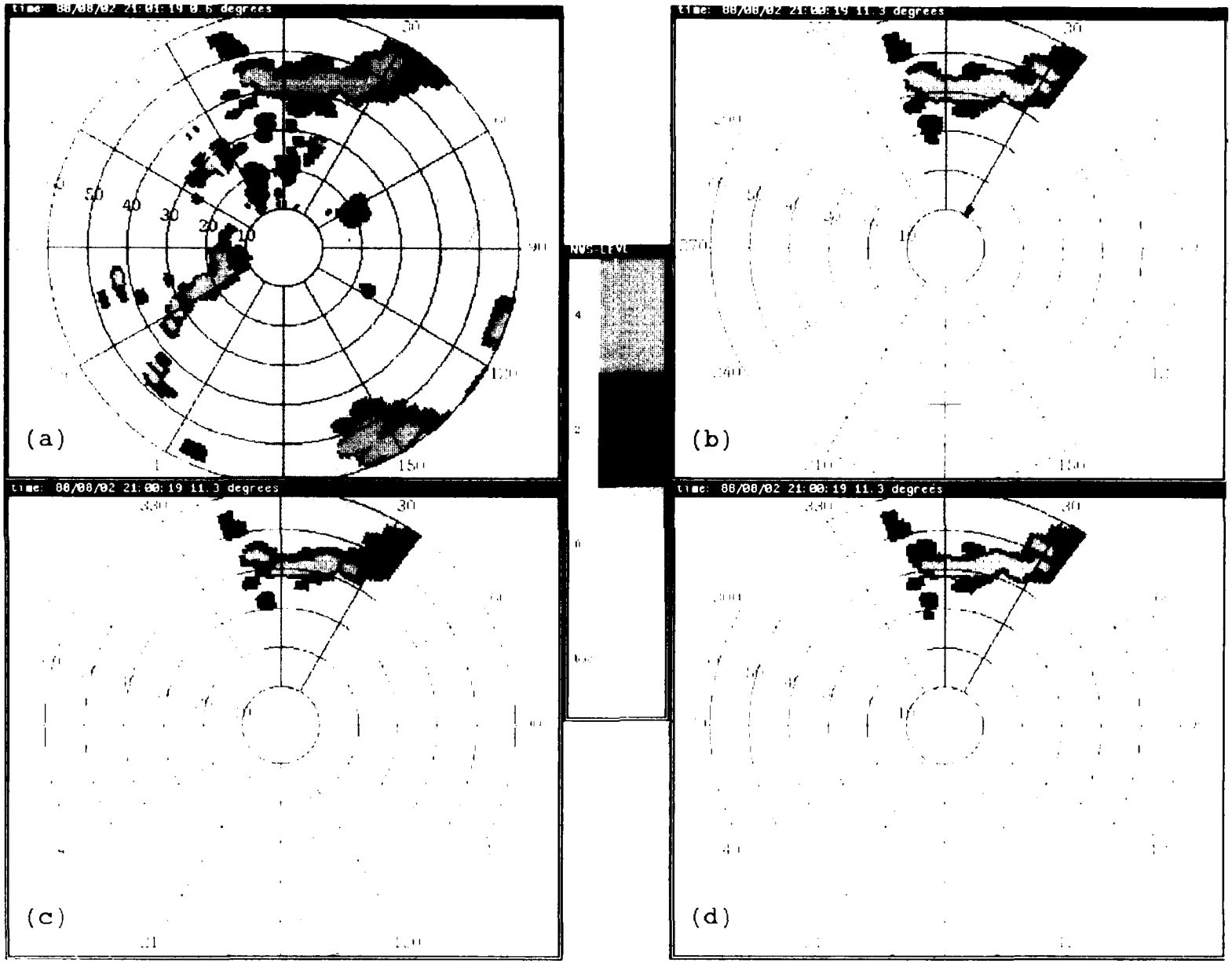

Figure 3-19. Comparison between (a) ASR-9 two-level and (b) MIT based maximum, (c) average, and (d) horizon-scan data, convective storm, 2 August 1988. Inspection indicates that the ASR-9 data agree best with the maximum reflectivity data, suggesting that the ASR-9 beamfill correction storm model is appropriate for this storm event.

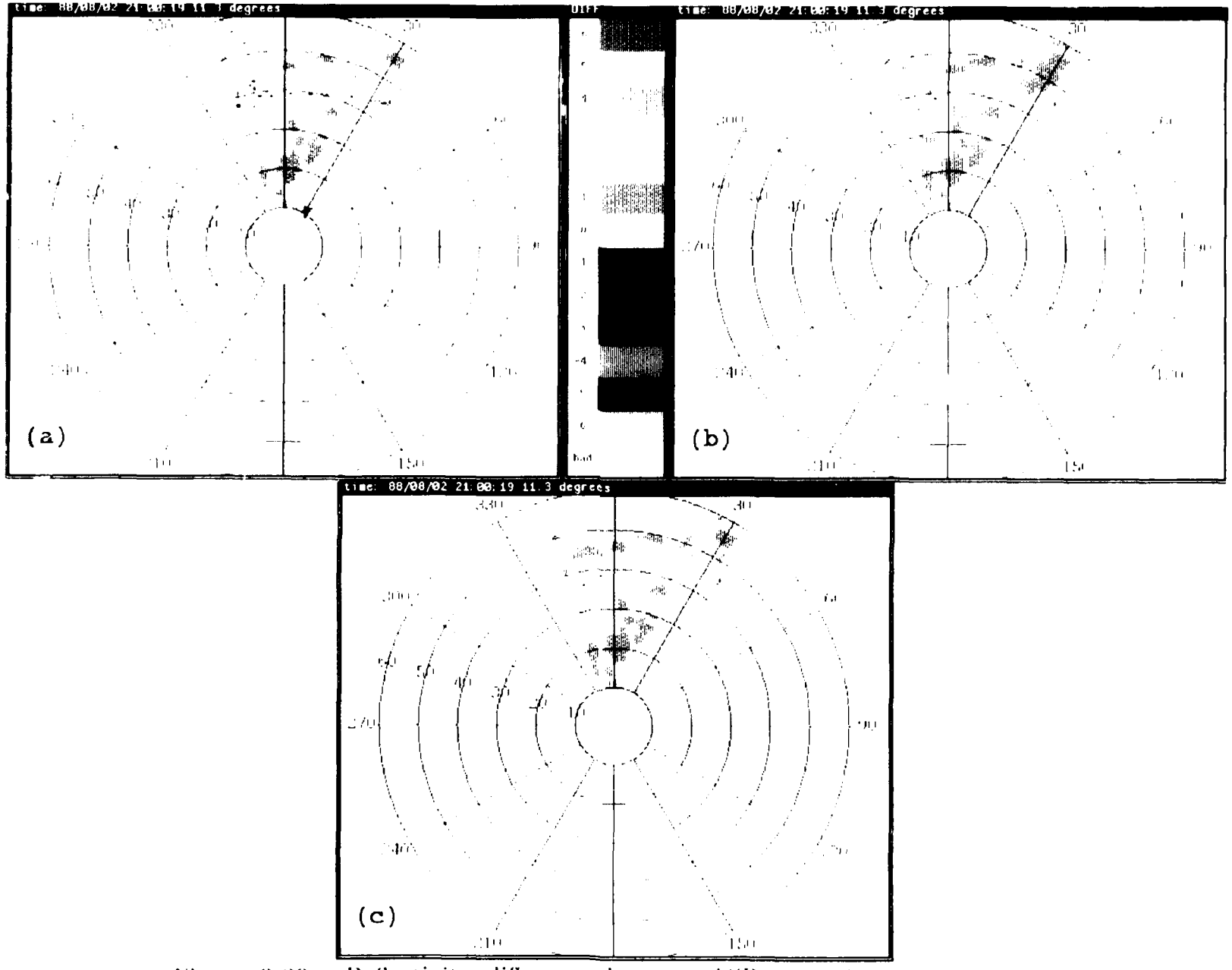

Figure 3-20. Reflectivity difference between ASR-9 two-level and (a) MIT based maximum, (b) average, and (c) horizon-scan data, convective storm, 2 August 1988. Statistics show that the ASR-9 data agree best with the maximum reflectivity data, with less agreement with the horizon-scan and average reflectivity data.

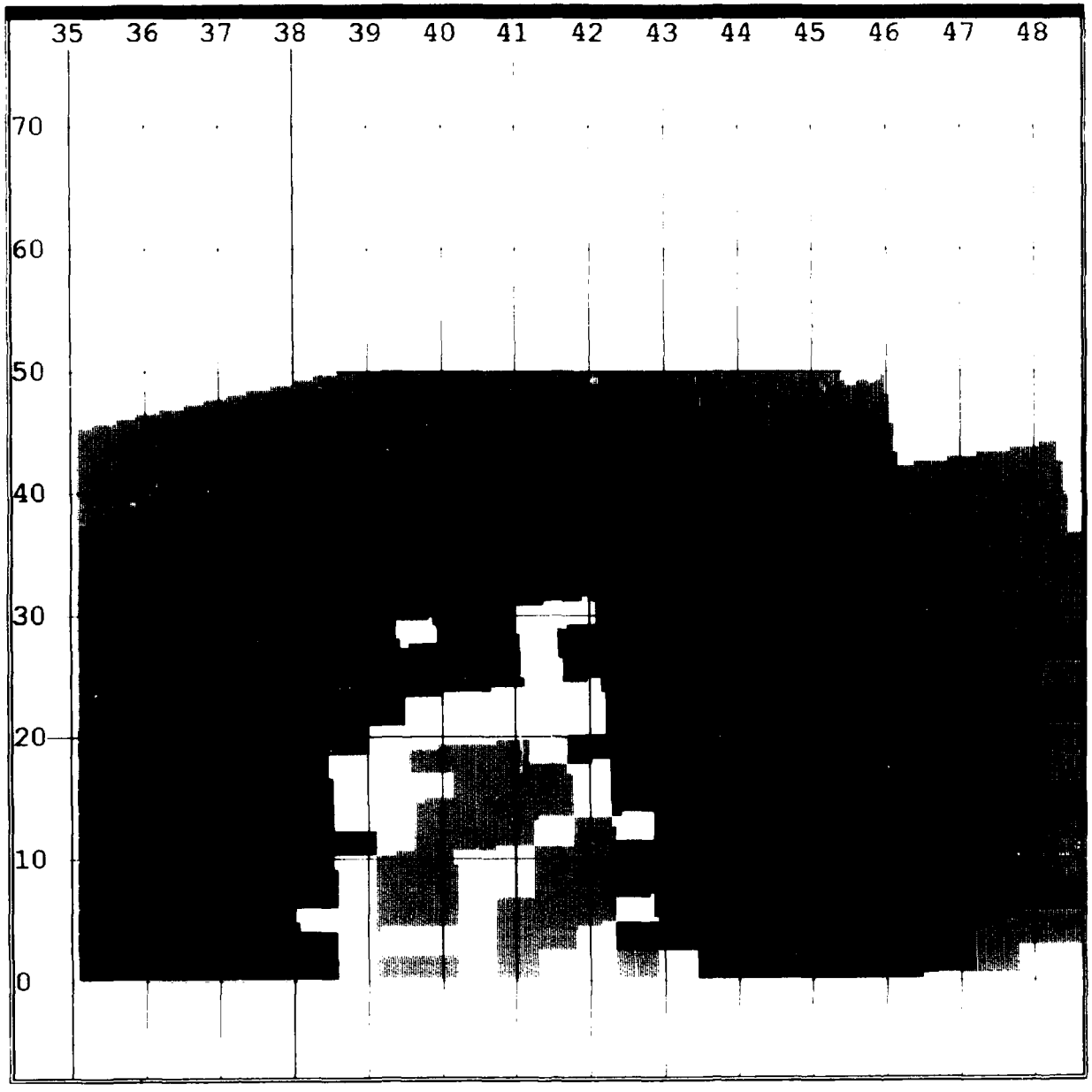

Figure 3-21. RHI at 10 degrees azimuth generated from MIT volume scan data for event shown in Figure 3-19. Range is in nautical miles; altitude is in thousands of feet. This figure shows the vertical reflectivity profile of the storm with its core extending from the ground up to about 3.5 km (11,480 ft.).

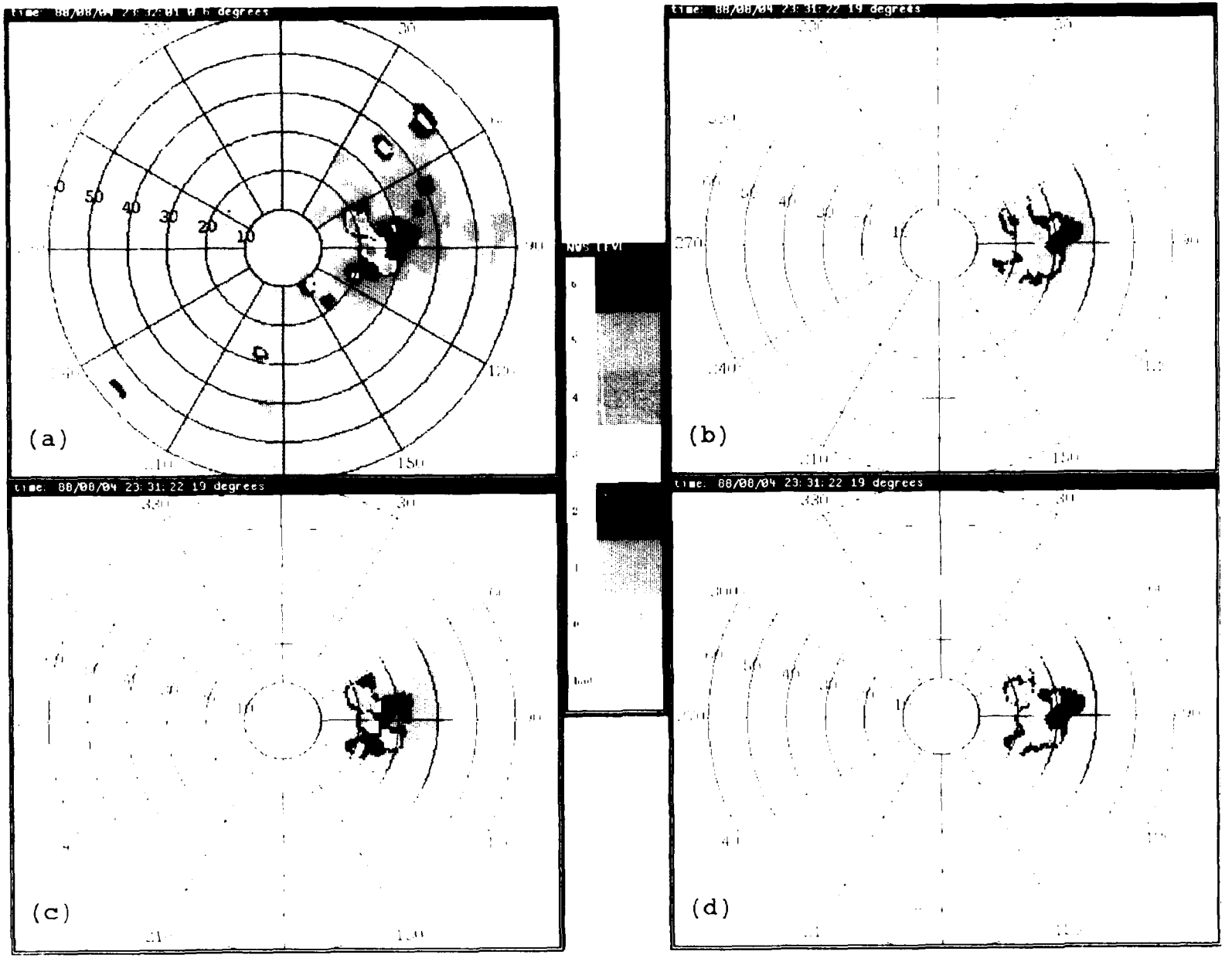

Figure 3-22. Comparison between (a) ASR-9 six-level and (b) MIT based maximum, (c) average, and (d) horizon-scan data, convective storm, 4 August 1988. Inspection indicates that the ASR-9 data agree best with the average and horizon-scan reflectivity data, suggesting that the ASR-9 beamfill correction storm model is not appropriate for this storm event.

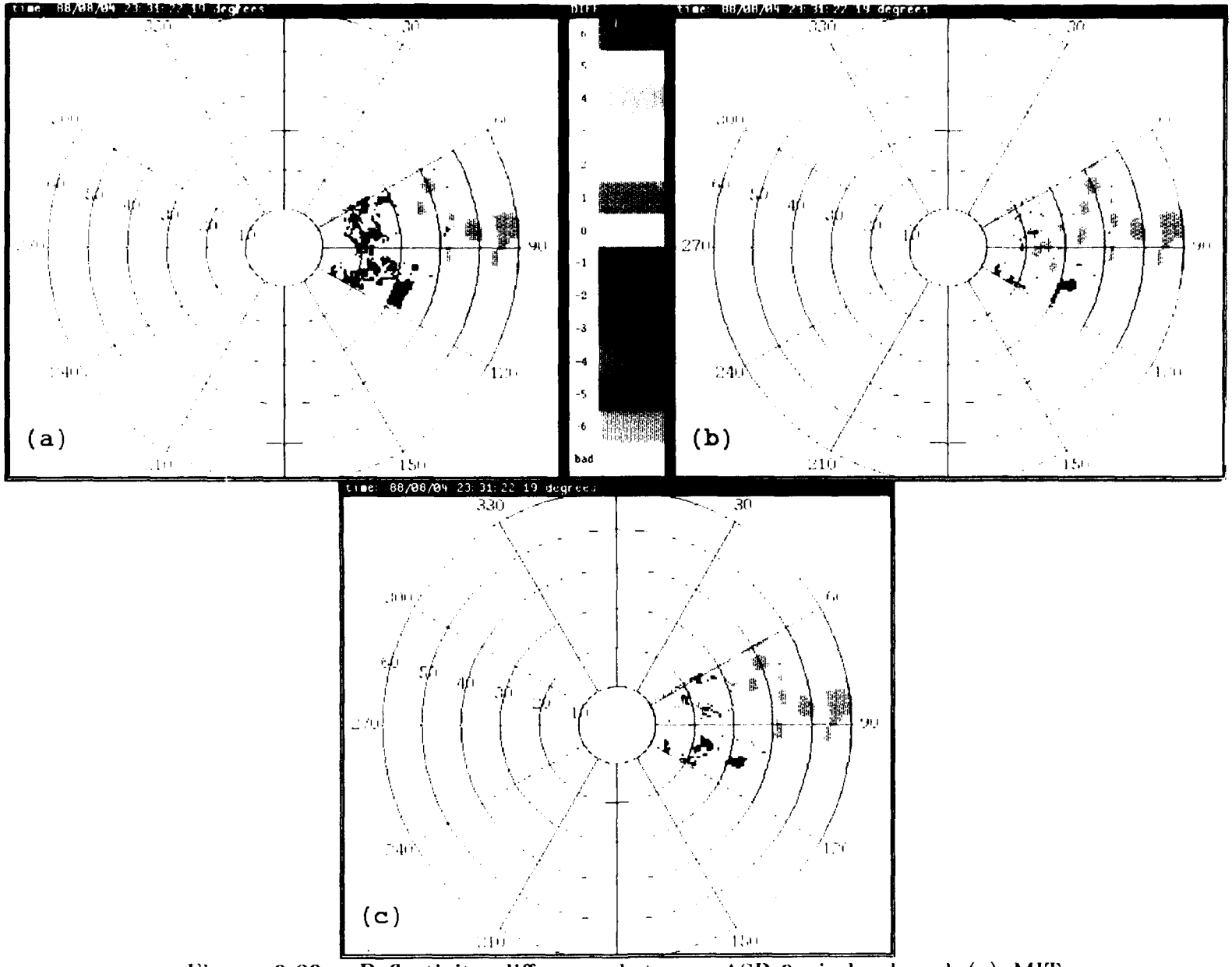

Figure 3-23. Reflectivity difference between ASR-9 six-level and (a) MIT based maximum, (b) average, and (c) horizon-scan data, convective storm, 4 August 1988. Statistics show that the ASR-9 data agree best with the average and horizon-scan reflectivity data, while the maximum data is sometimes two levels higher than the ASR-9 data.

TABLE 3-5

Probabilities Of Differences Between ASR-9 Six-Level And MIT Based Maximum, Average, And Horizon-Scan Data, Convective Storm, 4 August 1988

REFERENCE CAR INPUT FILE
Name: asrsix080488233201.rsm
Note: ASR-9
Tilt #: 1
Product #: 1
Date: 8/ 4/88
Time: 23:32: 1

COMPARISON CAR INPUT FILE
Name: mittru080488233122_smooth.r
Note: MIT max projection
Tilt #: 1
Product #: 4
Date: 8/ 4/88
Time: 23:31:22

DIFFERENCE CAR OUTPUT FILE: asrmax080488233201.rsm

Ref Level	X-3	X-2	X-1	X	X+1	X+2	X+3
0 (3958)	0.00	0.00	0.00	0.96	0.04	0.00	0.00
1 (1543)	0.00	0.00	0.23	0.71	0.05	0.01	0.00
2 (596)	0.00	0.00	0.14	0.66	0.18	0.02	0.00
3 (215)	0.00	0.00	0.02	0.60	0.30	0.07	0.00
4 (98)	0.00	0.00	0.00	0.52	0.47	0.01	0.00
5 (20)	0.00	0.00	0.00	0.85	0.15	0.00	0.00
6 (0)	0.00	0.00	0.00	0.00	0.00	0.00	0.00

REFERENCE CAR INPUT FILE
Name: asrsix080488233201.rsm
Note: ASR-9
Tilt #: 1
Product #: 1
Date: 8/ 4/88
Time: 23:32: 1

COMPARISON CAR INPUT FILE
Name: mittru080488233122_smooth.r
Note: MIT avg projection
Tilt #: 1
Product #: 3
Date: 8/ 4/88
Time: 23:31:22

DIFFERENCE CAR OUTPUT FILE: asravg080488233201.rsm

Ref Level	X-3	X-2	X-1	X	X+1	X+2	X+3
0 (3958)	0.00	0.00	0.00	0.98	0.02	0.00	0.00
1 (1543)	0.00	0.00	0.26	0.72	0.02	0.00	0.00
2 (596)	0.00	0.00	0.21	0.78	0.01	0.00	0.00
3 (215)	0.00	0.00	0.22	0.72	0.06	0.00	0.00
4 (98)	0.00	0.00	0.45	0.53	0.02	0.00	0.00
5 (20)	0.00	0.00	0.35	0.65	0.00	0.00	0.00
6 (0)	0.00	0.00	0.00	0.00	0.00	0.00	0.00

REFERENCE CAR INPUT FILE
Name: asrsix080488233201.rsm
Note: ASR-9
Tilt #: 1
Product #: 1
Date: 8/ 4/88
Time: 23:32: 1

COMPARISON CAR INPUT FILE
Name: mittru080488233122_smooth.r
Note: MIT-based horizon scan
Tilt #: 1
Product #: 5
Date: 8/ 4/88
Time: 23:31:22

DIFFERENCE CAR OUTPUT FILE: asrlow080488233201.rsm

Ref Level	X-3	X-2	X-1	X	X+1	X+2	X+3
0 (3958)	0.00	0.00	0.00	0.99	0.01	0.00	0.00
1 (1543)	0.00	0.00	0.29	0.69	0.02	0.00	0.00
2 (596)	0.00	0.00	0.14	0.74	0.11	0.00	0.00
3 (215)	0.00	0.00	0.03	0.91	0.07	0.00	0.00
4 (98)	0.00	0.00	0.02	0.88	0.10	0.00	0.00
5 (20)	0.00	0.00	0.45	0.55	0.00	0.00	0.00
6 (0)	0.00	0.00	0.00	0.00	0.00	0.00	0.00

horizon scan data, both of which are always within one NWS level of the ASR-9 data. The ASR-9 weather products are generally within one NWS level of the maximum reflectivity data.

Figure 3-24 shows an RHI generated from MIT PPI data at several elevations at 75 degrees in azimuth. This figure shows the vertical reflectivity profile of the storm with its core extending from the ground up to about 5 km (16,400 ft). Note the small area of high intensity weather at about 5 km, which may explain the maximum reflectivity data reporting one level higher than the ASR-9, average, and horizon-scan data at the core of the storm.

Case 3 8 August 1988 Six-Level Processor; Convective Storm

Figure 3-25 shows the output of the ASR-9 six-level weather channel and the maximum, average, and horizon-scan reflectivity data recorded during the convective storm on 8 August 1988 (same weather event as in Figure 3-6). The highest NWS level reported by the ASR-9 was Level 4. Based on visual comparisons, as in case 2 above, pencil-beam data processed to reflect the horizon scan reflectivity agrees best with ASR-9 data, followed by the layer average data, then the maximum reflectivity data. Figure 3-26 shows the plots of difference reflectivity between the ASR-9 and maximum, average, and horizon scan data, while Table 3-6 shows the associated probabilities of the same. Areas of white shown in the difference reflectivity plot indicate areas where the two particular data sets agree. Both the difference plot and statistics indicate that the ASR-9 agrees best with both horizon scan and layer average data, both of which are always within one NWS level of the ASR-9 data. The ASR-9 weather products are generally within one NWS level of the maximum reflectivity data.

Figure 3-27 shows an RHI generated from MIT PPI data at several elevations at 97 degrees in azimuth. This figure shows the vertical reflectivity profile of the storm with its core extending from the ground up to about 5 km (16,400 ft). Note the small areas of high intensity weather at several elevations, which may explain the maximum reflectivity data reporting one level higher than the ASR-9, average, and horizon-scan data at the core of the storm.

3.2.2 INTERPRETATION OF COMPARISONS

It is clear from the above comparisons that the ASR-9 weather data does not agree with any one representation of pencil beam volume data all the time. Recall from Section 1.2 that the ASR-9 beamfill correction storm model assumes a storm of constant reflectivity from the ground up to 4 km, with reflectivity decreasing at a rate of 3 dB per km, above 4 km. Therefore, the ASR-9 should provide the maximum reflectivity when the storm is characterized by the above model. However, as was shown in Figure 1-3 of Section 1.3, a static storm model will not accurately represent a storm's vertical reflectivity profile throughout its life-cycle. The best that can be achieved with a static storm model is to choose a model that characterizes the average vertical reflectivity profile of storms expected in the geographical area in which the ASR-9 will be operating.

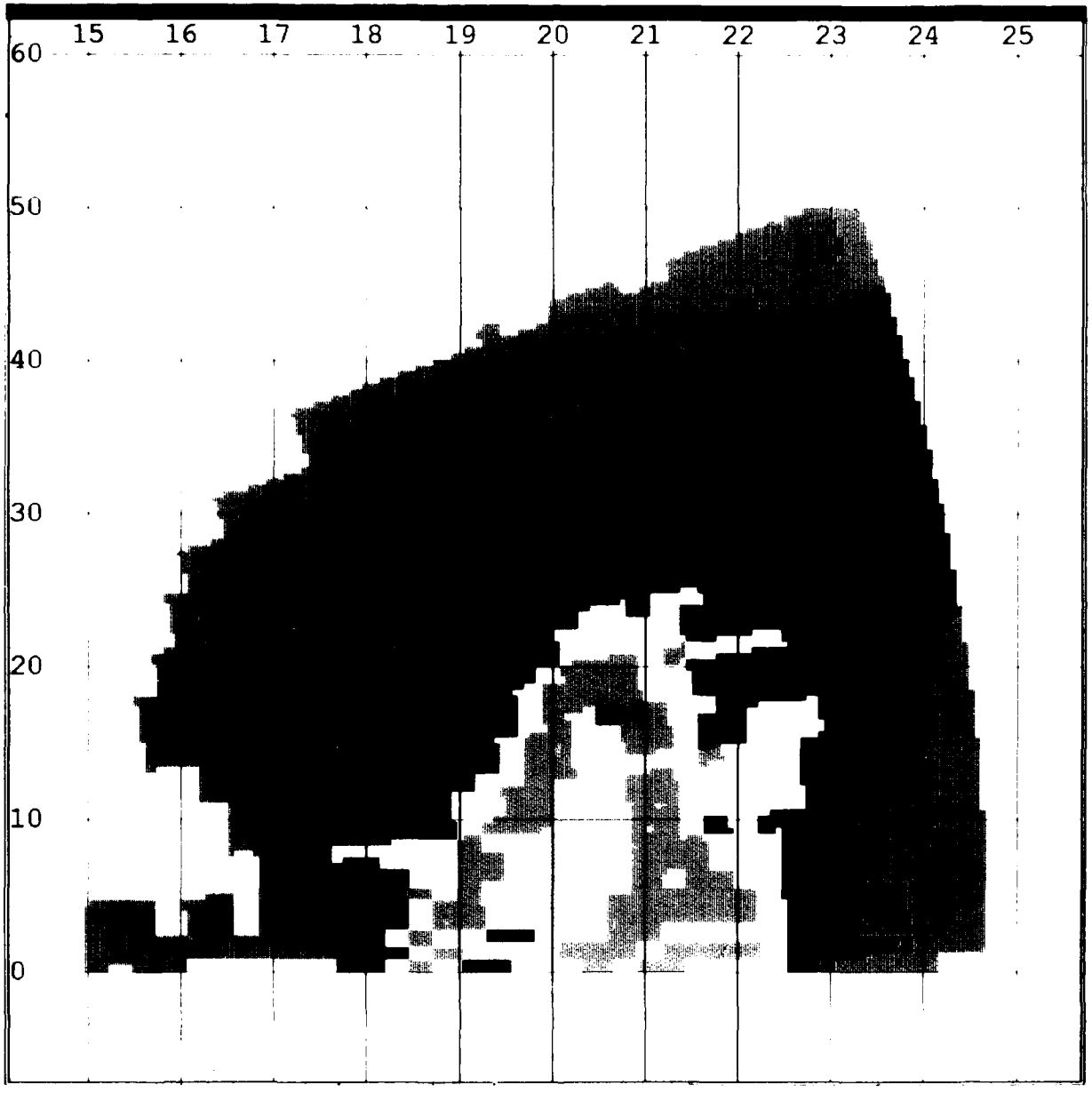

Figure 3-24. RHI at 75 degrees azimuth generated from MIT volume scan data for event shown in Figure 3-22. Range is in nautical miles; altitude is in thousands of feet. This figure shows the vertical reflectivity profile of the storm with its core extending from the ground up to about 5 km (16,400 ft.).

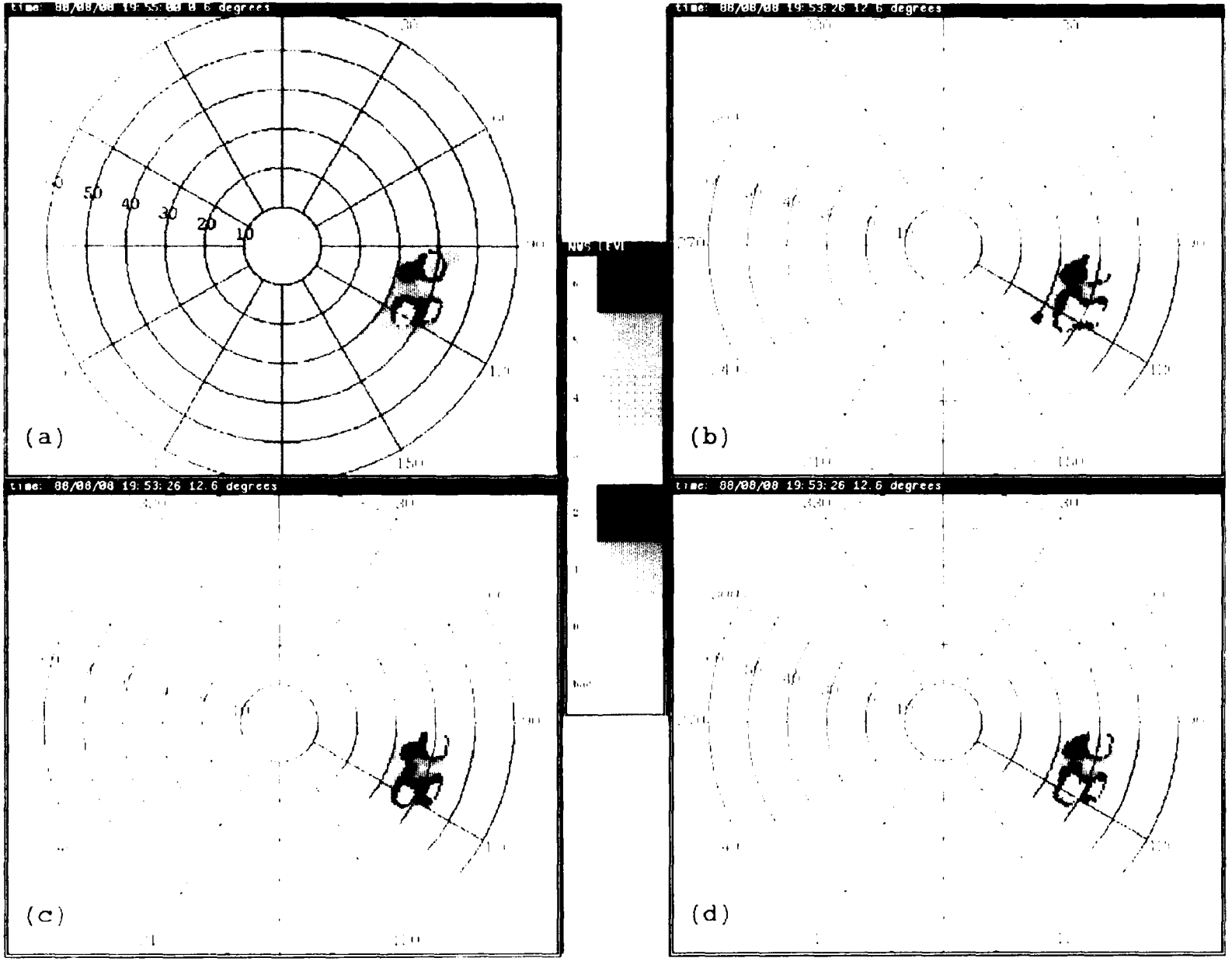

Figure 3-25. Comparison between (a) ASR-9 six-level and (b) MIT based maximum, (c) average, and (d) horizon-scan data, convective storm, 8 August 1988. Inspection indicates that the ASR-9 data agree best with the average and horizon-scan reflectivity data, suggesting that the ASR-9 beam fill correction storm model is not appropriate for this storm event.

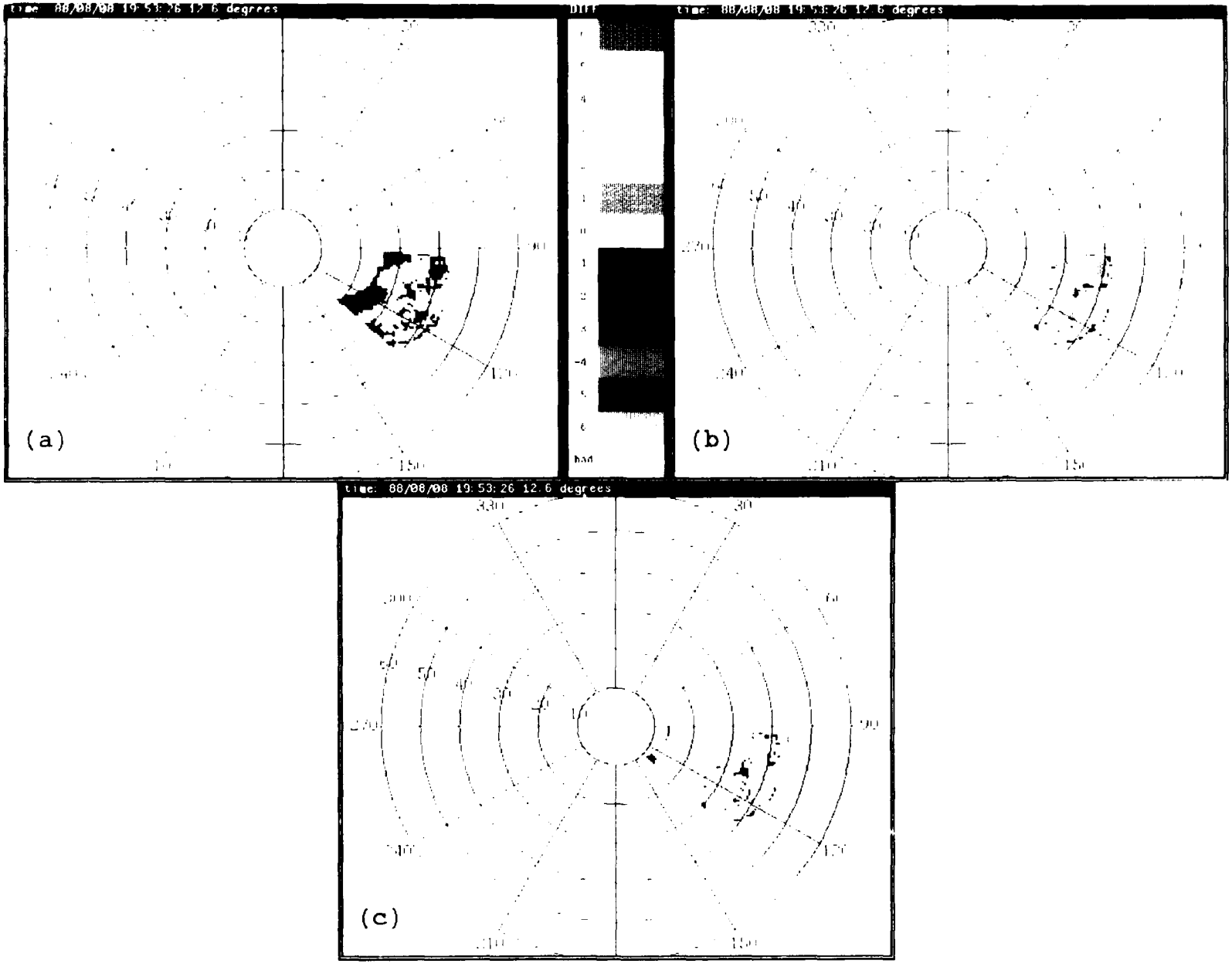

Figure 3-26. Reflectivity difference between ASR-9 six-level and (a) MIT based maximum, (b) average, and (c) horizon-scan data, convective storm, 8 August 1988. Statistics show that the ASR-9 data agree best with the average and horizon-scan reflectivity data, while the maximum data is sometimes two levels higher than the ASR-9 data.

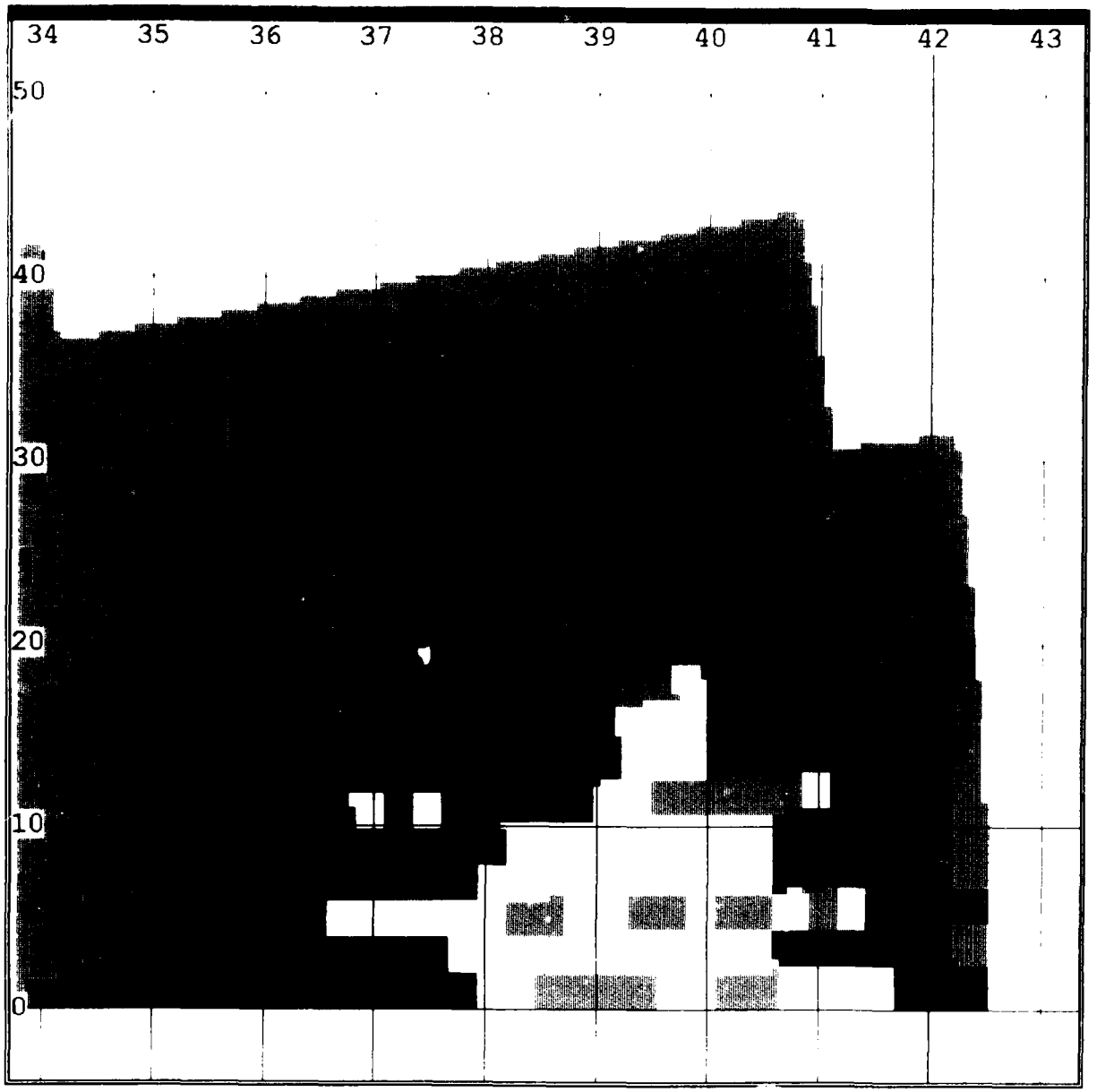

Figure 3-27. RHI at 97 degrees azimuth generated from MIT volume scan data for event shown in Figure 3-25. Range is in nautical miles; altitude is in thousands of feet. This figure shows the vertical reflectivity profile of the storm with its core extending from the ground up to about 5 km (16,400 ft.).

TABLE 3-6

Probabilities Of Differences Between ASR-9 Six-Level And MIT Based Maximum, Average, And Horizon-Scan Data, Convective Storm, 8 August 1988

REFERENCE CAR INPUT FILE
Name: asrsix080888195500.rsm
Note: ASR-9
Tilt #: 1
Product #: 1
Date: 8/ 8/88
Time: 19:55: 0

COMPARISON CAR INPUT FILE
Name: mittru080888195326_smooth.r
Note: MIT max projection
Tilt #: 1
Product #: 4
Date: 8/ 8/88
Time: 19:53:26

DIFFERENCE CAR OUTPUT FILE: asrmax080888195500.rsm

Ref Level	X-3	X-2	X-1	X	X+1	X+2	X+3
0 (3310)	0.00	0.00	0.00	0.89	0.11	0.00	0.00
1 (593)	0.00	0.00	0.03	0.84	0.13	0.01	0.00
2 (291)	0.00	0.00	0.00	0.80	0.18	0.03	0.00
3 (147)	0.00	0.00	0.03	0.63	0.29	0.05	0.00
4 (49)	0.00	0.00	0.00	0.47	0.53	0.00	0.00
5 (0)	0.00	0.00	0.00	0.00	0.00	0.00	0.00
6 (0)	0.00	0.00	0.00	0.00	0.00	0.00	0.00

REFERENCE CAR INPUT FILE
Name: asrsix080888195500.rsm
Note: ASR-9
Tilt #: 1
Product #: 1
Date: 8/ 8/88
Time: 19:55: 0

COMPARISON CAR INPUT FILE
Name: mittru080888195326_smooth.r
Note: MIT avg projection
Tilt #: 1
Product #: 3
Date: 8/ 8/88
Time: 19:53:26

DIFFERENCE CAR OUTPUT FILE: asravg080888195500.rsm

Ref Level	X-3	X-2	X-1	X	X+1	X+2	X+3
0 (3310)	0.00	0.00	0.00	0.99	0.01	0.00	0.00
1 (593)	0.00	0.00	0.03	0.92	0.05	0.00	0.00
2 (291)	0.00	0.00	0.01	0.96	0.03	0.00	0.00
3 (147)	0.00	0.00	0.08	0.91	0.01	0.00	0.00
4 (49)	0.00	0.00	1.00	0.00	0.00	0.00	0.00
5 (0)	0.00	0.00	0.00	0.00	0.00	0.00	0.00
6 (0)	0.00	0.00	0.00	0.00	0.00	0.00	0.00

REFERENCE CAR INPUT FILE
Name: asrsix080888195500.rsm
Note: ASR-9
Tilt #: 1
Product #: 1
Date: 8/ 8/88
Time: 19:55: 0

COMPARISON CAR INPUT FILE
Name: mittru080888195326_smooth.r
Note: MIT-based horizon scan
Tilt #: 1
Product #: 5
Date: 8/ 8/88
Time: 19:53:26

DIFFERENCE CAR OUTPUT FILE: asrlow080888195500.rsm

Ref Level	X-3	X-2	X-1	X	X+1	X+2	X+3
0 (3310)	0.00	0.00	0.00	0.99	0.01	0.00	0.00
1 (593)	0.00	0.00	0.05	0.89	0.07	0.00	0.00
2 (291)	0.00	0.00	0.01	0.93	0.06	0.00	0.00
3 (147)	0.00	0.00	0.03	0.90	0.08	0.00	0.00
4 (49)	0.00	0.00	0.00	1.00	0.00	0.00	0.00
5 (0)	0.00	0.00	0.00	0.00	0.00	0.00	0.00
6 (0)	0.00	0.00	0.00	0.00	0.00	0.00	0.00

SECTION 4

SUMMARY

ASR-9 weather channel data were recorded simultaneously with pencil-beam weather radar and ASR-8 (ASR-9 emulation radar) data in Huntsville, Alabama. During this time, the ASR-9 Field Test and Evaluation was underway, so the ASR-9 was not certified. A severe drought occurred in the Huntsville area during 1988, resulting in only nineteen weather events being recorded, processed, and analyzed for inclusion in this assessment (see Table 2-2). However, these data allowed for analysis of four basic types of weather: stratiform rain, air mass storms, squall lines, and cold fronts.

Separate cases for the two- and six-level processor were required because the processors are independent subsystems, and do not provide weather data simultaneously to a remote site. Operationally, the six-level weather processor is the primary source of weather while the two-level weather processor is the back-up source. This is reflected in the greater amount of six-level weather data available for assessment.

Separate cases for the ASR-9 operating with circular polarization and linear polarization were required for two reasons. First, the front-end path losses and STC functions differ depending on the polarization and processor chosen. Accordingly, the two- and six-level processors compensate for RF path losses and STC functions. Second, as discussed in the introduction and Appendix H, there may be polarization loss dependent on the sense of polarization (orthogonal or same sense) of the receiver and the ellipticity of the rain drops. Perfectly spherical raindrops propagate opposite sense polarized signals back to the radar.

The nineteen weather data sets (see Table 2-2) were used to address two primary issues:

(1) Does the ASR-9 weather channel, as implemented, perform according to FAA specification?

(2) Does the ASR-9 weather channel adequately represent weather reflectivity pertinent to ATC?

To determine whether or not the ASR-9 weather channel performs according to specification, ASR-9 weather channel data were compared both subjectively and quantitatively with:

(a) Simulated ASR-9 weather data using pencil-beam (MIT) radar data.

(b) Emulated ASR-9 weather data using fan-beam (FL-3) radar data.

The first three cases (see Table 2-2) included both simulation and emulation data. Subsequent cases included only FL-3 based emulation data for comparison to ASR-9 weather products. Analysis of the first three cases shows good agreement between ASR-9, C-band based simulation data, and FL-3 based emulation data. Analysis of all subsequent cases indicates about a 3 dB difference between ASR-9 and FL-3 based emulation data. This bias seems to be independent of range and reflectivity level, suggesting a simple

calibration difference between the two radars. When the FL-3 based emulation was adjusted to compensate for the 3 dB difference, results showed good agreement between ASR-9 and FL-3 based emulation data. An ensemble of statistics generated based on all the data (see Table 3-3), indicates reflectivity levels reported by the ASR-9 were within plus-or-minus one level of the emulation data at least 78.2 % of the time for unadjusted emulation products and at least 95.6 % of the time for adjusted emulation products. With the exception of the apparent 3 dB offset needed in thresholding the emulation data, ASR-9 weather channel performance is consistent with both expected and emulated performance, indicating that the ASR-9 weather channel was implemented according to FAA specification.

To determine whether or not the ASR-9 weather channel adequately represents weather reflectivity, ASR-9 weather channel data were compared both subjectively and quantitatively with three representations of data obtained from the MIT pencil-beam weather radar based on:

(1) The maximum reflectivity observed over the vertical extent of the storm.

(2) The average reflectivity observed over the the vertical extent of the storm.

(3) The reflectivity observed at the horizon (NWS equivalent).

These specific measurement criteria were chosen because they may all be relevant from ATC viewpoint (see Section 2.1). Comparisons show that the ASR-9 weather channel data agrees generally within one level of the maximum, average, and horizon scan (NWS equivalent) reflectivity data. Strong agreement was found between ASR-9 data and maximum and horizon-scan reflectivity data when the storm core was close to the ground. This was expected because the beamfill correction is based on the contractor's storm model which assumes the maximum reflectivity of the storm is between the ground and 4 km. Strong agreement was found between ASR-9 data and average reflectivity data when the storm core was aloft. Clearly, because the ASR-9 beamfill correction uses a static storm model, and storms in any given geographical region vary in vertical reflectivity profile, the ASR-9 weather products cannot be expected to correlate with any one storm model for all weather observed.

The ASR-9 weather channel gives controllers access to weather reflectivity information, quantized in six NWS levels and updated every 30 seconds. The novel processing features incorporated in the weather channel include spatial and temporal smoothing and elimination of second-trip weather echoes and ground clutter. The ASR-9 weather products are based on observations from the entire volume scanned by its antenna, thus, the controller will have timely weather information from storms developing aloft. Overall, the ASR-9 should represent a significant improvement over its predecessors in providing air traffic controllers with useful weather data.

SECTION 5

ADDITIONAL RESEARCH

As stated in the conclusion section, the ASR-9 weather channel operating in Huntsville appears to give a useful representation of weather reflectivity within its 60 nmi operational range. The apparent 3 dB discrepancy is most likely caused by a difference in calibration between the ASR-9 and FL-3 emulation radar. Without a simultaneous calibration of these two radars using common calibration equipment and a common calibration target (e.g. sphere, corner-reflector), it may not be possible to reconcile this difference. For example, just a 0.5 dB error in the antenna gain measurement for each radar could result in as much as a 2 dB difference in the reflectivity measured by each.

There are two issues relating to the ASR-9 weather channel in general, that have been discussed in this report because of their possible impact on weather channel performance, but have not been analyzed in detail. These are the optimization of the beamfill correction implemented by the weather processor and the polarization losses due to both elliptical and opposite sense polarization (see Section 1.3).

5.1 OPTIMIZATION OF BEAMFILL CORRECTION

The Huntsville climate represents only one of the climatic regions that will be encountered by ASR-9 systems. Although the results herein found that ASR-9 products agreed to within one NWS level of profile maximum, provile average, and horizon-scan reflectivity data, it is clear that the amount of agreement is dependent on the storm characteristics and the appropriateness of the static storm model used to determine the range-dependent beamfill correction. Optimal performance from the beamfill correction can only be obtained if the static storm model accurately characterizes the ensemble of storms that the ASR-9 is likely to encounter in its region. The following steps for developing region-specific storm models have been proposed and are currently being researched by Lincoln Laboratory:

(1) Determine the desired weather reflectivity product.

The most conservative approach would be to always report the maximum reflectivity at any altitude. However, the maximum reflectivity product is insensitive to the vertical extent of the maximum reflectivity region, and hence gives no indication of the percentage of the profile over which the most hazardous conditions will prevail. Since this may not always be representative of conditions encountered by a plane along its glide slope, such a product could over-warn, but at the same time might provide a desirable margin of safety. Different reflectivity parameterizations should be examined to determine the weather product which will be most useful to ATC

(2) Determine the magnitude of error which may result from an invalid storm model.

This represents a preliminary research step needed to ascertain the degree of accuracy needed in developing and selecting storm models as well as the impact of using an invalid storm model in producing the desired weather

reflectivity reports. The coarse quantization of the NWS levels would certainly reduce the impact of an invalid model.

(3) Identify geographical regions which could be represented by a single storm model.

The conterminous United States should be divided into regions where similar atmospheric conditions governing the height and structure of storms prevail. Somewhere on the order of five regions will probably suffice given the crudeness of the beamfilling correction.

(4) Develop a model for each region based on climate.

The contractor's present model may be appropriate for some regions, and could be adapted for those regions where it is inappropriate. These modifications would incorporate meteorological characteristics of the region such as vertical moisture distribution, cloud base and extent, freezing level, and temperature distribution. If meteorological characteristics of a particular region exhibit large seasonal variation, it may be necessary to develop seasonal models for that region.

(5) Where possible, verify the models by comparison with weather radar data data from selected representative sites.

Regional and seasonal storm models developed from climatology should be verified by comparing these models against site-specific models computed from actual radar data recorded at several locations within each region. For example, data recorded by FL-3 and the FAA Terminal Doppler Weather Radar FL-2 (pencil-beam) at Kansas in 1989 could be used to generate an optimal beam storm model for that site. This data-derived model would then be compared to the regional model which was developed from climatological data characterizing Midwest thunderstorms.

5.2 INVESTIGATION OF POLARIZATION LOSSES

Although the results herein found no obvious signs of ASR-9 weather reflectivity error due to polarization loss, numerous studies have shown this to be a potential problem (see Appendix H). Lincoln Laboratory plans to use the FL-3 radar at the Kansas City field site in 1989 to record simultaneous CP and LP data during significant and spatially extensive high reflectivity precipitation. ASR-9 six-level weather channel emulation software will then be used to determine the effect of depolarization attenuation on ASR-9 reflectivity estimates.

REFERENCES

[1] J. Pell, "The Use of Broad-Beam Radar for Quantitative Analysis of Severe Storms", J. Appl. Meteor. Dec 1971.

[2] E. B. Dobson et al, "Detection of Severe Weather by FAA Radars", Report No. FAA-RD-79-91, Applied Physics Laboratory (September 1979).

[3] K. E. Wilk and J. T. Dooley, "FAA Radars and Their Display of Severe Weather (Thunderstorms)", Report No. FAA-RD-80-65, National Severe Storms Laboratory (July 1980).

[4] D. L. Hopson and K. E. Coonley, "Use Of Air Traffic Control Radars For Hazardous Weather Data", FAA, Washington, D.C. (June 1978).

[5] M. E. Weber, "Assessment of ASR-9 Weather Channel Performance: Analysis and Simulation", Report No. ATC-138, MIT Lincoln Laboratory (31 July 1986).

[6] D.S. Zrnic, "Effects of Propagation on the Measurement of the Reflectivity Factor with Circularly Polarized Waves", Memorandum, NSSL, 1988.

[7] FAA's controller handbook, *Air Traffic Control*, (FAA 7110.65D).

[8] M. I. Skolnik, *Introduction to Radar Systems*, McGraw-Hill p 450 (1962).

[9] V.N. Bringi and T.A. Seliga, "Statistical Properties of the Dual-Polarization Differential Reflectivity (Z_{DR}) Radar Signal", IEEE Trans. Geoscience and Remote Sensing, Vol. GE-21, No. 2 (April 1983).

[10] W. Sichak and S.Milazzo, "Antenna for Circular Polarization", Proc. IRE, Vol. 56, pp 997-1002 (August 1948).

[11] V.N. Bringi and T.A. Seliga, "Potential Use of Radar Reflectivity Measurements at Orthogonal Polarizations for Measuring Precipitation", J. Appl. Meteor., Vol 15, (January 1976).

[12] R. J. Doviak and D. S. Zrnic, *Doppler Radar and Weather Observations*, Academic Press, [illegible], pp 212-217 (1984).

[13] D.R. Mann,"TDWR Clutter Residue Map Generation and Usage", Project Report ATC-148, Lincoln Laboratory, MIT, FAA-PM-87-26, 1988.

[14] M.D. Eilts and S.D. Smith,"Doppler Velocity De-aliasing", Informal Documentation (Publication Pending), NOAA Environmental Research Laboratories, National Severe Storms Laboratory, 1988.

APPENDIX A

PROBLEMS WITH EARLIER ASR WEATHER PRODUCTS

The primary responsibility of the ATC system is to maintain separation of aircraft [7]. Therefore, the radars employ techniques to enhance aircraft detection while rejecting all forms of clutter, including rain, to the greatest extent possible. Even so, there are sensor characteristics of the ASRs which, although chosen for optimal target detection, are well suited for weather detection:

- Transmitter Frequency (S-band)
- Transmitter Pulse Duration (1 μs)
- Transmitter Output Power (1 MW)
- Pulse Repetition Frequency (1 kHz)
- Azimuthal Beam Width (1.4 °)

There are several characteristics of earlier ASRs, described below, that are not optimal and, in fact, severely limit the detection of weather.

- **Uncalibrated and non quantized weather reflectivity levels.** The weather echoes seen on the PPI display are generated based on video from either the normal or MTI channel. Figure A-1 shows a PPI display with normal video detected weather. Even though the displayed intensity is dependent on the weather reflectivity, it is also dependent on the sensitivity time control (STC), polarization, velocity (MTI filter response), range, and storm characteristics.

- **Use of circular polarization when severe weather is observed.** Normally, in good weather, ASRs operate in the VP mode. In the presence of significant precipitation, the ASRs fitted with appropriate antennas are typically operated with circular polarization (CP) to improve target detection. CP, while having a small effect on the detection of aircraft, generally reduces the detection of weather on the order of 15 dB in the target channel. Reception of the opposite sense of circular polarization in a separate channel can recover useful weather signals.

- **MTI effects on near stationary weather.** Weather targets are best detected when the normal video (no MTI) is used. However, in the presence of ground clutter, the MTI channel is more effective for target detection. The detection of weather by MTI depends on velocity, i.e., weather targets with velocities near zero will be affected by the MTI rejection, which is chosen based on ground clutter levels. Therefore, weather detection is typically poor in areas of significant ground clutter, typically within 15 nmi from the airport. The area close to the airport is where weather detection is most critical due to the concentration of aircraft in a constricted air space.

- **Broad vertical antenna beam width.** The fan-beam of an ASR encompasses heights from the surface up to 35,000 feet. Storms, in general, will not fill the beam, thus some means for compensating for this partial beam filling situation is needed. Prior to the advent of a digital weather processor, compensation techniques were not feasible.

- **Low time on target/high antenna scan rate.** Due to the fluctuating nature of the weather echo (i.e., an accumulation of independent point scatterers in a particular volume), typical weather radars integrate many return pulses from each spatial sampling cell to lessen the variance on the estimate. For example, the current NWS radar systems integrate either 15 or 31 pulses for each range-azimuth cell. The antenna scan rate of the typical ASR is 12.5 rpm compared to the typical scan rate of a weather radar of 3 rpm. The ASR scan rate and azimuthal antenna beam width limits the number of integrated pulses to each CPI (coherent processing interval). Thus, a large reflectivity estimate variance is inherent in a simple processor.

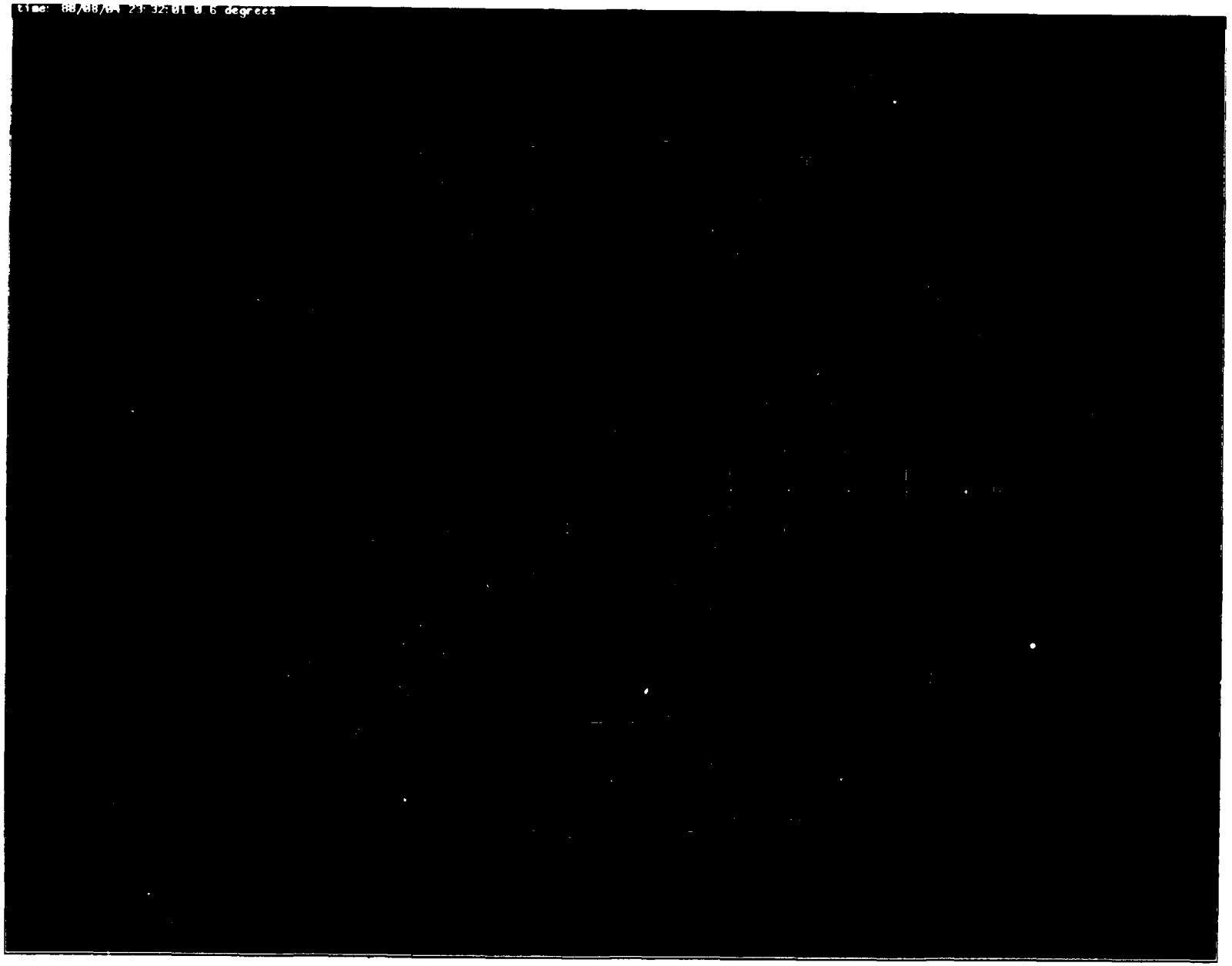

Figure A-1. Typical weather display of current ASR systems. Differences in weather intensity cannot be discerned.

APPENDIX B

ANALYSIS OF ASR-9 WEATHER CHANNEL PERFORMANCE[1]

A computer program that uses pencil beam Doppler weather radar data and ground clutter measurements was developed to simulate the output of an ASR-9 weather channel. The simulation allows for adjustment of weather velocity parameters --mean radial velocity and spectrum width-- as well as radar parameters (e.g., beam switching range, weather thresholds). This facilitates an understanding of the interaction between storm structure, the ground clutter environment and the radar operating configuration.

B.1 SPATIAL AND TEMPORAL SMOOTHING

In Figure B-1, a Monte-Carlo simulation [5] is used to illustrate the statistical spread in reported weather levels at the various stages in the smoothing sequence. The plots show the limits within which 90 percent of reported weather levels would fall as a function of the true weather reflectivity factor. At the output of the final spatial filtering stage, the width of the transition interval between weather levels has been reduced to 1-2 dB. On the controller's display, the statistical displacement of contour boundaries from scan to scan is determined by this transition width and the horizontal gradient of precipitation reflectivity at the boundary. In most cases of operational concern, reflectivity gradients will be 2 dB/km or more, so that contour boundary fluctuations will be smaller than the 0.5 nmi by 1.4 degree resolution cell size of the ASR-9 weather map. Simulations and maps recorded from the ASR-9 in Huntsville, Alabama confirm this conclusion that, after smoothing, statistical fluctuations of the weather reports are not significant.

B.2 CLUTTER FILTERING

The ASR-9 "adaptively" selects the degree of clutter suppression required on a resolution cell-by-cell basis. With this processing scheme, a probabilistic statement of the impact of ground clutter residue and the ground clutter filters on weather reflectivity estimates can be derived from the joint distribution of weather velocity, spectrum width, and ground clutter intensity [5]. Table B-1 lists, as a function of range and weather (Wx) level, the probability for clutter-induced censoring by the clutter filters, using representative environmental measurements. The weather mean velocity and spectrum width distributions used in the calculation were derived from radar volume scans of thunderstorms and stratiform rain in the New England area; the ground clutter intensity distribution (which determines the proportion of resolution cells where clutter filtering must be invoked) was measured at Dallas-Ft. Worth Airport.

[1] * Information contained herein was extracted from an earlier Lincoln Laboratory report assessing ASR-9 weather channel performance [6]

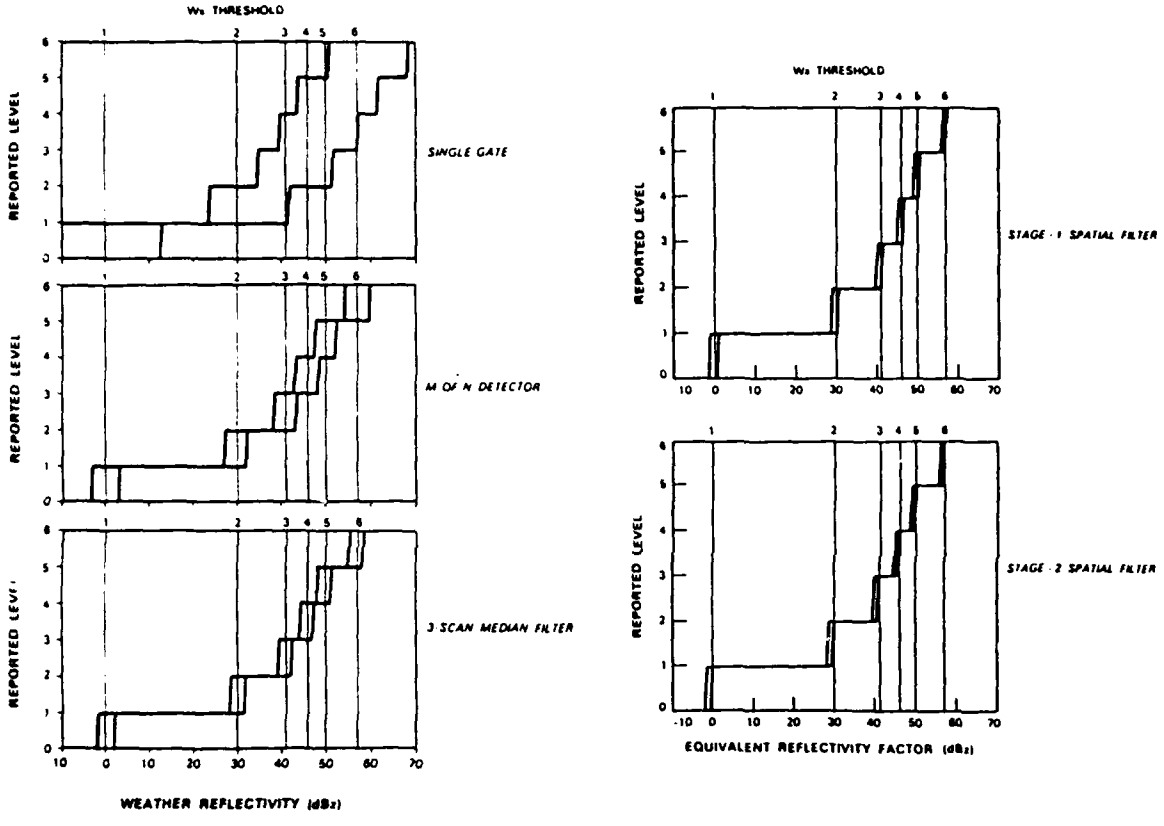

Figure B-1. Statistical spread of ASR-9 weather channel reports. (The two lines are the upper and lower limits within which 90% of the reports fall, plotted as a function of weather reflectivity)

TABLE B-1

PROBABILITY FOR CENSORING OF WEATHER DUE TO GROUND CLUTTER			
	Probability		
Wx Level	0-5 nmi	5-10 nmi	10-15 nmi
1	0.43	0.11	0.09
2	0.06	0.03	0.01
3	0.07	0.02	0.02
4	0.04	0.02	0.01
5	0.01	0.01	0.00
6	0.00	0.00	0.00

The table shows that, with the exception of Level 1 weather within 10 nmi of the radar, 90 % or more of the ASR-9's resolution cells should report the correct weather level in a typical ground clutter environment. The spatial filters in the smoothing and contouring processor will, in general, further reduce the impact of ground clutter on the final weather maps. This robust clutter suppression capability has been confirmed with simulations using ground clutter data observed at operational radar sites and through field measurements with an ASR-8.

B.3 BEAM FILL CORRECTIONS

The ASR-9 features dual cosecant-squared elevation receiving patterns with nominal 3 dB widths of 5 degrees. The "high" beam, employed at short range to reduce ground clutter intensity, has maximum gain about 6.5 degrees above the horizon. Beyond roughly 10 nmi, the receiver is switched to the "low" beam, with peak response at 2 degrees elevation. At long range, the fan beam integrates precipitation echoes over much or all of a storm's depth; if the beam volume is only partially filled with precipitation, the measurement will underestimate even the vertically averaged reflectivity. At short range, the fixed elevation scan results in maximum sensitivity for precipitation in the lower portion of the storm.

The ASR-9 uses programmable, range-dependent weather thresholds that can be set to reduce reflectivity estimate biases caused by the beam pattern. As the processor is currently configured, these thresholds are quasi-static (to be set up, for example, on a site-seasonal dependent basis). Weber [4] examined the performance of this technique by using pencil-beam, Doppler radar volume scans from summertime storms in Eastern Massachusetts. Each volume scan was resampled onto a Cartesian coordinate grid. Fixing the x,y coordinates then defined a profile of precipitation reflectivity versus height. From the resulting ensemble of reflectivity profiles, range-dependent threshold corrections were derived that minimized the least squares difference between the (corrected) ASR-9 reflectivity estimate and a two-dimensional parameterization of the three-dimensional reflectivity field. This section treats one example of such a parameterization, the maximum reflectivity (over elevation angle) for each range-azimuth resolution cell.

Figure B-2 plots an example of the average vertical distribution of reflectivity (relative to the peak) and the corresponding threshold correction; the figure was derived from that subset of the profiles where the maximum reflectivity corresponded to Level 3

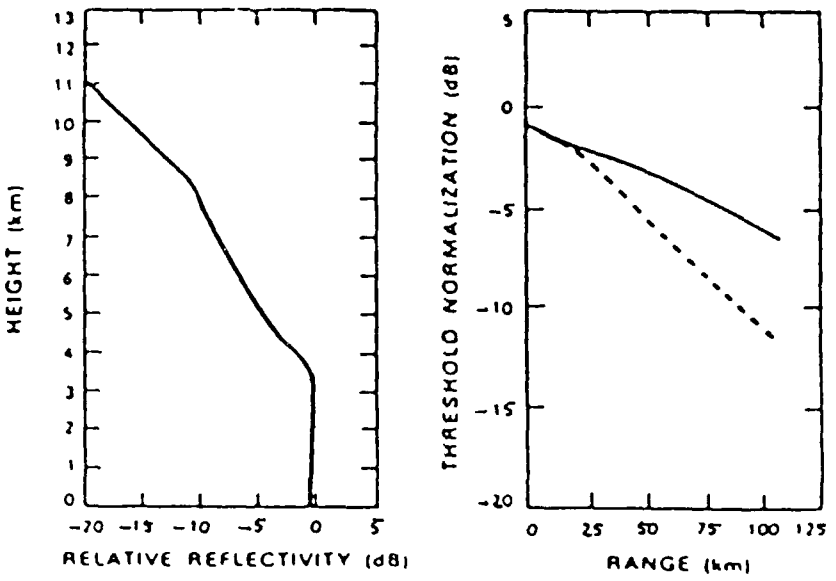

Figure B-2. Mean profile of weather reflectivity versus height, and corresponding weather threshold adjustment (Level 3 weather).

weather (41-46 dBZ). The mean profile is flat up to 4 km above ground level (AGL) and falls off at an average rate of 3 dB/km at greater heights. Associated threshold corrections for the "maximum-in-height" reflectivity field parameterization approach 6 dB in the low beam at 60 nmi range. Results from subsets of the profiles corresponding to other NWS levels are similar, aside from a weak trend towards more rapid fall-off of reflectivity factor with height as the precipitation level increases.

The efficacy of the derived beam-shape corrections was then tested against the individual storm cases by comparing simulated ASR-9 weather maps against "maximum-in-height" truth generated from the same Doppler radar volume scans. The simulation procedure included all important attributes of the ASR antenna pattern and weather processor. Results from a number of such comparisons are shown in Figure B-3 where the average error between simulated ASR reports and truth is plotted as a function of storm centroid range. This accuracy metric was calculated by means of a resolution cell-by-cell comparison and is approximately the fraction of resolution cells where the ASR report and truth differ.

Error probabilities are low, in the range of 0.1 to 0.25. In most cases, the differences correspond to mismatch in size and shape of precipitation contours and not to actual missed detections or false alarms. The trend towards lower average error at long range was shown to indicate that the profile maximum reflectivity factor correlates more strongly with a vertically averaged (i.e., long range) ASR measurement than with its short range measurement of reflectivity in the lower part of the cloud. Additional methods of accuracy assessment were discussed by Weber [5] as was the accuracy of other possible two-dimensional parameterizations of the reflectivity field (e.g., averages over specified altitude intervals). Results were equivalent to those shown in Figure B-3, indicating relative errors between ASR reports and "truth" that were generally no larger than 2 to 3 dB. This corresponds at most to a one level change in the reported NWS level.

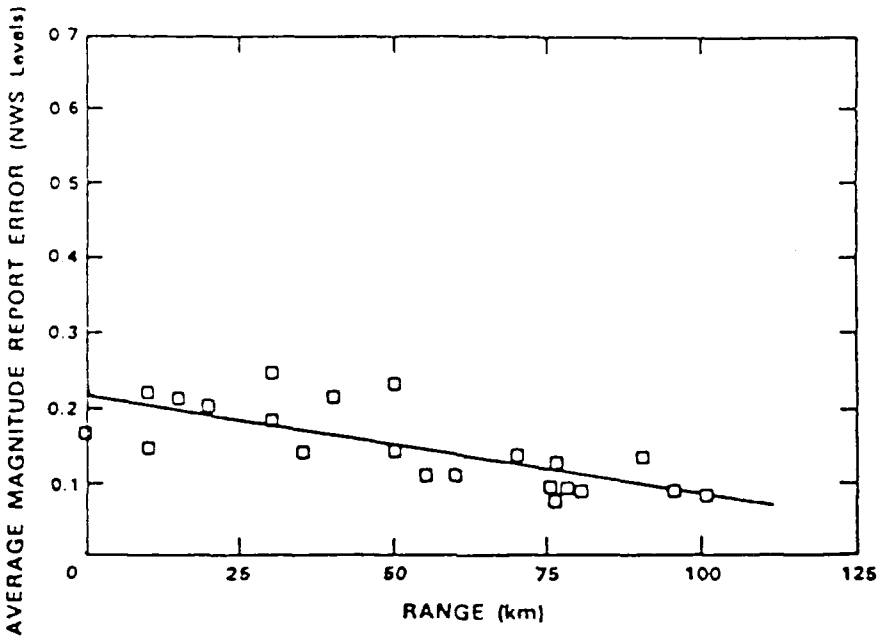

Figure B-3. Average weather report error (NWS levels) versus storm range from radar.

APPENDIX C

SIMULATION OF THE ASR-9 WEATHER CHANNEL USING MIT PENCIL-BEAM WEATHER RADAR DATA

This appendix describes a reflectivity simulation program which converts pencil-beam volume-scan data collected by the MIT weather radar into either six or two-level format described in the ASR-9 specification.

It contributes to the validation of the ASR-9 weather channel in three ways. (1) It enables independent testing of the ASR-9 weather channel processing algorithms. (2) It allows confirmation of observations made by the FL-3 emulation radar. (3) It provides a reference data set for direct comparison with ASR-9 weather products.

C.1 PREPROCESSING OF MIT DATA

Before MIT pencil-beam data is input to the simulation program, the radar data are preprocessed for quality assurance. The preprocessor involves SNR thresholding, residual clutter editing, and radial velocity de-aliasing.

The first phase of the preprocessor, the SNR thresholding, is accomplished by comparing the SNR of each data point against a threshold value, nominally 10 dB. If the SNR is less than or equal to threshold, the corresponding reflectivity, velocity and spectrum width estimates are flagged as invalid.

Residual clutter editing is performed during the second phase of the data preprocessing. This is necessary because the 25 dB clutter rejection capability of the MIT radar system is insufficient to completely suppress all of the local ground clutter. A clear-day map of the residual clutter is generated by the MIT radar for each of the predefined low elevation scans up to and including 4.5 degrees. This clutter residue map is then used to flag those input weather cells whose reflectivity does not exceed a certain threshold above the corresponding clutter map cell value. Flagged values are not included in the subsequent generation of integrated fan beam estimates. Methods for generating and implementing clutter residue maps are discussed in [Mann, 1988][13].

The MIT radar transmitter wavelength of 5.375 cm and PRF of 924 Hz yield a maximum unambiguous Doppler velocity of only 12.4 m/s. This could easily be exceeded, especially in the vicinity of thunderstorm outflows. Since the radial fan beam equivalent velocity is used in simulating the effects of the ASR-9 clutter filter bank, the radial velocity estimates are de-aliased (unfolded) during the final phase of the preprocessor using the Local Environmental Check (LEC) algorithm developed at the National Severe Storms Laboratory in Norman, Oklahoma [Eilts, 1988] [14]. The algorithm uses a combination of single radial continuity along with neighboring radial comparison techniques to edit and unfold Doppler radial velocity data.

C.2 SIMULATION ALGORITHM DESCRIPTION

Figure C-1 is a flow diagram of the MIT-based ASR-9 simulation. The logic flow is very similar to that of the ASR-9 weather channel itself (Figure C-2). PPI radial moments data (Z, V, σ_V) from the MIT pencil-beam radar are used as input to the simulation program. There are six processing steps involved in the simulation program:

- Elevation integration of volume scan data
- Clutter filtering
- Spatial smoothing (in range)
- Beam-fill loss correction
- Conversion to NWS six-level intensity scale
- Spatial smoothing (neighboring cells)

The MIT pencil beam data, consisting of multiple elevation scans, is first integrated in elevation to yield a range-azimuth domain representation of the volume reflectivity weather field as observed by the ASR-9. Based on a clear-air clutter map recorded by FL-3, the clutter filter attenuation is calculated and added to each range-azimuth cell. The data are then spatially smoothed in range and converted to their NWS six-level equivalents. Finally, the data are passed through the 5-of-9 and the highest-of-nine spatial filters to produce the final equivalent ASR-9 six-level weather report. The following sections contain detailed descriptions of these processing steps.

C.2.1 ELEVATION INTEGRATION OF MIT VOLUME SCAN DATA

MIT data consists of a series of azimuthal PPI scans at different elevation angles, covering the same volume seen by an ASR-9. Because the elevation beamwidth of the ASR-9 is 4.8 degrees, compared to the 1.4 degree elevation beamwidth of the MIT radar, MIT moment estimates $[f(r, \theta, \phi)]$ must be integrated in elevation while being weighted by the ASR-9 beam pattern. This results in an ASR fan-beam equivalent reflectivity, velocity, and spectrum width estimates $[f(r, \theta)]$.

Figure C-3 is a plot of the vertical ASR-9 beam patterns. To simulate the effects of the cosecant-squared fan-shaped beam pattern of the ASR-9 antenna, the individual MIT reflectivity, radial velocity, and spectrum width samples are first weighted as a function of elevation angle by the appropriate ASR-9 transmit/receive beam pattern (low or high). Low or high beam pattern weighting will be chosen based on a contractor furnished beam switching map. In lieu of the beam switching map, the simulation program allows for definition of up to eight primary beam selection regions and up to four secondary beam selection regions. The current implementation of this option results in selection of the high receiving beam for ranges less than 24 km and selection of the low beam for ranges greater than 24 km.

The data used to compute the ASR-9 beam patterns were hand digitized from a graph of the ASR-9 elevation beam patterns provided by Westinghouse and encoded into the simulation program in the form of a look-up table which contains values of dB below peak for every degree of elevation over the span of -10 to 40 degrees. The table contains 102 values (51 values each for the two beams) and is reproduced in Table C-1 for reference. Note that the table assumes an ASR-9 antenna tilt of zero degrees, that is, the peak of the elevation beam pattern is at zero degrees with the lower and upper -3 dB

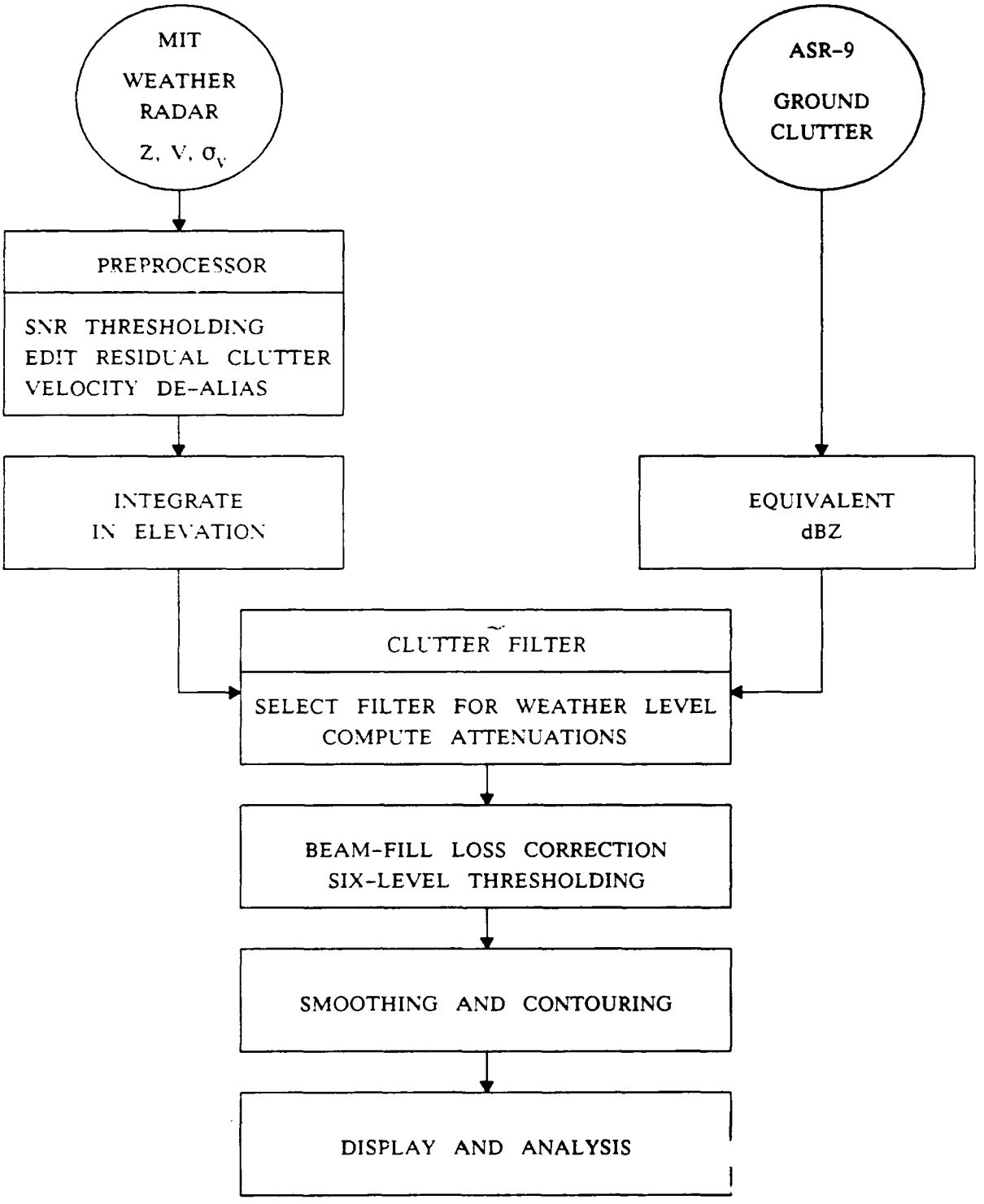

Figure C-1. ASR-9 weather channel simulation block diagram.

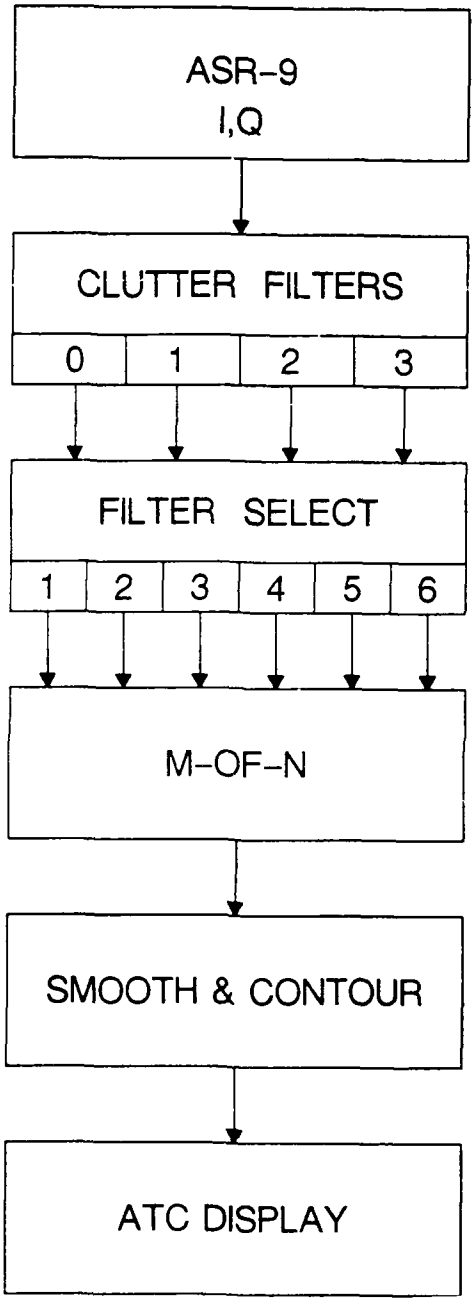

Figure C-2. Simplified ASR-9 six-level weather channel block diagram.

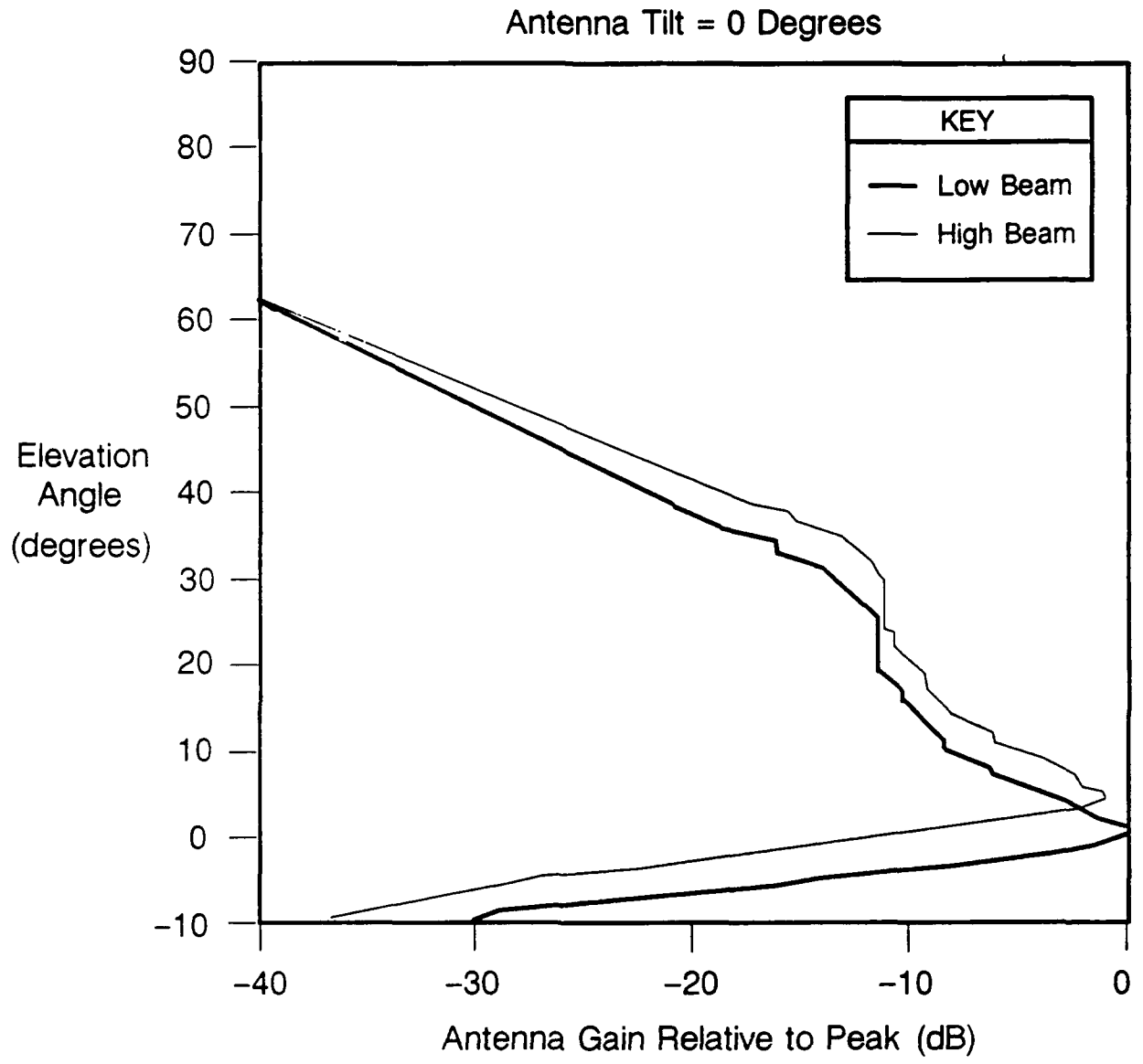

Figure C-3. ASR-9 antenna elevation beam patterns.

points occurring at -2.0 degrees and +4.0 degrees respectively. This conforms to the 4.8 degree minimum -3 dB elevation beamwidth specified by the FAA [DOT-FAA-E-2704A, 1984]. The simulation program includes an antenna tilt offset parameter (typically 2.0 degrees) which is taken into account when accessing the look-up table.

Equations (1) to (3) are used to compute the ASR-9 equivalent reflectivity $\tilde{Z}$, radial velocity $\tilde{V}_R$, and spectrum width $\tilde{\sigma}_v^2$ quantities. (See Weber, 1986 [5])

$$\tilde{Z}(R,\phi) = \frac{\int Z(R,\phi,\theta)\, B_T(\theta)\, B_R(\theta)\, d\theta}{\int B_T(\theta)\, B_R(\theta)\, d\theta} \tag{1}$$

$$\tilde{V}_R(R,\phi) = \frac{\int V_R(R,\phi,\theta)\, Z(R,\phi,\theta)\, B_T(\theta)\, B_R(\theta)\, d\theta}{\int Z(R,\phi,\theta)\, B_T(\theta)\, B_R(\theta)\, d\theta} \tag{2}$$

$$\tilde{\sigma}_v^2(R,\phi) = \frac{\int \sigma_v^2(R,\phi,\theta)\, Z(R,\phi,\theta)\, B_T(\theta)\, B_R(\theta)\, d\theta}{\int Z(R,\phi,\theta)\, B_T(\theta)\, B_R(\theta)\, d\theta} + \sigma_{em}^2$$

$$+ \frac{\int V_R^2(R,\phi,\theta)\, Z(R,\phi,\theta)\, B_T(\theta)\, B_R(\theta)\, d\theta}{\int Z(R,\phi,\theta)\, B_T(\theta)\, B_R(\theta)\, d\theta} - \tilde{V}_R^2(R,\phi) \tag{3}$$

TABLE C-1
ASR-9 Beam Pattern Data Base

Low Beam

Angle (deg)	Relative Gain (dB)									
-10 to -1	-30.0	-28.5	-24.0	-21.0	-16.0	-14.0	- 9.0	- 6.2	- 3.0	- 1.2
0 to 9	0.0	- 0.2	- 1.5	- 2.3	- 3.0	- 4.0	- 5.5	- 6.3	- 6.5	- 7.5
10 to 19	- 8.5	- 8.5	- 9.0	- 9.3	- 9.5	-10.0	-10.5	-10.5	-11.0	-11.5
20 to 29	-11.5	-11.5	-11.5	-11.5	-11.5	-11.5	-12.0	-12.0	-12.5	-13.0
30 to 39	-13.5	-14.0	-15.0	-16.0	-16.0	-18.0	-19.0	-20.0	-20.5	-21.0
40	-22.0									

High Beam

Angle (deg)	Relative Gain (dB)									
-10 to -1	-36.0	-34.8	-36.0	-30.5	-28.0	-26.5	-22.0	-19.2	-17.0	-13.3
0 to 9	- 9.0	- 6.5	- 4.0	- 2.1	- 1.0	- 1.0	- 2.0	- 2.3	- 3.0	- 3.7
10 to 19	- 5.0	- 6.0	- 6.0	- 7.0	- 8.0	- 8.3	- 8.7	- 9.0	- 9.0	- 9.3
20 to 29	-10.0	-10.3	-10.5	-10.5	-11.0	-11.0	-11.0	-11.0	-11.0	-11.0
30 to 39	-11.5	-11.5	-12.0	-12.5	-13.0	-14.0	-15.0	-15.5	-17.0	-17.5
40	-19.0									

$\tilde{Z}$ is computed by first establishing a temporary 2-dimensional polar coordinate grid with origin coincident to the MIT radar and an azimuth resolution of 1.4 degrees. The range resolution of the temporary grid matches that of the input MIT data range resolution (typically 0.5 km or 1.0 km). Then, starting with the first (lowest) input MIT constant elevation scan, the individual reflectivity estimates are first weighted by the ASR-9 antenna pattern and then stored in the appropriate temporary range-azimuth grid cell. If two or more of the MIT data quantities are coincident with respect to a particular temporary grid cell, averaging is performed. If no MIT data values fall within a particular temporary grid cell, the cell is assigned a value of zero. This weighting-resampling-averaging procedure is repeated for each of the input MIT constant elevation scans, producing separate 2-dimensional temporary output arrays containing cell-averaged, beam-weighted reflectivity estimates for each tilt of the MIT radar. The 3-dimensional (r,ϕ,θ) representation is collapsed to the 2-dimensional fan beam realization (r,ϕ) by integration of corresponding 2-dimensional array cells across the MIT constant-elevation scan surfaces. The integrated reflectivities are then normalized by the total integrated antenna pattern (the denominator of Equation (1)) to yield $\tilde{Z}$.

The mechanics of integration are similar for obtaining $\tilde{V}(R,\phi)$ and $\tilde{\sigma}_V^2(R,\phi)$. In addition to the antenna pattern weighting, the individual V_R and σ_V^2 quantities are weighted by their corresponding reflectivities Z. The equation for the computation of $\tilde{\sigma}_V^2$ contains extra terms to account for contributions from the high ASR-9 antenna rotation rate (σ_{sm}^2) and the vertical wind shear. σ_{sm}^2 is a constant equal to 0.75 m/s for the ASR-9. Since the MIT radar produces poor estimates of the velocity spectrum width, the simulation has the option of utilizing a user-specified constant σ_s^2 in place of the measured estimate. A constant velocity spectrum width of 2 m/s will be used in place of the measured estimates.

C.2.2 CLUTTER FILTERING

For each of the ASR-9 range-azimuth cells, and for each of the six weather levels, the least attenuating of the four clutter filters is selected such that the median ground clutter reflectivity corresponding to the ASR-9 cell will be reduced 3 dB or more below the weather level threshold under test.

The filter selections are generated by a separate preprocessor computer program which takes as input a site-specific clear-day map of the ground clutter from the ASR-9 clutter map generator. However, due to the lack of an actual ASR-9 clutter map, the preprocessor program uses a clutter map generated from the FL-3 fan-beam radar. Since the FL-3 clutter data are reported with a granularity of 1.4 degrees in azimuth and 120 meters in range, the preprocessor program computes the median of the clutter reflectivity for each 1.4 degree, 1.0 nmi range cell. This produces a clutter map with similar granularity to the ASR-9 clutter map generator. Then, based on the criteria in the preceding paragraph, six filter selections corresponding to the six weather level thresholds are generated for each ASR-9 equivalent clutter map cell. If none of the filters is sufficient to suppress the ground clutter 3 dB or more below the given weather level threshold, a clutter sensor flag value of -1 is set for that weather level at that range-azimuth cell. The result of the preprocessor program is a disk-file containing a map of filter selections -1 (censored), 0 (all-pass), 1, 2, 3 for each weather level and for each 1.4 degree azimuth by 1.0 nmi range cell. Since the choice of filters for the six weather levels depends only on the site-specific clear-day map, it is not necessary to generate a map of filter selections for every run of the ASR-9 simulation program.

The method currently implemented for simulating the effects of the ASR-9 clutter filter bank assumes a Gaussian velocity distribution within the ASR-9 equivalent sample volume. Using this assumed velocity distribution, a disk-file was generated which contains the weather attenuations for each filter for velocity values ranging from 0 to +30 m/s, and velocity spectrum width values ranging from 0 to 20 m/s. The curves plotted in Figure C-4 were generated using filter attenuation values contained in the disk-file. Based on the elevation-integrated reflectivity, the appropriate filter is selected from the corresponding cell of the filter selection map, and that filter selection is used along with the associated velocity and spectrum width to get a weather attenuation value from the look-up table. The elevation-integrated reflectivity is subsequently reduced by the extracted weather attenuation value.

C.2.3 RANGE SMOOTHING

Simulation of the 0.5 nmi range granularity of the ASR-9 "M-of-N" processor is accomplished by appropriate range smoothing of the elevation-integrated MIT radar data. These data are sampled at azimuth intervals of 1.4 degrees and range intervals of either 0.5 km (0.27 nmi) or 1.0 km (0.54 nmi). For MIT data with range intervals of 0.5 km, every other range-azimuth cell value is replaced by the average of it and its four neighboring range cell values. For MIT data with range gate spacings of 1.0 km, each range-azimuth cell reflectivity estimate is replaced by the average of it and its two nearest neighboring range cells. This procedure is applied to each of the 256 azimuth sectors, resulting in data which are smoothed in range over 1.08 nmi and reported every

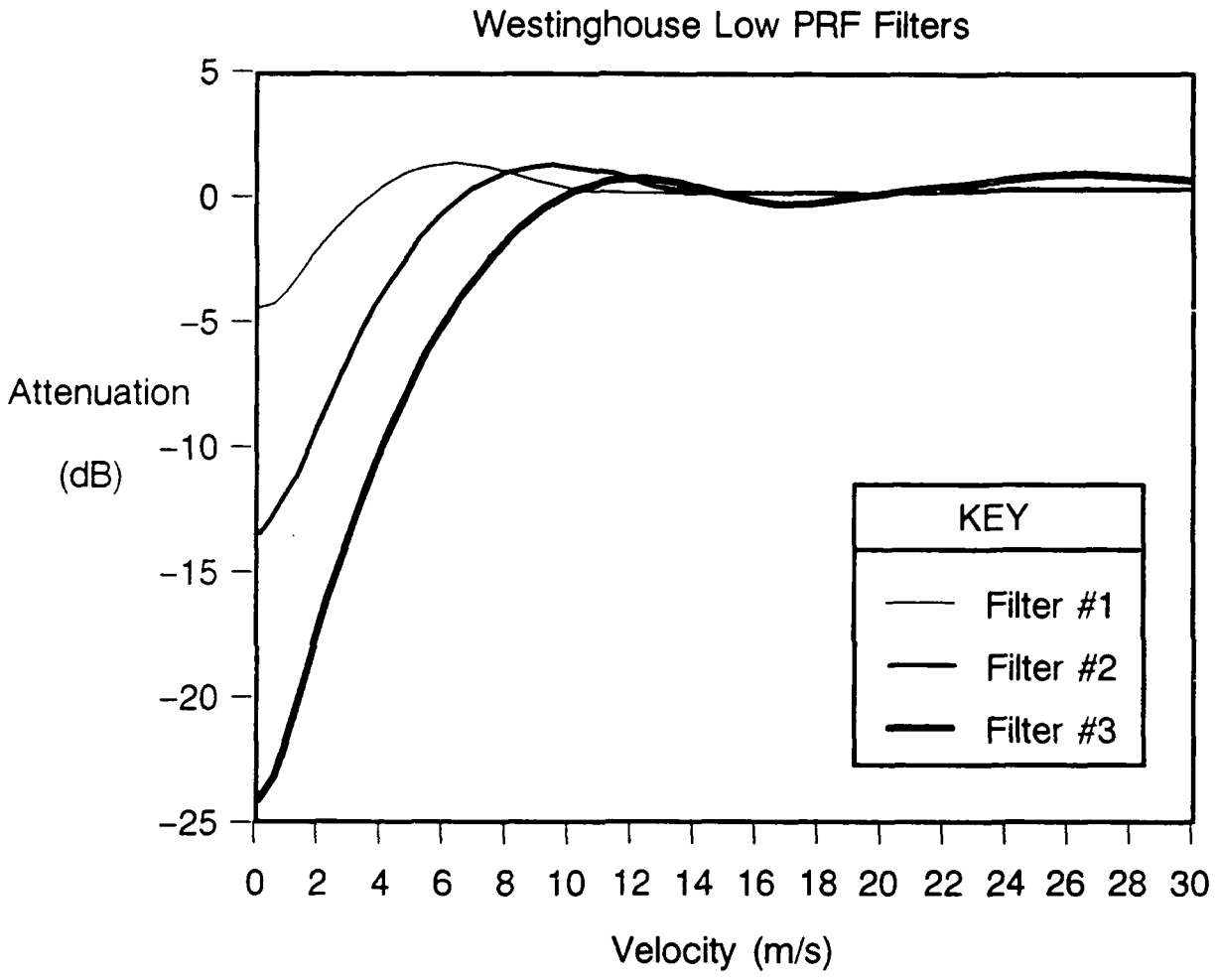

Figure C-1. Attenuation versus velocity for the three attenuating clutter filters.

0.54 nmi.

C.2.4 BEAMFILL LOSS CORRECTION

Because of the large altitude coverage of the broad ASR-9 fan beam, storm cells at far ranges may only partially fill the beam. Since the standard radar reflectivity estimate assumes that precipitation echoes are distributed uniformly throughout the sample volume [12], the ASR-9 will tend to underestimate the true reflectivity at far ranges. To correct for this, the ASR-9 weather processor channel will employ a storm reflectivity structure model to compute and apply a range-dependent beamfill loss correction to the reflectivity estimates.

For the current ASR-9 test configuration, the storm reflectivity model assumes constant reflectivity from the surface to 4 km AGL, and -3 dBZ/km decrease above 4 km. This model may be expressed mathematically by:

$$Z'(R,\theta) = \begin{cases} 1 & H \leq H_t \\ 10^{\frac{-3(H - H_t)}{10}} & H > H_t \end{cases} \qquad (4)$$

where,

$Z'(R,\theta)$ = relative reflectivity
H = height above ground (km)
H_t = height of constant reflectivity layer above ground (km)

H is calculated, accounting for Earth curvature, as follows:

$$H = \sqrt{R_e^2 + R^2 + 2\,R_e\,R\,\sin(\theta)} - R_e \qquad (5)$$

where

R_e = radius of the Earth (6.37×10^3 km)

Figure C-5 is a plot of the dBZ loss as a function of range for each of the two ASR-9 beams. An ASR-9 antenna tilt of 2.0 degrees was assumed and the forementioned reflectivity model was used to calculate the loss. Since the low receiving beam is generally used beyond 30 km, the maximum loss would be about 3.8 dBZ.

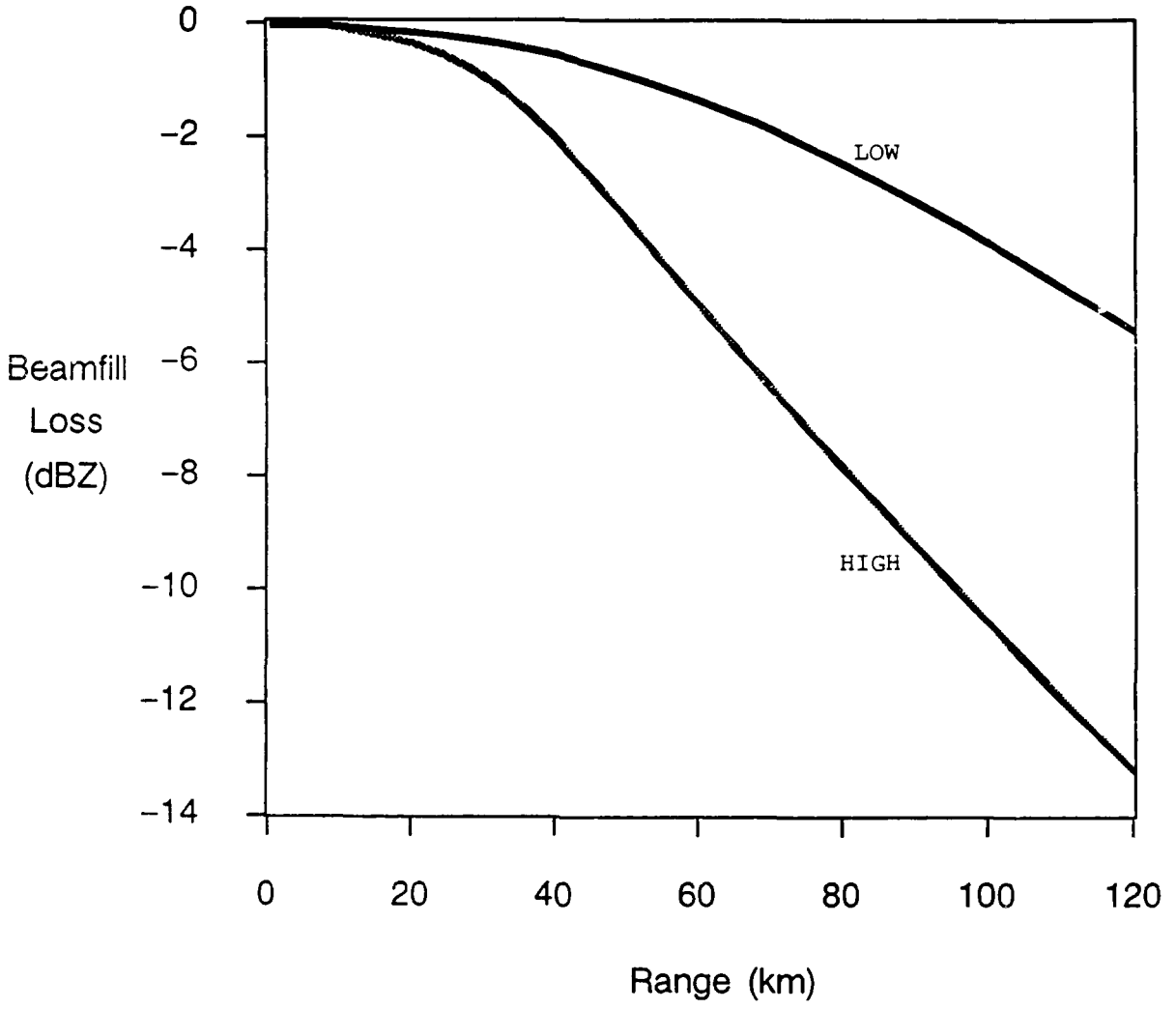

Figure C-5. Beamfill loss versus range for low and high antenna beams.

While the narrow pencil-beam antenna pattern of the MIT radar is more adequately suited for volumetric weather sensing, simulation of the ASR-9 weather channel output requires that the same beamfill loss correction be applied to the elevation-integrated MIT reflectivity estimates. To implement this in the ASR-9 simulation, the beamfill loss correction Z_{cor} is computed for each 1 km range interval by integrating the model-based relative reflectivity profile $Z^*(r\ \theta)$ over the entire vertical extent of the ASR-9 fan beam:

$$Z_{cor}(R) = \frac{\int Z^*(R,\theta)\, B_T(\theta)\, B_R(\theta)\, d\theta}{\int B_T(\theta)\, B_R(\theta)\, d\theta} \tag{6}$$

The range-dependent beamfill loss corrections are then applied to the vertically-integrated MIT reflectivity estimates:

$$\hat{Z}(R,o) = Z(R,o) \cdot Z_{cor} \tag{7}$$

C.2.5 CONVERSION TO NWS SIX-LEVEL INTENSITY SCALE

The corrected reflectivity estimates are then converted to their corresponding NWS six-level scale values by means of a look-up table (Table C-2). Reflectivities less than the lower threshold for Level 1 are assigned a level value of 0.

TABLE C-2
NWS Standard Reflectivity Levels

Level	Reflectivity (dBZ)
1	18* - 30
2	30 - 41
3	41 - 46
4	46 - 50
5	50 - 57
6	57+

* Actual minimum used on level 1 was 6 dB above system noise as is done in the ASR-9 weather channel. 18 dBZ is the actual minimum currently being used by the NWS.

C.2.6 SPATIAL SMOOTHING

The six-level intensity data are then smoothed in two stages. The first stage consists of taking each range-azimuth cell value and its eight surrounding cell values, and replacing it with the highest level found in at least "WWW" (an adjustable parameter) of the nine cells. WWW is reduced proportionately when clutter-censored cells are

encountered. To implement this for a given range-azimuth cell, the value of each of the nine neighbors is checked and the appropriate level accumulator is incremented. Clutter-censored cells are also tallied. After all levels have been tallied, WWW is adjusted for clutter-censored cells using:

$$WWW_{new} = WWW \times \frac{9 - N_{censored}}{9} \tag{8}$$

Finally, the value of the central cell in the cluster is assigned the highest level whose accumulator plus the sum of all higher level accumulators is greater than or equal to WWW_{new}. If the number of clutter-censored cells exceeds six of the nine cells in the cluster, the central weather cell in the cluster is assigned -1.

The final smoothing of the six-level intensities is performed on the output of the first-stage spatial filter by examining the level assigned to each range-azimuth cell and its eight surrounding cells, and replacing it with the highest level of the nine cells. Figure C-6 is a schematic depiction of the two-stage spatial smoothing process.

C.2.7 SIMULATION PRODUCTS

The final result of the ASR-9 simulation program is a 2-dimensional (range-azimuth) map containing six-level reflectivity estimates as seen by an ASR-9 equipped with the weather channel processor. The final six-level weather product has a granularity of 0.5 nmi by 1.4 deg and a resolution of 1 nmi by 4.2 deg. In addition to the final six-level weather product, the simulation program produces output at several intermediate stages. These intermediate data products are stored along with the final weather product in a disk-file that adheres to the radar common data format (CFT) used at Lincoln Laboratory. The intermediate product data include: (1) ASR-9 equivalent reflectivity, (2) ASR-9 equivalent radial velocity, (3) ASR-9 equivalent velocity spectrum width, (4) ASR-9 equivalent reflectivity after output of clutter filter bank, (5) ASR-9 equivalent reflectivity after range-smoothing, (6) beamfill loss correction and conversion to six-level intensity (M-OF-N), (7) first spatial filter, and (8) second spatial filter (final product). Product data generated by the simulation are resampled onto a 1 km [.54 nmi] resolution Cartesian grid centered over the ASR-9 for further analysis and display.

C.3 TEST CASE RESULTS

PPI volume data were taken with the MIT weather radar at Huntsville, Alabama during a convective air mass thunderstorm event which occurred around 23:32 GMT on August 4, 1988. The scan configuration used during the August 4 test is presented in Table C-3.

AD-A211 745 ASR-9 WEATHER CHANNEL TEST REPORT(U) MASSACHUSETTS INST 2/2
OF TECH LEXINGTON LINCOLN LAB D C PUZZO ET AL.
03 MAY 89 ATC-165 DOT/FAA/PS-89-3 F19628-85-C-0002
UNCLASSIFIED F/G 17/9 NL

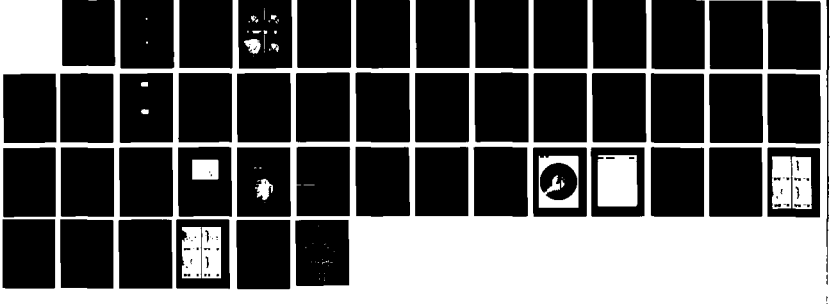

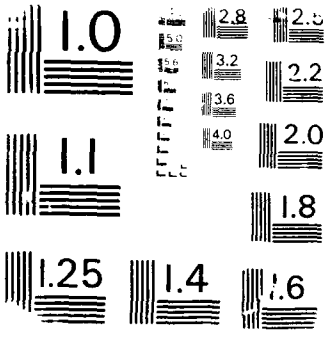
1.0
1.1
1.25
1.4
1.6
1.8
2.0
2.2
2.8
3.2
3.6
4.0

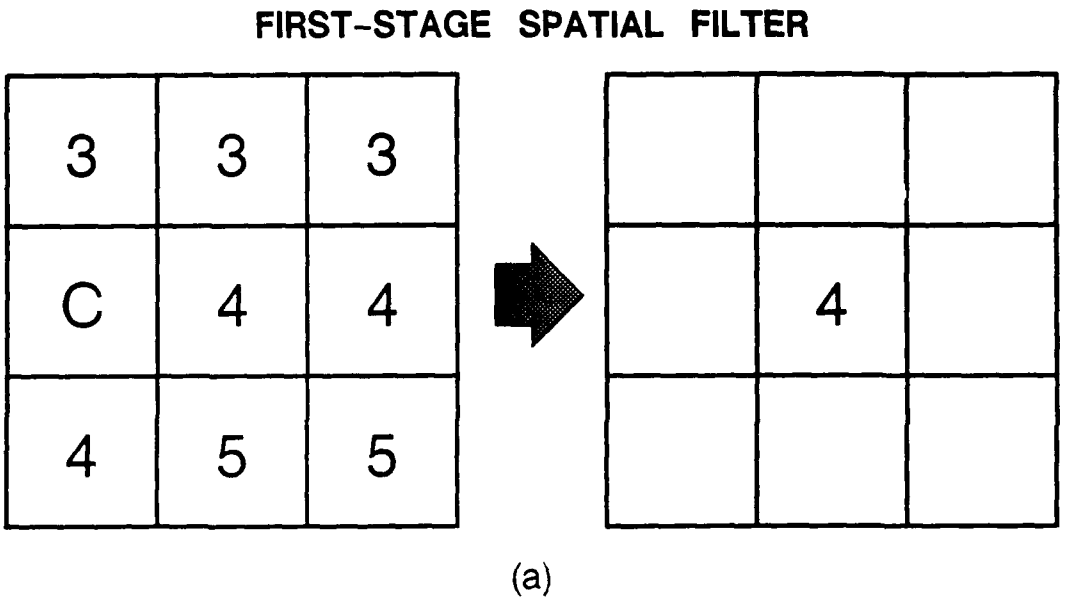

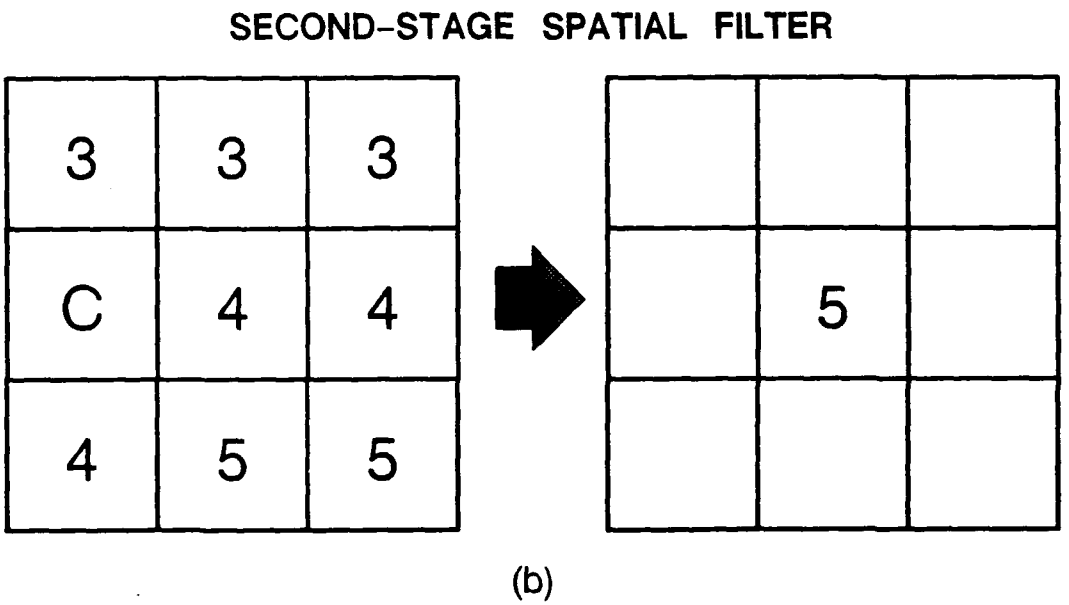

Figure C-6. Schematic depiction of 2-stage spatial filter.

TABLE C-3

Scan Configuration for 4 August 1988

Tilt #	Time	Azimuths	Elevation	# Radials	Range Spacing
1	23:31:22 - 23:31:25	59.1 to 123.1	0.7	48	0.5 km
2	23:31:30 - 23:31:33	120.7 to 56.6	1.5	47	0.5 km
3	23:31:39 - 23:31:42	61.1 to 125.2	3.1	48	0.5 km
4	23:31:47 - 23:31:50	116.8 to 53.5	4.7	47	0.5 km
5	23:31:55 23:31:59	60.1 to 123.8	6.3	48	0.5 km
6	23:32:03 - 23:32:07	117.1 to 53.6	7.9	48	0.5 km
7	23:32:12 - 23:32:16	61.5 to 125.2	9.5	48	0.5 km
8	23:32:20 - 23:32:24	116.5 to 53.4	11.1	47	0.5 km
9	23:32:29 - 23:32:33	61.6 to 125.2	12.7	48	0.5 km
10	23:32:37 - 23:32:41	116.9 to 53.0	14.3	50	0.5 km
11	23:32:46 - 23:32:50	61.6 to 125.5	15.9	48	0.5 km
12	23:32:54 - 23:32:57	116.5 to 52.1	17.5	47	0.5 km
13	23:33:03 - 23:33:07	61.6 to 124.9	19.1	48	0.5 km

These data were used to simulate the ASR-9 weather channel using the simulation program. Figure C-7 shows intermediate and final simulator output.

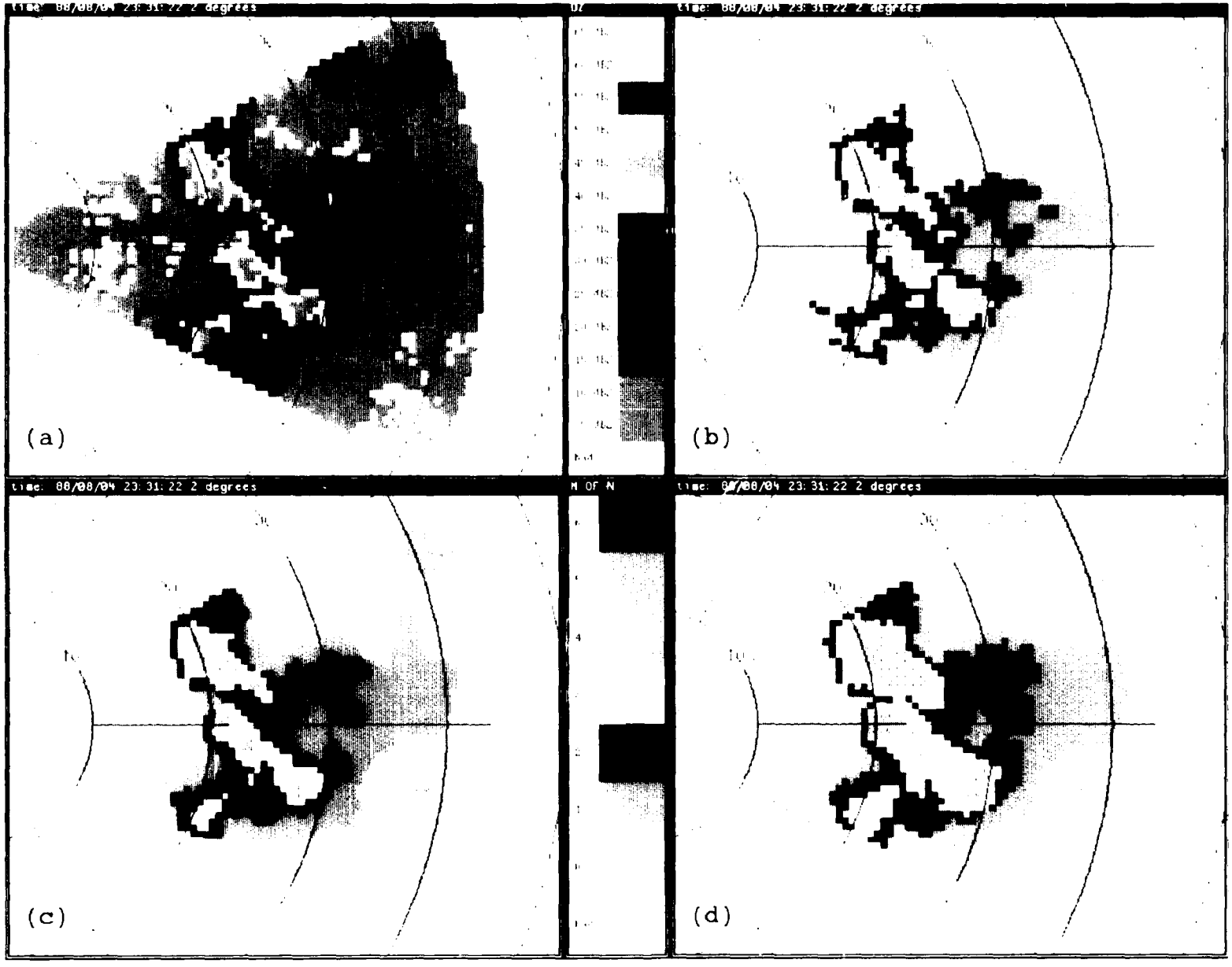

Figure C-7. Output of the ASR-9 weather channel processor simulation after: (a) Fan beam integration of MTI reflectivity data, (b) M-of-N processor, (c) First spatial filter, (d) Second spatial filter (final product)

APPENDIX D

EMULATION OF THE ASR-9 WEATHER CHANNEL USING FL-3 FAN-BEAM RADAR DATA

D.1 INTRODUCTION

This appendix describes the ASR-9 reflectivity channel emulation program. This program converts time-series radar data collected by the FL-3 fan-beam radar into the six-level format described in the ASR-9 specification.

It contributes to the validation of the ASR-9 system in three ways. (1) It enables independent testing of the ASR-9 processing scheme. (2) It confirms observations made by the MIT pencil beam radar. (3) It provides a second set of observations for direct comparison with the ASR-9.

D.2 EMULATION PROGRAM DESCRIPTION

Figure D-1 is a flow diagram of the emulation, which is essentially a duplicate of the ASR-9 weather channel. The FL-3 radar system is designed to be the functional equivalent of an ASR-9. It consists of an ASR-8 antenna and S-Band transmitter (on loan from the U.S. Navy) with a Lincoln Laboratory designed signal recording system attached. Since FL-3 is itself an airport surveillance radar, its beam shape is a fan-beam similar to that of the ASR-9.

FL-3 data are recorded on high density tape in time-series format. As a result, emulation of the ASR-9 signal processing can be performed in the time domain, as is done in the ASR-9 processor. Subsequently, the data processing scheme in the FL-3 emulation directly follows the ASR-9 processing scheme (summarized in Section 1.2. of this report).

D.2.1 DATA STORAGE FORMAT

FL-3 data are stored on 1/2 inch tape in integer format, with a scan-sector-pulse-gate hierarchy. Multiple consecutive scans (a scan being data collected during one complete rotation of the antenna) can be stored in a single tape file. Each 360 degree scan is comprised of 256 sectors, so the angular resolution in the data is about 1.4 degrees, one azimuthal beamwidth. When data are collected in block staggered mode, the first eight pulses of a sector comprise the low PRF coherent processing interval (CPI), and the next 10 comprise the high PRF CPI. Two to three filler pulses are placed between sectors so that the CPIs always occur over the same angular regions. Azimuthal and PRF information is stored in headers before every pulse. Gate spacing is 120 meters, making one nmi of data equivalent to 16 gates.

D.2.2 CPI ACCUMULATION

Each scan is processed sector by sector; high and low PRF CPIs of a sector are

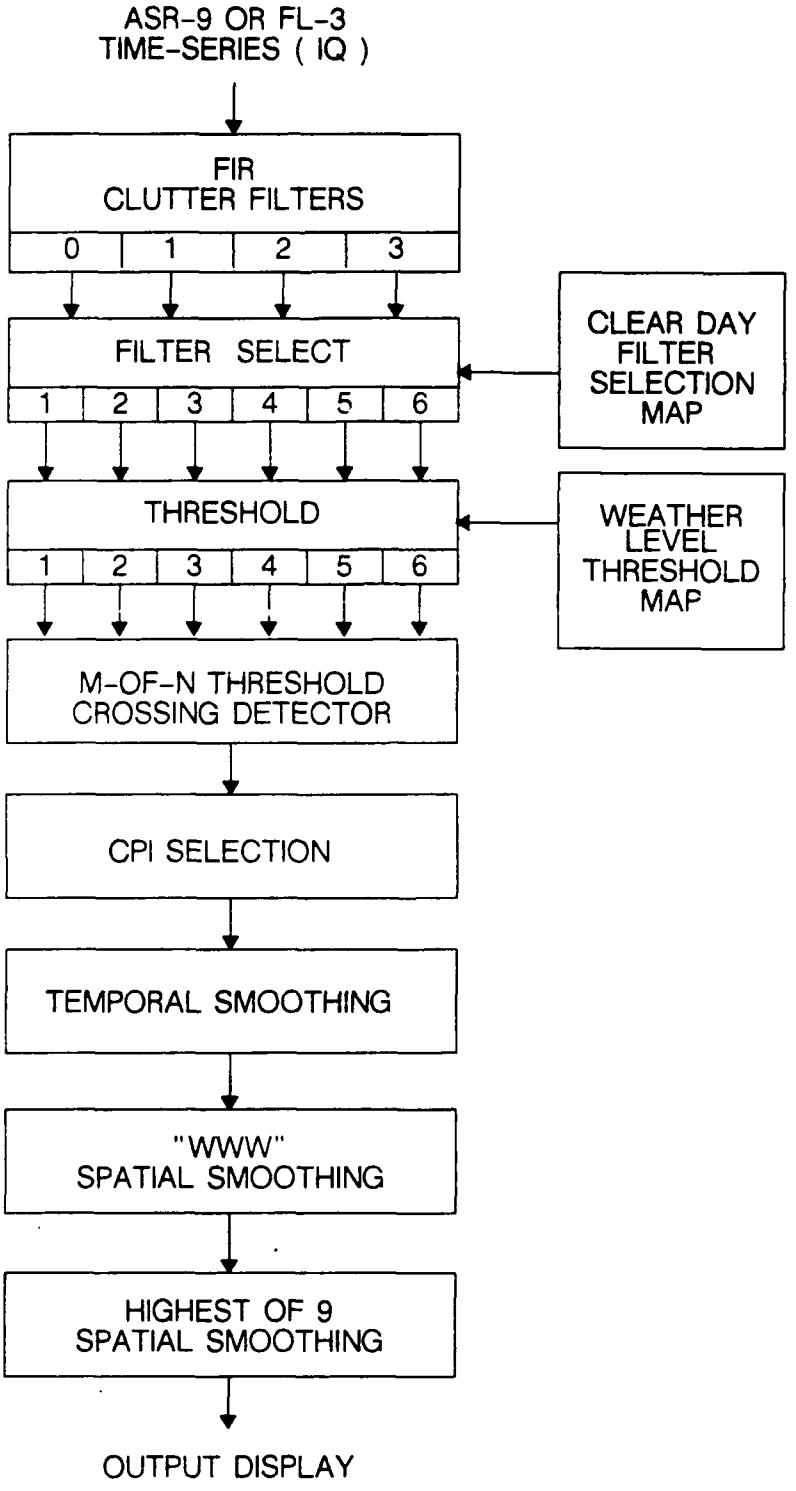

Figure D-1. ASR-9 six-level reflectivity channel emulation block diagram

separately processed. A CPI (either 8 or 10 pulses) is accumulated, then converted from integer to real values.

D.2.3 BEAM SELECTION

High or low beam selection can be user-specified for up to 12 separate regions. Input variables describe two types of channel selection structures, **wedges** and **regions**.

The **wedges** are consecutive sectors in which the beam selection is switched to the high beam out to a specified range gate. Up to eight wedges can be specified by entering eight pairs of integer values; each pair consists of the outer-bound's gate number and the sector number corresponding to the clockwise side of the wedge. The first wedge begins at sector 0 (0°), and the wedges are contiguous.

The **regions** are "rectangular" areas, defined by two sector boundaries and two ranges. Up to four regions can be specified. In these regions, each beam selection flag is switched from value to which it was set after the wedges were applied. Two overlapping regions will cause the flags to flip twice. The user specifies the inner and outer range gates (g1 and g2), and the two sector boundaries (s1 and s2).

D.2.4 CLUTTER FILTERING

The data are split into four streams, each stream is sent to one of four FIR clutter filters. Two sets of four filters exist: one set of 8 point filters for low PRF signals, one set of 10 point filters for high PRF signals. The first filter in both sets is an all-pass filter. The impulse response curves of the remaining six attenuating filters are shown in Figure D-2. These impulse responses, furnished by Westinghouse, are the same as those used in the ASR-9 processor.

A site-specific map determines which FIR clutter filter output is to be used for the detection of a particular NWS weather level at a particular gate. This map is generated from data taken from a single scan of the FL-3 antenna on a clear day. The resolution of the resultant filter selection map is 1 nmi by 1.4 degrees. For each cell, the map contains six filter selections, one for each NWS reflectivity level. The map also contains censoring flags, denoting cells where clutter intensity is such that reliable detection of a particular weather level is not possible.

The radial resolution of the map, one gate (1/16 nmi), is finer than that specified for the ASR-9, which requires filter selection map resolution to be 1 nmi. However, the map conforms to the ASR-9 resolution by repeating the same value for 16 consecutive gates.

D.2.4.1 Filter Selection Map Generation

The filter selection map is generated by running the emulation in filter selection map generation mode. When the emulation operates in this mode, the filter selection map is generated and written to the user-specified filter selection map file. A single scan

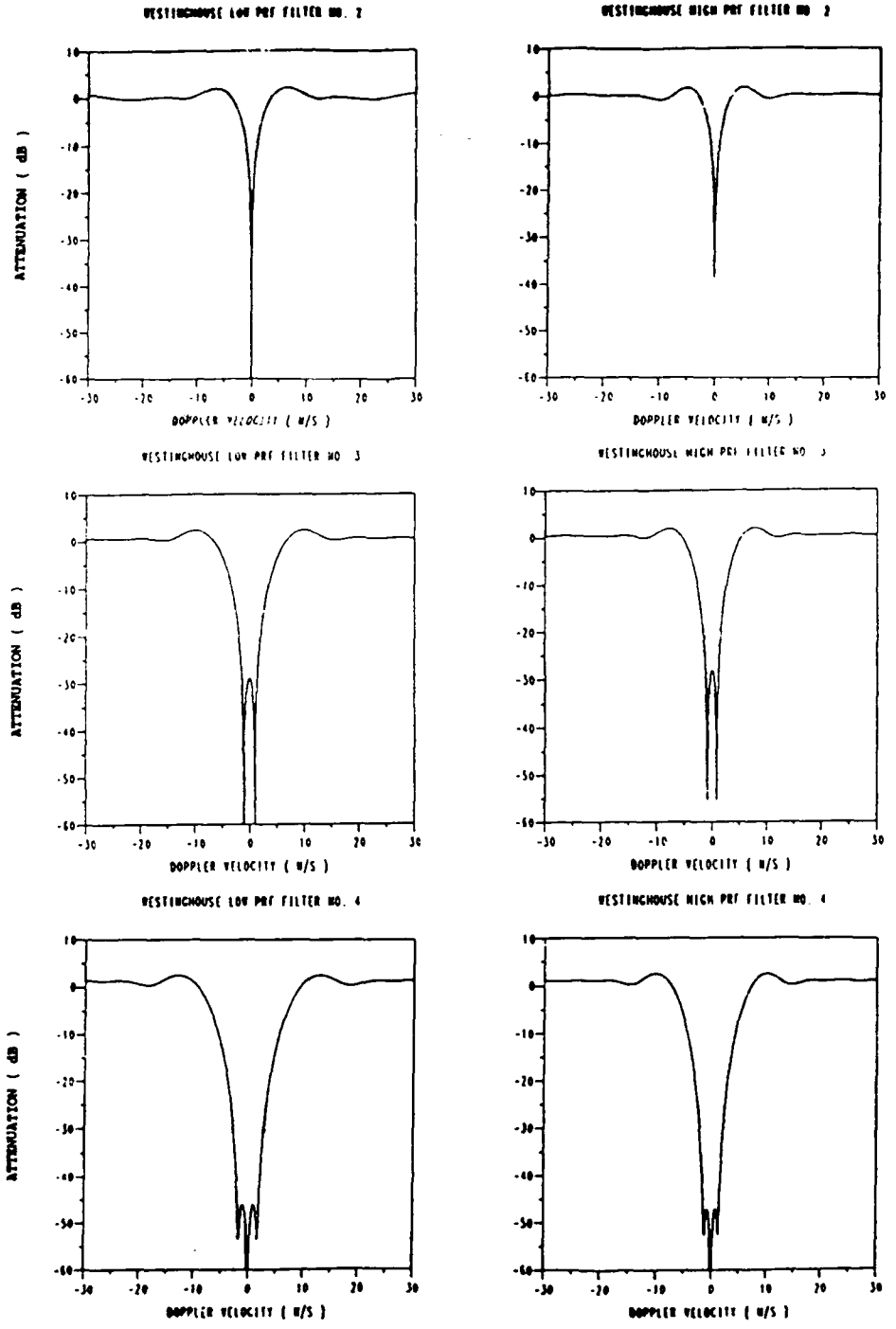

Figure D-2. Transfer functions of low and high PRF FIR clutter filters suggested by Westinghouse

of FL-3 data collected on a clear day is used as time-series input. Since only one scan is used, the emulation performs no temporal filtering. Data are processed as in normal mode, with the following exception: For each sector of data, the outputs of the four FIR filters is buffered until both CPI's of data have been processed. The filter selection procedure is then performed as follows:

(1) All four filter outputs for both CPIs are converted from $counts^2$ to their equivalent Z values by applying equation (D-1) (see Section D.2.5. of this appendix).

(2) For every 1 nmi (16 gates), the maximum median dBZ level (M_f) of each of the two CPI's is extracted. This operation is repeated for all four filter outputs.

(3) For all six NWS levels L (dBZ), four values Δ_{Lf} have been computed, such that

$$\Delta_{Lf} = M_f - (L - 5.0)$$

The output of least attenuating filter f where Δ_{Lf} does not exceed 0 dBZ is selected. If breakthrough still occurs at the highest clutter attenuation (i.e., $\Delta_{L4} > 0$), a clutter censor flag is placed in the map in lieu of a filter selection. This flag denotes that too much clutter exists in that particular 1 nmi increment for reliable detection of the given NWS level.

(4) Filter selections are written to the file designated to contain the filter selection map. The radial resolution of the emulation's filter selection map is one gate, (1/16 nmi). The map conforms to the 1 nmi resolution of the ASR-9 specification by repeating the same value for 16 consecutive gates.

D.2.5 WEATHER LEVEL THRESHOLDING

After appropriate filter outputs have been selected, the six resultant data streams (one for each NWS level) are each compared gate by gate with a weather threshold map. The map is computed at the beginning of program execution. The values in the map are functions of range and NWS level: such factors as STC attenuation, beamfill correction, A/D conversion, antenna gain, and system noise are included in the computation of these thresholds. The values of each map element are generated from the following equation:

$$T(level, chan, r) = \left[\frac{Z(level)}{C_{radar}^{chan}\, r^2}\right]\left[\frac{P_{ac}(r)}{k_{med}\, l(chan, r)}\right] \qquad \text{(D-1)}$$

where

$$T(level, chan, r) \equiv Weather\ level\ threshold(count^2)$$

$$Z(level) \equiv NWS\ reflectivity\ level\left(\frac{mm^6}{m^3}\right)$$

$$r \equiv Weather\ target\ range(m)$$

$$C_{radar}^{chan} \equiv Radar\ system\ constant\left(\frac{mm^6}{count^2\ m^5}\right)$$

$$P_{stc}(r) \equiv STC\ attenuation\ correction$$

$$k_{med} \equiv 8-of-16\ filter\ bias\ correction$$

$$l(chan,r) \equiv Beam\ fill\ correction$$

D.2.5.1 Computation of the Unattenuated Weather Level Thresholds

The purpose of this section is to explain the first set of terms in equation (D-1):

$$T_s(level,chan,r) = \frac{Z(level)}{C_{radar}^{chan}\ r^2} \tag{D-2}$$

T_s is the unattenuated weather level threshold.

The power received from an echo by an antenna can be expressed in terms of basic radar theory as the product of the power density of the echo at the antenna and the effective aperture area of the receiving antenna.

$$P_r = S_r\ A_e \tag{D-3}$$

where

$$P_r \equiv Power\ received(mW)$$

$$S_r \equiv Echo\ power\ density\left(\frac{mW}{m^2}\right)$$

$$A_e \equiv Effective\ antenna\ aperture\ area(m^2)$$

The threshold term, T_s, is expressed in $counts^2$, the "power" recorded at the FL-3 receiver's digital output. Both an antenna-to-receiver loss term, l_{REC}^{chan}, and a receiver "gain" term, $G_{A/D}^{chan}$, must be included to convert the power at the antenna to $counts^2$. $G_{A/D}^{chan}$ is a term that converts the milliwatt antenna power into $count^2$. Since FL-3 has two separate receivers channels, both $G_{A/D}^{chan}$ and l_{REC}^{chan} are channel dependent. The adjusted threshold equation is

$$T_s = S_r\ A_e\ G_{A/D}^{chan}\ l_{REC}^{chan} \tag{D-4}$$

where

$$G_{A/D}^{chan} \equiv Receiver\ A/D\ gain\left(\frac{count^2}{mW}\right)$$

$$l_{REC}^{chan} \equiv loss\ from\ antenna\ waveguide\ to\ receiver\ input$$

$$A_e \equiv Effective\ antenna\ aperture\ area(m^2)$$

The echo power density, S_r, expands to the following equation

$$S_r = \frac{1}{4\pi r^2} S_i \eta V \tag{D-5}$$

where

$S_i \equiv$ *Incident radiation power density* $(\frac{mW}{m^2})$

$\eta \equiv$ *Reflectivity density* $(\frac{m^2}{m^3})$

$V \equiv$ *Weather target volume* (m^3)

The incident radiation power density, S_i expands to

$$S_i = \frac{1}{4\pi r^2} G_{ANT}^{LO} P_{pulse} l_{TRANS} \tag{D-6}$$

where

$G_{ANT}^{LO} \equiv$ *Directive antenna gain*

$P_{pulse} \equiv$ *Transmitter pulse power* (mW)

$l_{TRANS} \equiv$ *Loss from transmitter to antenna*

The transmitter pulse power is a function of the average pulse power, the pulse width, and the average pulse repetition interval.

$$P_{pulse} = \left(\frac{\bar{T}_{PRI}}{\tau}\right) \bar{P}_T \tag{D-7}$$

where

$\bar{T}_{PRI} \equiv$ *Averagepulse repetition interval* (sec)

$\tau \equiv$ *Pulse width* (s ^)

$\bar{P}_T \equiv$ *Average transmitter power* (mW)

Combining Equations (D-6) and (D-7) yields

$$S_i = \frac{1}{4\pi r^2} G_{ANT}^{LO} \left(\frac{\bar{T}_{PRI}}{\tau}\right) \bar{P}_T l_{TRANS} \tag{D-8}$$

The weather reflectivity density, η, is expressed by

$$\eta = 10^{-18} \frac{\pi^5}{\lambda^4} |K_w|^2 Z \tag{D-9}$$

where

$\lambda \equiv$ *Pulse wavelength* (m)

$K_w \equiv$ *Constant derived from the complex refractive index of water*

$Z \equiv$ *Effective reflectivity factor* $(\frac{mm^6}{m^3})$

The above equation applies when λ is significantly larger than the diameter of the

weather target water droplets. This condition is satisfied for the 10 cm wavelength of both the FL-3 and AWR-9 systems.

The value of the constant $|K_w|$ used in the emulation is

$$|K_w| = 0.964 \tag{D-10}$$

Z, the NWS reflectivity value, represents a density of diameter weighted water droplets, i.e.,

$$Z = \frac{1}{\Delta V} \sum_{V} D^6 \tag{D-11}$$

where

$$D \equiv Droplet\ diameter(mm)$$

$$V \equiv Weather\ target\ volume(m^3)$$

Since Z is traditionally represented in units of $\frac{mm^6}{m^3}$, the reflectivity factor equation contains a conversion factor, 10^{-18}, so that η is expressed in MKS units.

The weather target volume is represented by the equation

$$V = \frac{1}{1.85\ \ln 2} \left[\pi \frac{\theta r}{2} \frac{\phi r}{2}\right] \left[\frac{c\ \tau}{2}\right] \tag{D-12}$$

where

$$\theta \equiv Azimuthal\ beamwidth(radians)$$

$$\phi \equiv Elevational\ beamwidth(radians)$$

$$c \equiv Speed\ of\ light(\frac{m}{\sec})$$

The range-azimuth cell is modelled as a "pill-box" shape with ellipsoidal ends of area $\pi \frac{\theta}{2} \frac{\phi}{2} r^2$ and length $\frac{c\ \tau}{2}$. The cell is, of course, not really a perfect "pill-box", as the beam intensity actually follows a Gaussian contour. The $\frac{1}{1.85\ \ln 2}$ term corrects for this.

Combining Equations (D-5), (D-8), (D-9), and (D-12), the echo power density, S_r, is expressed by

$$S_r = \frac{G_{ANT}^{LO} \left(\frac{\bar{T}_{PRI}}{\tau}\right) \bar{P}_T\ l_{TRANS}\ \pi^4\ \theta\ \phi\ c\ \tau\ |K_w|^2\ Z}{1.85\ \ln 2\ 128\ \lambda^4\ 10^{18}\ r^2} \tag{D-13}$$

The effective antenna aperture area, A_e of equation (D-3), is derived from basic antenna theory as

$$A_e = G_{ANT}^{chan} \frac{\lambda^2}{4\pi} \tag{D-14}$$

The antenna aperture represents the effective cross-sectional area of the antenna in the direction it is pointing.

Combining equations (D-4), (D-13), and (D-14), the unattenuated threshold equation becomes

$$T_u = \frac{G_{ANT}^{LO}\ G_{ANT}^{chan} \left(\frac{\overline{T}_{PRI}}{\tau}\right) \overline{P}_T\ l_{TRANS}\ l_{REC}^{chan}\ \pi^3\ \theta\ \phi\ c\ \tau\ |K_w|^2\ G_{A/D}^{chan}\ Z}{1.85\ \ln 2\ 512\ \lambda^2\ 10^{18}\ r^2} \tag{D-15}$$

Defining C_{radar}^{chan} as

$$C_{radar}^{chan} = \frac{1.85\ \ln 2\ 512\ \lambda^2\ 10^{18}}{G_{ANT}^{LO}\ G_{ANT}^{chan} \left(\frac{\overline{T}_{PRI}}{\tau}\right) \overline{P}_T\ l_{TRANS}\ l_{REC}^{chan}\ \pi^3\ \theta\ \phi\ c\ \tau\ |K_w|^2\ G_{A/D}^{chan}} \tag{D-16}$$

the unattenuated threshold becomes

$$T_u = \frac{Z}{C_{radar}^{chan}\ r^2} \tag{D-17}$$

D.2.5.2 STC Attenuation

The purpose of the sensitivity time control (STC) is to prevent saturation of the radar receiver at close ranges. This is done by attenuating the signal before it enters the receiver. The STC attenuation is a range dependent function. In the FL-3 system, the STC function is defined by three parameters, p_1, p_2, and p_3, as follows:

$$P_{stc}(r) = MIN\left(p_1 + \left(\frac{r}{p_2}\right)^{-p_3}, 1\right) \tag{D-18}$$

D.2.5.3 M-of-N Bias Correction

As mentioned previously, both the FL-3 and the ASR-9 systems sample data in 1/16 nautical mile (nmi) increments. For each 0.5 nmi, the six-level processor selects the highest weather level exceeded in half or more of the surrounding nautical mile's gates, i.e. the highest weather level in 8 of 16 gates is extracted. This has the effect of median filtering the data. This process is repeated for both CPIs and the lowest of the two weather level detections is selected. This process of median filtering and lowest of two selection affects the probability of detection of a particular weather level. The probability of detection of a threshold crossing after the CPI selection stage should be 50%. In order

for this requirement to be fulfilled, the probability of detection at every 1/16 nmi gate must be increased. To effect this, the weather level thresholds must be lowered.

Let p_s be the probability that a threshold crossing will be detected in a single cell. From basic combinatorics, the probability of M or greater crossings in N cells, p_M, is

$$p_M = \sum_{j=M}^{N} p_s^j (1 - p_s)^{N-j} \frac{N!}{j!\,(N-j)!} \tag{D-19}$$

By setting $M = 8$ and $N = 16$, then applying the restriction $p_M^2 = 0.5$, the above equation for p_s has the solution

$$p_s = 0.5364 \tag{D-20}$$

Weather echo powers are exponentially distributed. As a result, the probability density function for p_s is

$$P_s(x) = \frac{1}{\alpha} e^{-\frac{x}{\alpha}} \tag{D-21}$$

where

$\alpha \equiv$ *Average value (true echo power)*

From this density function, it can be determined that the probability that a weather sample exceeds the weather threshold T is

$$\begin{aligned} p_s(x \geq T) &= \int_{x=T}^{\infty} P(x)\, dx \\ &= \int_{x=T}^{\infty} \frac{1}{\alpha} e^{-\frac{x}{\alpha}}\, dx \\ &= e^{-\frac{T}{\alpha}} \end{aligned} \tag{D-22}$$

Setting $p_s = 0.5364$,

$$\frac{T}{\alpha} = -ln(0.5364) = 0.623$$

Therefore, weather level thresholds should be lowered by a factor of 0.623, or 2.06 dB. The coefficient used in the threshold equation (D-1) should therefore be

$$k_{med} = \frac{1}{0.623} = 1.605 \tag{D-23}$$

D.2.5.4 Beamfill Correction

The third attenuation factor in the threshold equation (Equation D-1) is a correction for beamfill loss. As range increases, the vertical cross-section of the fan-beam also increases, while that of the weather structures to be detected does not. Storms at long range do not quite "fill" the beam and the returned power is decreased. This problem is illustrated below. For simplicity, the two storms in Figure D-3 are identical in size, shape, and reflectivity density; they differ only in range from the radar. The storm near the radar completely fills its fan-beam; the second storm is illuminated only by half the beam. With no correction for beamfilling, reflectivity estimates would differ for the two storms by a factor of 2 (~3 dBZ).

A beamfill correction provides a level of compensation for this loss. To implement such a correction, assumptions about storm structure must be made. In the above example, a change in the height of the idealized storm would change the amount of beam left "un-filled" at long range, thus affecting attenuation. In the emulation, the storm model adopted is the same as that used by the Westinghouse ASR-9 six-level processor. All weather is assumed to be of a constant reflectivity from the Earth's surface to 4 kilometers (13,123 feet) altitude, with the reflectivity falling off at a rate of 3 dB for every kilometer (3281 feet) higher. Mathematically, this storm weighting function can be expressed as

$$p(h) = \begin{cases} 1 & h \leq 4 \\ 10^{\left(\frac{-3(h-4)}{10}\right)} & h > 4 \end{cases} \qquad \text{(D-24)}$$

where

$p(h) \equiv Storm\ model\ weighting\ function$

$h \equiv Height(km)$

The height can be expressed in radar coordinates,

$$h'(r,\phi) = r \sin\phi \qquad \text{(D-25)}$$

where

$r \equiv Range(km)$

$\phi \equiv Elevation(radians)$

In the above expression, however, it is assumed that the Earth is flat. At the outermost range of the ASR-9, 115 kilometers (60 nmi), the Earth's surface has curved approximately 1 km below the 0 degree level of the beam. At that range, a 0.5 dB error in the beamfill estimate would result, assuming that the Westinghouse storm model is used. Therefore, a compensation for Earth curvature is warranted. The height function, accounting for a curved Earth, is

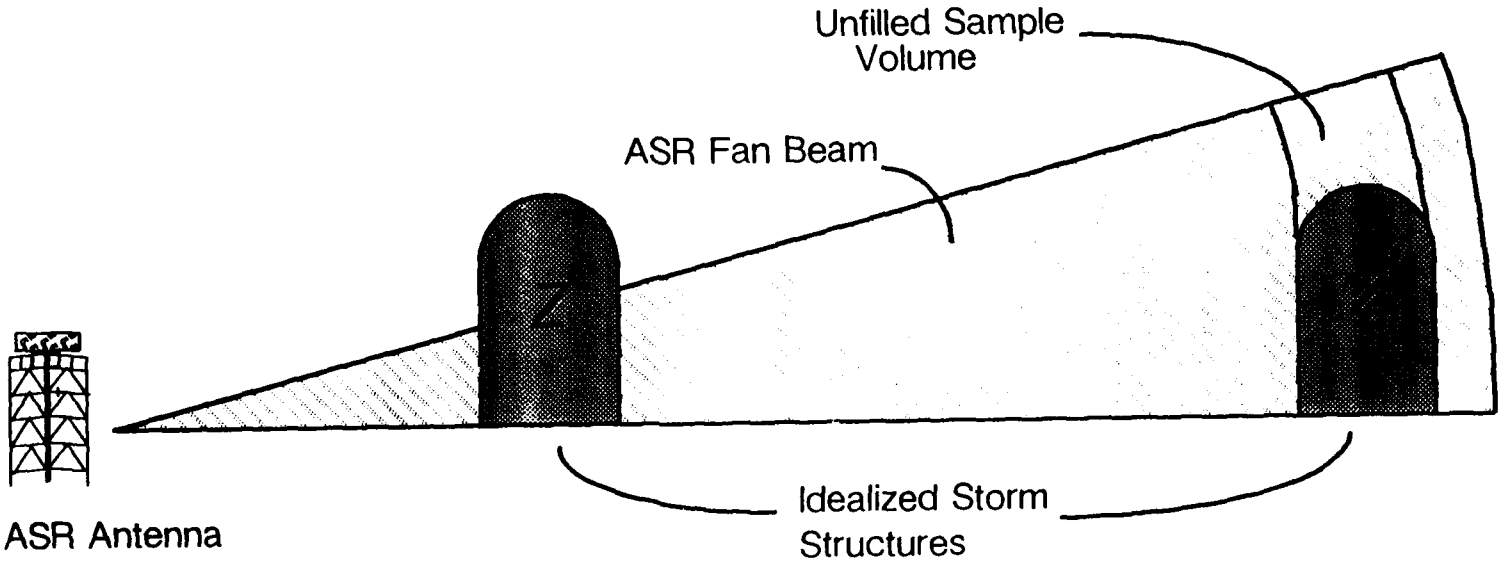

Figure D-3. Idealized depiction of range-dependent beamfill loss

$$h(r,\phi) = r\sin\phi + \left[\sqrt{r^2 + R_e^2} - R_e\right] \qquad \text{(D-26)}$$

where

$$R_e \equiv Radius\ of\ the\ Earth = 6370\ km$$

The storm model is weighted by the antenna beam pattern of the ASR-9. The beam weighting functions are plotted in Figure D-4. The attenuation factor is calculated in the expression:

$$l_{BEAM}^{chan} = \frac{\int_{\phi=0}^{\frac{r}{2}} p(r,\phi)\, f_{LO}(\phi)\, f_{chan}(\phi)}{\int_{\phi=0}^{\frac{r}{2}} f_{LO}(\phi)\, f_{chan}(\phi)} \qquad \text{(D-27)}$$

where

$$f_{chan}(\phi) \equiv One-way\ antenna\ \ B_T(\theta)\, B_R(\theta)\, d\theta\ pattern$$

Implementation of the above correction proceeds as follows: For each 1/16 nmi gate, the beam attenuation equation is numerically calculated with the following

$$l_{BEAM}^{chan} = \frac{\sum_{phi=0}^{\frac{r}{2}} stormweight(range, phi)\ bpattern(phi, tilt, low)\ bpattern(phi, tilt, chan)\ \Delta phi}{\sum_{phi=0}^{\frac{r}{2}} bpattern(phi, tilt, low)\ bpattern(phi, tilt, chan)\ \Delta phi} \qquad \text{(D-28)}$$

The *stormweight* function explicitly calculates the height dependent storm model parameter. The *bpattern* function returns the one-way antenna beam weighting as a function of antenna tilt, receiver channel, and elevation; it utilizes a lookup table containing the beam weights of the ASR-9 from -10 to 40 degrees, with 1-degree resolution. To increase accuracy, the function performs a linear interpolation for all values between -10 and 40 degrees. For all elevations outside that range, the weights are computed from exponential drop-off functions modelled after the actual beam patterns of the ASR-9.

The resolution, i.e., the size of Δphi, is varied to improve computation time. For values of less than 10 degrees, Δphi is set to 1/8 of a degree, and *phi* is incremented by that amount. After 10 degrees, Δphi is set to 1/2 a degree. This reduction in resolution alters the calculated beamfill attenuation by less than 0.02 dB.

D.2.6 M-OF-N DETECTION

Six streams of threshold-crossing flags are passed to the M-of-N detection module. For each 0.5 nmi increment (8 gates), a 1 nmi (16 gate) range interval is examined; the highest NWS weather level that has its threshold exceeded in 8 of the 16 gates is

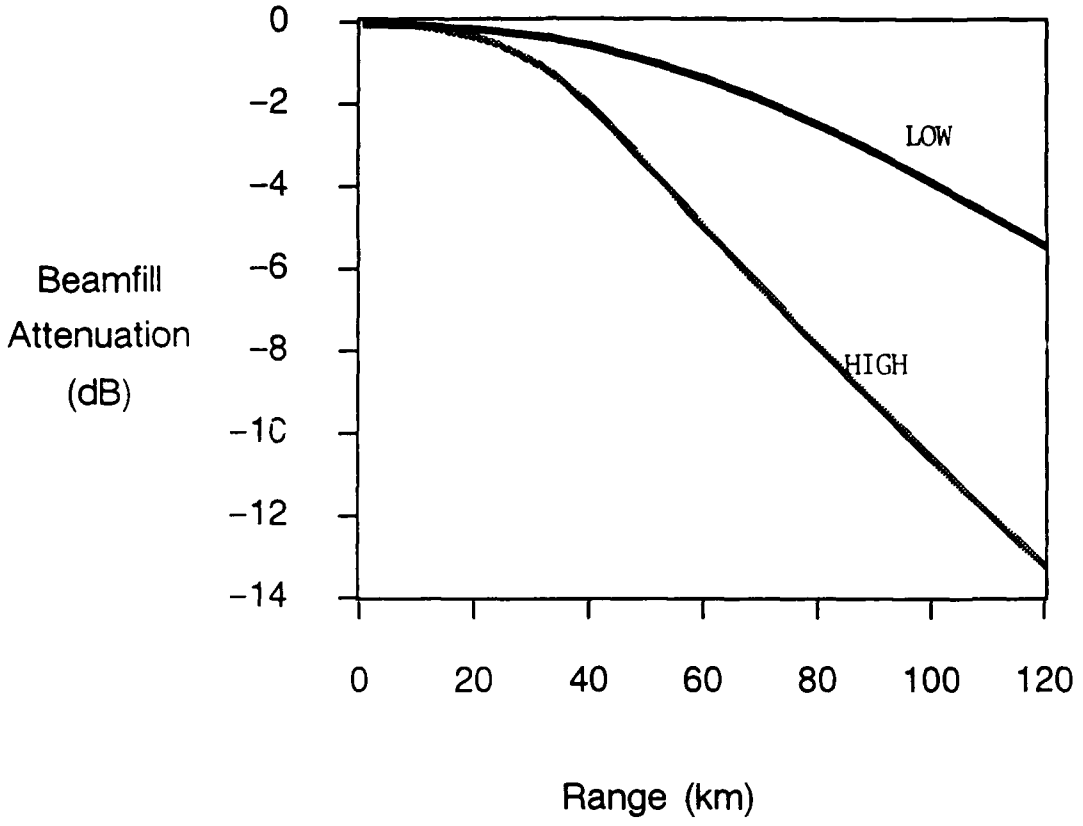

Figure D-4. Beamfill loss versus range for low and high antenna beams

selected. If no level meets that criterion, a zero level is selected. If the selected weather level is censored in that 0.5 nmi increment due to high clutter, then a censoring flag, passed along with the output data stream, is set.

D.2.7 CPI SELECTION

The above processing is performed on both low and high PRF CPIs. For every 0.5 nmi gate, the lowest of the two CPIs selected levels is chosen; this is done to eliminate second trip echoes.

D.2.8 SENSITIVITY TIME CONTROL (STC)

The ASR-9 six-level channel's processing scheme entails operating with the STC attenuation switched off on every other scan. NWS Level 1 weather is processed on scans in which the STC is turned off; all other weather levels are processed with STC attenuation turned on. Since the FL-3 signal processor lacks STC switching capability on a per scan basis, all weather levels in the FL-3 emulation program are generated from the same set of STC attenuated scans.

D.2.9 TEMPORAL FILTERING

Three scans are processed in the manner described above. Every other scan (rotation of the antenna) is used to ensure the proper temporal variation in the collected data (see preceding section). Temporal filtering is performed by extracting the median value of the three scans for each 0.5 nmi gate.

D.2.10 "WWW" SPATIAL FILTER

The first spatial filter extracts a value from each nine cell, nearest neighbor cluster by first sorting the six-level values from lowest to highest, then selecting the WWW-th element of the list, WWW being a user-specified parameter. For example, if the WWW value is 5, then the fifth highest of the nine cells is selected. Any clutter censored cells are excluded from the cluster before the value is extracted, and WWW is decreased accordingly. If five or more cells in the cluster are censored, then the cell in question is declared to be censored.

D.2.11 HIGHEST-OF-9 SPATIAL FILTER

Implementation of the second spatial filter is essentially identical to that of the first, the only difference being that the highest weather level is always selected, i.e., the WWW parameter value is always 9.

D.2.12 OUTPUT FORMAT

Emulation output data are stored in polar form. Radial resolution of the output data is 0.5 nmi, and azimuthal resolution is 1.4 degrees.

In addition to the final product (the output from the second spatial filter), products from two intermediate stages (the temporal filter and the first spatial filter) are also stored in separate output files.

All output data can be displayed in numerous ways. All six NWS levels can be displayed on a single image. Alternatively, any two levels can be shown in either discrete or summation mode.

APPENDIX E

MIT C-BAND PENCIL-BEAM RADAR SYSTEM OVERVIEW

E.1 INTRODUCTION

This appendix provides a general description of the MIT C-band Doppler weather radar system fielded in Huntsville AL during 1987 and 1988. The MIT radar collected volume-scan data for use in the assessment of ASR-9 weather channel performance. MIT radar data was used to simulate the ASR-9 weather channel output and to provide volume reflectivity data for direct comparison to ASR-9 weather channel products.

E.2 SYSTEM OVERVIEW

The MIT system (Figure E-1) is a pencil beam, pulsed Doppler radar that can measure, display, and record reflectivities and velocities of weather events in real time within a 226 km radius. This coherent-on-receive system employs a magnetron transmitter, independent log and linear receivers (for producing power and phase information, respectively), and an efficient Doppler signal processor to produce simultaneous reflectivity and mean velocity information on weather events. A host computer is interfaced to the signal processor for control of scan sequences and data storage. The large dynamic range of the log receiver, coupled with the sensitivity time control (STC) incorporated in the linear receiver, results in a large overall system dynamic range. General system characteristics are summarized in *Table E-1*.

E.2.1 TRANSMITTER

The transmitter (Figure E-2) consists of a coaxial magnetron whose output frequency is set to 5590 MHz. Automatic frequency control (AFC) on the magnetron is incorporated to compensate for any possible long term (greater than a few seconds) frequency drifts of the magnetron. Transmitter output signal power is approximately 160 kW peak (as measured at the 30 dB coupler) with a 1 μs duration. The transmitter is triggered by the signal processor at a PRF on the order of 1 kHz.

E.2.2 RECEIVER

The receiver (Figure E-2) consists of a log channel (non-coherent) and a linear channel (coherent). The two channels share a common RF section and are separated in the IF section. The log channel output voltage is proportional to the logarithm of the input power and is accurate to 1 dB over its 90 dB dynamic range. The signal processor measures this voltage to produce reflectivity information. The linear coherent-on-receive channel produces quadrature video information which is input to the signal processor to produce mean velocity estimates. An STC function is implemented via a variable gain IF amplifier to compensate for the range squared power loss of the weather return signal. This results in a linear channel dynamic range that is range independent. The 10 bit A/Ds used to sample the quadrature video signals allow for a 55 dB instantaneous dynamic range. The STC function is set to allow the processor's coherent channel to

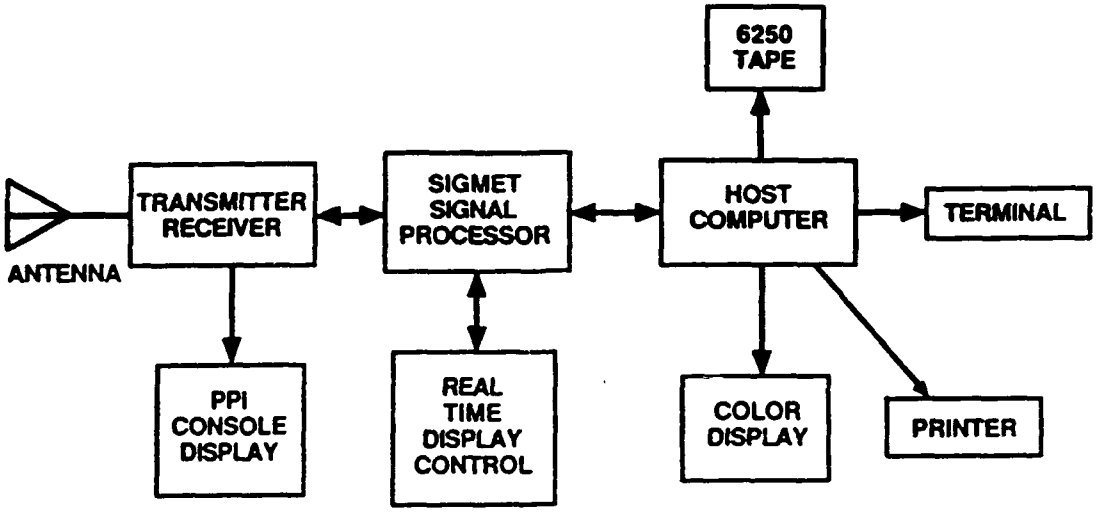

Figure E-1. MIT radar system block diagram.

TABLE E-1

MIT WEATHER RADAR PARAMETERS

Transmitter	
Type:	Coaxial magnetron (5570-5670 MHz, 0.0012 duty max)
Output Power:	160 kW peak (82 dBm)
RF Losses:	1.7 dB (coupler to antenna feed)
Pulse Width:	1 μs (0.5 μs alternate)
PRF:	924 Hz (1000 Hz max)
Antenna	
Type:	99 inch parabolic reflector/pencil beam
Power Gain:	41.1 dB
Polarization:	Horizontal
Beamwidth:	1.4 degrees (both axes)
Scan Rate:	25 s per PPI (160 range bins)
Receiver	
Type:	Log/linear coherent-on-receive
STALO:	5620 MHz crystal controlled
COHO:	30 MHz phase locked
Noise Figure:	6 dB *(excluding waveguide losses)*
Sensitivity:	
	Log: -106 dBm
	Linear: -104 dBm
Dynamic Range:	
	Log: 90 dB
	Linear: 106 dB (55 dB for A/Ds)
Weather Dynamic Range:	0 to 55 dBZ nominal
STC Function:	Inverse range squared
Bandwidth:	1 MHz (at video)
Clutter Rejection:	30 dB max
Processor	
A/Ds:	
	Log: 8 bit (0.344 dB per LSB)
	Linear: 10 bit (limits dynamic range to 55 dB)
Range Resolution:	1/4 km, 1/2 km, 1 km
Range Coverage:	40 km, 80 km, 160 km (160 range bins)
Processor Time:	
	64 point FFT: 101 ms (226 bins)
	64 point FFT: 66 ms (160 bins)
	Absolute min: 35 ms
Degrees per CPI:	1.4 degrees nominal (256 degrees per PPI)

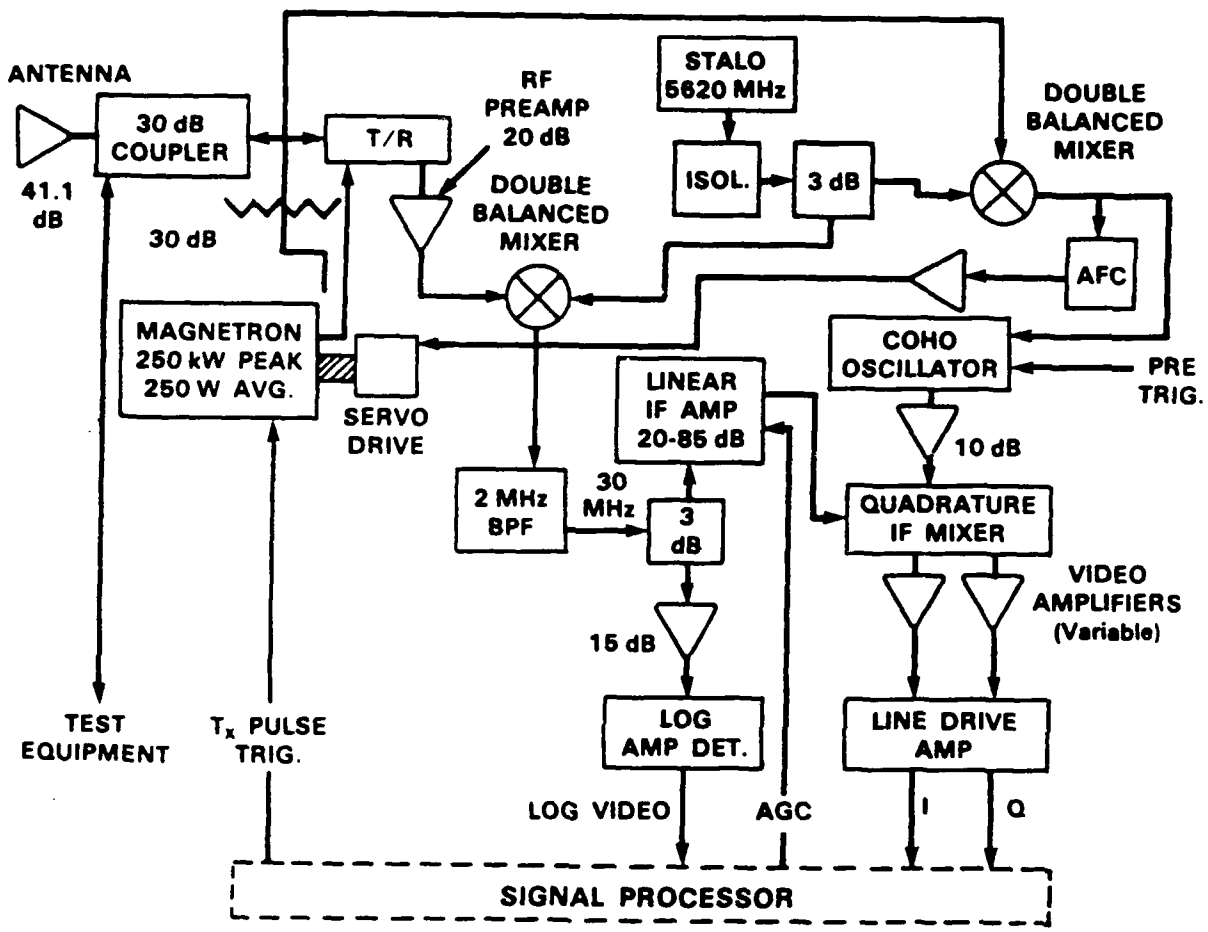

Figure E-2. MIT radar front end block diagram.

measure velocity for weather events having reflectivities between 0 and 55 dBZ.

E.2.3 SIGMET SIGNAL PROCESSOR

The signal processor consists of two parallel processing channels, one using information from the log channel and the other using information from the linear channel. The end product of the log processing channel is reflectivity in dBZ while the end product of the linear processing channel is mean velocity and spectral width in meters per second. A complete description of the signal processor is given in *The Doppler Signal Processor User's Manual* by Richard E. Passarelli, Jr. (Sigmet, Inc., 1985).

The linear processing channel digitizes the I and Q voltage outputs of the quadrature video detector. The processor then performs a 64-point fast Fourier transform (FFT) for each range-azimuth cell. Frequency domain clutter filtering is performed by notching out several FFT points about the zero frequency line. The processor "fills in" the deleted points by interpolation based on the information contained in the FFT points closest to the notch area. The processor performs an inverse FFT and estimates mean velocity using a pulse pair algorithm.

Two byproducts produced by the linear processor on a cell-by-cell basis are a signal-to-noise ratio (S/N) estimate and a clutter to signal ratio (C/S) estimate. The S/N information is typically used to reject those data where the signal strength is below or near system noise. Lincoln Laboratory performed its own S/N thresholding in post processing. Thus, the processor's S/N threshold is normally deactivated during data collection. The C/S information is typically used to reject those data where the signal power is below or near the stationary clutter power. If, in a particular cell, the C/S is greater than 25 dB (the clutter rejection capability of the MIT system), that cell is flagged as containing bad data. The linear channel also uses the C/S information to calculate a correction factor which it subtracts from the log channel reflectivity measurement to yield a reflectivity estimate based on weather echoes only.

The log processing channel digitizes and averages 64 samples of the log video detector output voltage. Using a preprogrammed equation that is a function of the digitized measurement of the log detector output voltage and range, the log processing channel calculates the weather reflectivity. The log processing channel incorporates a noise threshold which is typically set so that system noise will not be interpreted as a signal. The log channel reflectivity measurement has no clutter rejection. Thus, its output consists of a measurement including both clutter and signal. As mentioned above, one of the byproducts of the linear channel velocity calculation is a measure of clutter power relative to signal power which is used to subtract the clutter power's contribution from the log channel reflectivity estimate.

E.2.4 OVERALL SYSTEM PERFORMANCE

Assuming 64 pulses were used by the signal processor and assuming a nominal weather spectrum width of 3 meters per second, the equivalent number of independent pulses was on the order of 35.[1] This resulted in an expected weather reflectivity estimate standard deviation of about 1 dB.[2] There was an additional 1 dB error on the reflectivity estimate due to the linearity limitation of the log video detector. Therefore, the accuracy of the reflectivity estimate was expected to be on the order of 2 dB. The error on the velocity estimate was expected to be on the order of 0.4 meter per second.[3] Clutter suppression measure 30 dB out to 4 km, degrading to 24 dB at 17 km. Range dependence of clutter rejection was attributed to the time dependence of COHO phase jitter.

---

[1] R. J. Doviak and D. S. Zrnic, DOPPLER RADAR and WEATHER OBSERVATIONS, Figure 6.3c, Academic Press (1984).

[2] See Figure 6.2b, *ibid.*

[3] See Figure 6.6, *ibid.*

APPENDIX F

The FAA - Lincoln Laboratory ASR-9 Radar Emulation Facility (FL-3)

The FAA - Lincoln Laboratory ASR-9 radar emulator (FL-3) was built in 1986 for collecting raw (I and Q) radar data for a variety of studies. The predominant use of the system has been in the collection of data on severe weather conditions which has been used for the verification of the ASR-9 weather channel, and to provide data for use in determining the feasibility of using the ASR-9 as a sensor for the detection of windshear and microbursts.

The FL-3 radar is built from stock ASR-8 radar components, commercial computer equipment and custom interfaces designed and built at Lincoln Laboratory. Figure F-1 shows the system in block-diagram form. The following paragraphs describe the major functional components.

F.1 TOWER, ANTENNA, TRANSMITTER AND RECEIVERS

The antenna, rotary joint and tower are all standard ASR-8 components. The antenna produces a cosecant-squared beam similar to the ASR-9 antenna. The antenna has two feed horns which produce a high-beam pattern and a low-beam pattern. These beams are displaced 3.5 degrees in elevation. The antenna rotates at 12.5 rpm and is mounted on a 57 foot tower. A motorized lead screw has been added to the antenna mount to allow the antenna elevation to be set to either -1.0 or 0.0 degrees above the horizon while the antenna is rotating.

FL-3 uses a modified ASR-8 transmitter. The ASR-8 transmitter operates in S-band (2700-2900 MHz) and produces 1.1 Megawatts peak at the antenna. The transmitted pulse width is 600 nanoseconds, and the pulse repetition rate is adjustable (under computer control) between 650 and 1220 Hz. The diode-bridge based core-bias power supply has been replaced with a low-noise switching power supply, and the klystron filament supply has been replaced with a Lincoln built supply which switches the filament off during the high-voltage pulse. Both of these modifications were installed to reduce 60Hz noise components in the transmitted signal. The system uses a pair of identical receivers which allow simultaneous reception of both high and low beam signals. The receivers use standard ASR-8 components from the waveguide down to the IF output stage. The IF outputs and ASR-8 COHO oscillator output are supplied to a pair of Lincoln built synchronous receivers. The in-phase and quadrature (I and Q) outputs of both receivers are passed to four 12-bit A/D converters which are sampled at 1.25 MHz. This provides a range gate spacing of 120 meters.

F.2 RADAR CONTROLLER

FL-3 radar timing is controlled by a Lincoln built timing and data collection controller. This device supplies all of the necessary triggers to the transmitter to emulate the block-staggered PRF operation of the ASR-9 radar. It is also capable of operating

the radar ir constant PRF mode. The radar controller provides the digital control signals to the programmable STC attenuators at the receiver front-ends. All of the radar controller functions are programmable and are setup by the system control computer. The controller also collects ancillary information regarding system operation which is passed on to the digital recording system. This information consists of radar power output, satellite time-of-day clock, current PRF, antenna position, pulse location within staggered block, etc. A complete set of this ancillary information is passed to the digital recording system along with the I and Q data for each transmitted pulse from the radar.

F.3 DIGITAL RECORDING SYSTEM

The digital recording system is built primarily from commercially available computer equipment and is centered around an Aptec 2400 Input/Output computer (IOC). The IOC contains two megabytes of memory on a high-speed (24 megabytes per second) I/O bus. The radar controller, a high-density digital tape drive, a pair of standard 9-track tape drives and a DEC MicroVAX computer are each connected to the IOC via individually programmable I/O processors which all have access to the IOC memory over the high-speed bus. The digital recording system is capable of recording all of the digitized I and Q data generated by the radar and the ancillary information collected by the radar controller on the high-density digital tape drive. This corresponds to a transfer rate of approximately 10 megabytes per second when recording I and Q from both upper and lower beams to the full 60 nautical mile range of the radar. The data stored on the high-density drive can be played back at a much lower data rate for the purpose of transcribing the data to 9-track tape for use on standard data processing computers.

F.4 SYSTEM SOFTWARE

The menu-driven software in the system control computer controls all of the functions of the radar and the recording system. Radar operators select PRF, stagger mode and STC parameters which are then loaded into the radar controller. Operators also control the amount of data being recorded on the high-density recorder (either or both receivers, range extent, etc.) from the system computer terminals. All operator commands are logged in a database in the system computer which maintains a complete record of of all of the recording sessions. The database system also records comments made by the operators while data is being recorded. These comments usually include information obtained from outside sources as to potential mic[illegible] and gust-front activity. When a data request is made, the operators use this database system to locate the correct high-density tape and the location on the tape that corresponds to the date and time for the data request.

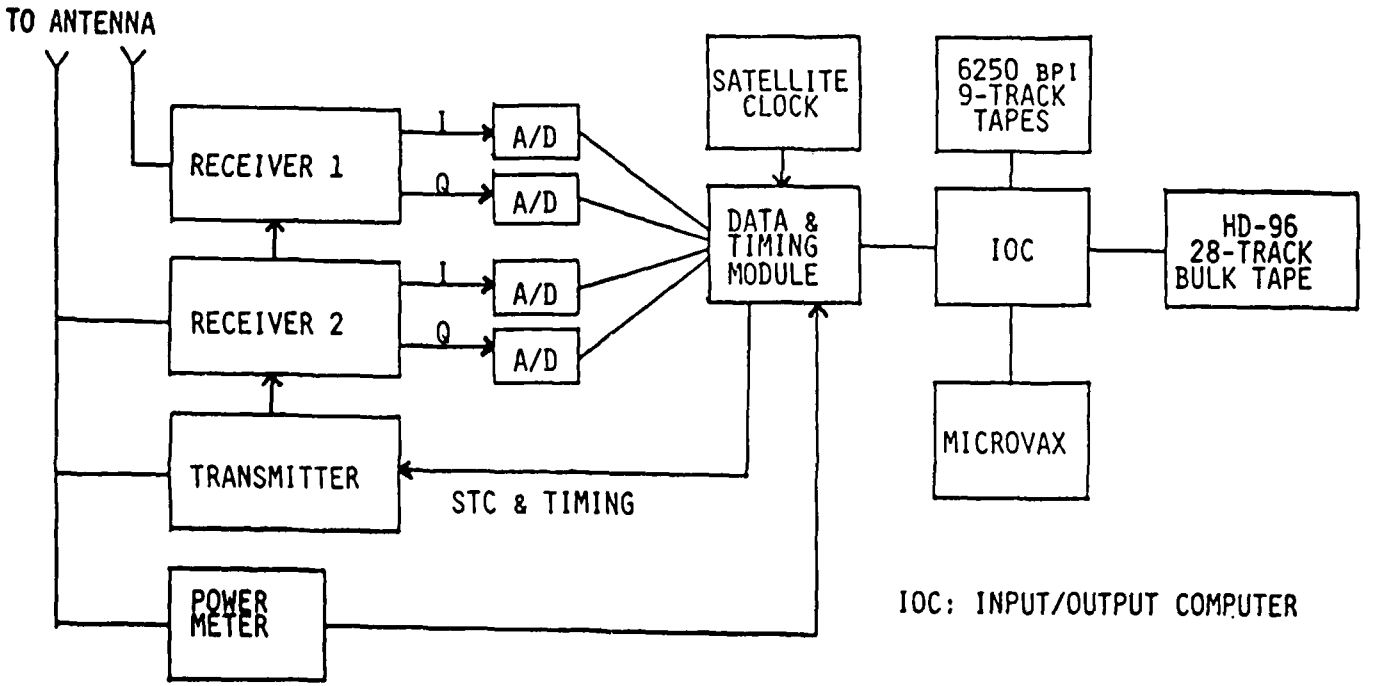

Figure F-1. FL-3 system block diagram.

APPENDIX G

OVERVIEW OF CURRENT NWS RADARS AND NEXRAD

The current NWS radar system inventory consists of both C-band (WR-74) and S-band (WR-57) pencil-beam radars. There are several features listed below of these radars (including the NWS radar at the Huntsville airport) that make them undesirable for use in the assessment of the ASR-9 weather channel and, for that matter, make them undesirable for measurement of terminal area weather for ATC.

- Antenna scanning primarily limited to horizon scans
- Lack of ground clutter rejection
- Data update time of approximately 5 minutes due to data transmission

The NWS pencil-beam antenna permits examination of a narrow elevation sector of a weather event in a single PPI scan. The NWS radar must employ many PPI scans at incremental elevation angles to cover the entire volume of a storm. However, its scanning strategy consists of near-horizon PPI scans with relatively infrequent range-height indications (RHI), i.e., vertical scans through areas of interest. This scanning strategy prevents the NWS radar from covering frequently the weather conditions from ground level to 35,000 feet. For example, Figure G-1 shows an RHI plot of a storm with its core aloft and another storm with its core on the ground. The NWS radar horizon scan would not see the storm aloft.

The present NWS radar systems have no clutter rejection capability. This prevents the measurement of weather reflectivity when the clutter echo is greater than, or equal to, the weather echo. The return from ground clutter is greatest when the NWS radar antenna scans the horizon -- its normal mode of operation. The NWS radars typically have clutter return levels (Figure G-2) comparable to operationally significant weather reflectivities within 30 km (15 nmi) of the NWS site. Localized clutter often limits the use of NWS reflectivity data near the airport.

The NWS radar has a slow azimuthal scan rate typical of weather radars. The relatively slow scan rate, although resulting in more time on target and thus reducing the variance of the reflectivity estimate, requires more time (approximately 30 seconds) to cover a 360-degree PPI. The NWS mode of data transmission to the end user (e.g., ATC personnel) further reduces the weather PPI update rate to about once every 5 minutes, a rate that may be too slow to allow ATC tactical use of the data in the case of rapid storm growth and movement.

In the future, the NWS will replace the existing radar with new systems, called NEXRAD (Next Generation Weather Radar). A most significant improvement will be the addition of clutter rejection capability. NEXRAD will provide information on storm height, gust front, and other parameters of interest in strategic ATC operations. However, the scanning strategy is expected to result in update times on the order of 5 minutes, with another 5 minutes for data processing. Therefore, NEXRAD will not be able to produce the timely weather information needed for tactical use in the terminal area.

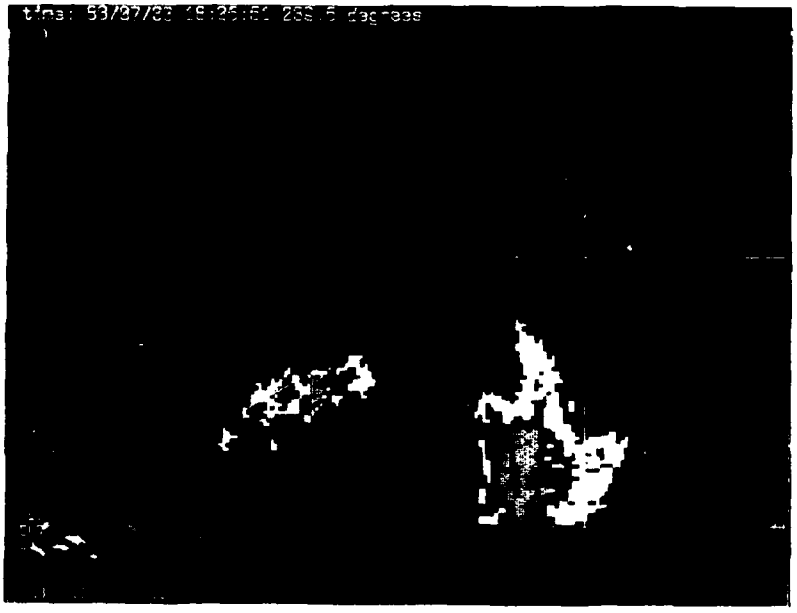

Figure G-1. RHI taken through a convective storm developing aloft and a convective storm extending from the ground up to 12 km. The NWS radar horizon-scan may not detect the presense of the storm aloft until it falls within its view.

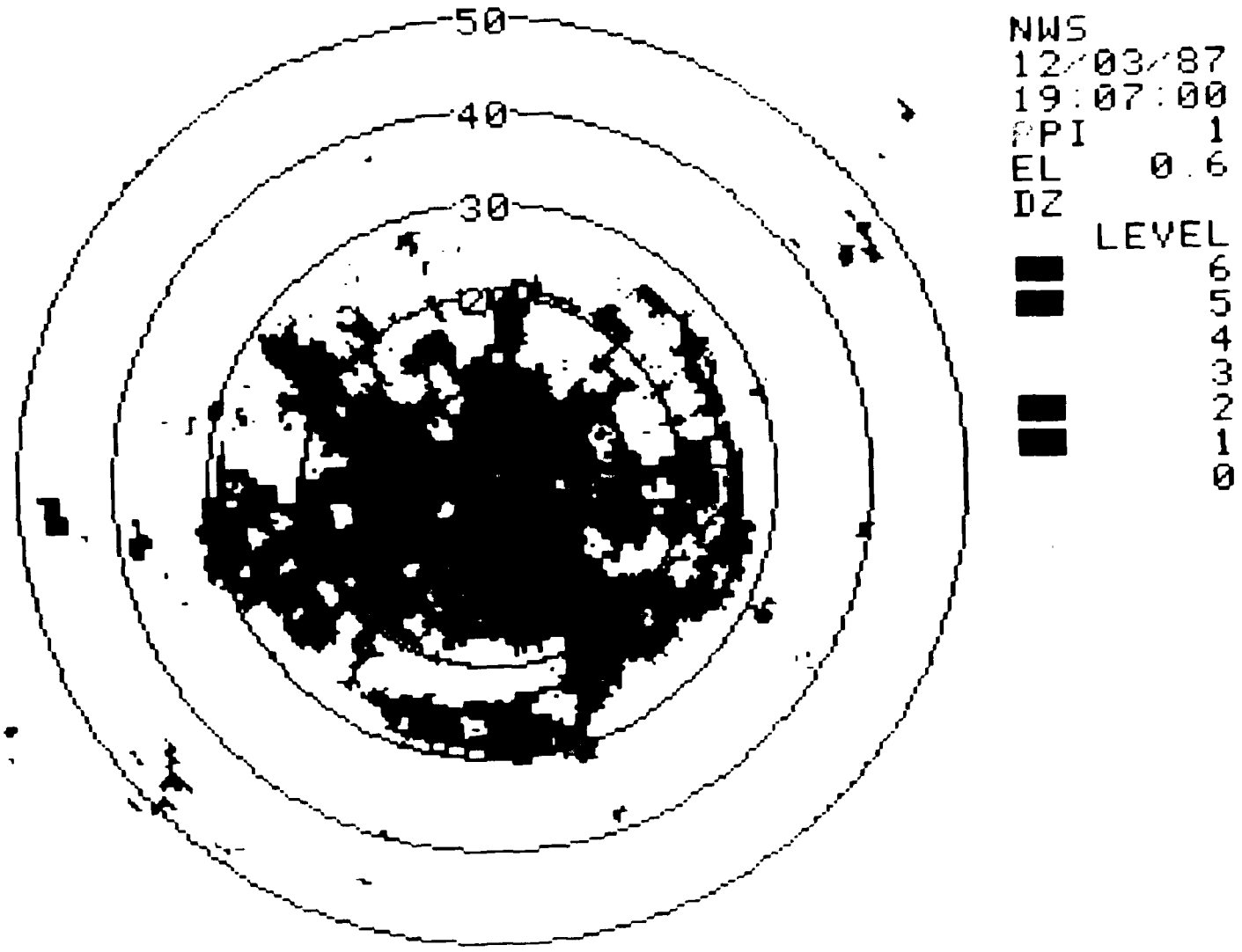

Figure G-2. Clear air ground clutter observed by the Huntsville NWS radar system. (Fall 1987)

APPENDIX H

EFFECTS OF DEPOLARIZATION ON ASR-9 WEATHER CHANNEL PRODUCTS

To investigate the effect that non-spherical scatterers may have on the reflectivity estimate measured by the ASR-9, the case of a circularly polarized wave reflected off of a single raindrop was considered. It was assumed that the rain drop's horizontal dimension was larger than its vertical dimension (i.e., elliptical in shape). Figure H-1 contains a plot of the ratio of horizontal to vertical back-scatter cross sections σ_H/σ_V for an oblate spheroidal scatterer as a function of the ratio of its width to thickness, or axial ratio, b/a. Note that, when approaching the breakup limit, the width to thickness ratio is about 2:1. Note also that this occurs for a differential reflectivity, Z_{DR}, of about 6 dB; i.e., the horizontally polarized reflectivity measurement is 6 dB higher than the vertically polarized reflectivity measurement. This is also supported by Bringi and Seliga [9] who found that Z_{DR} in rain can vary between -3 and 6 dB, but typically lies between 0 and 5 dB.

Equation (1) below is a simplified version of a relationship derived by Sichak and Milazzo [10] for the polarization loss factor (PLF) for a CP antenna receiving the same sense elliptically polarized wave whose vertical to horizontal electric field intensity ratio is a/b. It is assumed that there is no cross polarization energy present.

$$PLF = \frac{1}{2}\,\frac{(a/b+1)^2}{((a/b)^2+1)} \qquad (1)$$

The assumption made that the electric field intensity ratio is equivalent to the ratio of the vertical and horizontal dimensions of an elliptical scatterer radiated with a CP signal. [11] Substitution of a/b equal to 2 into Equation (1) yields a polarization loss factor of 0.9, or about 0.5 dB. Clearly, the effect of elliptically shaped scatterers does not result in significant errors to the CP reflectivity estimate, especially when considering that the estimate is so coarsely quantized as in the ASR-9.

Note from Equation (1) that the maximum PLF is 3 dB. In other words, the vertical component of reflectivity can be zero, and the CP weather channel will underestimate the true reflectivity by only 3 dB. This brings to light a potential problem with the use of vertical polarization (VP) by the ASR-9. When horizontal polarization (HP) and VP reflectivity measurements on an elliptical scatterer are compared to reflectivity based on an equivalent spherical scatterer with equal area, horizontal (vertical) reflectivity measurements tend to overestimate (underestimate) the reflectivity of the equivalent sphere. Furthermore, the HP measurement is closer to the reflectivity of the equivalent sphere than the VP measurement. [12] This is attributed to the scatterer being elliptical with the major axis in the horizontal plane. Therefore, when operating with VP, the weather channel may have significant errors, depending on the ellipticity of the scatterers. However, the vertical integration of the wide vertical beam may tend to offset any errors due to the ellipticity.

Assuming that the ASR-9 will use CP for high levels of weather (e.g. Level 3 and above, where elliptical scatterers are more prominent) and VP for low levels of weather (say Level 2 and below, where spherical scatterers are more prominent), then the reflectivity errors due to polarization loss should not be significant. There may be times when the radar is operated with VP and there are a few intense weather cells that are potentially hazardous to aircraft, but not spatially extensive enough to warrant switching to CP. It is quite possible that the use of VP will result in a level being underreported by one level, especially for higher reflectivities (recall from Section 1.2 that the higher levels cover small increments of reflectivity). One solution, if indeed the cell is of limited spatial extent, may be to vector the aircraft around the storm cell and, if there is doubt, switch to CP.

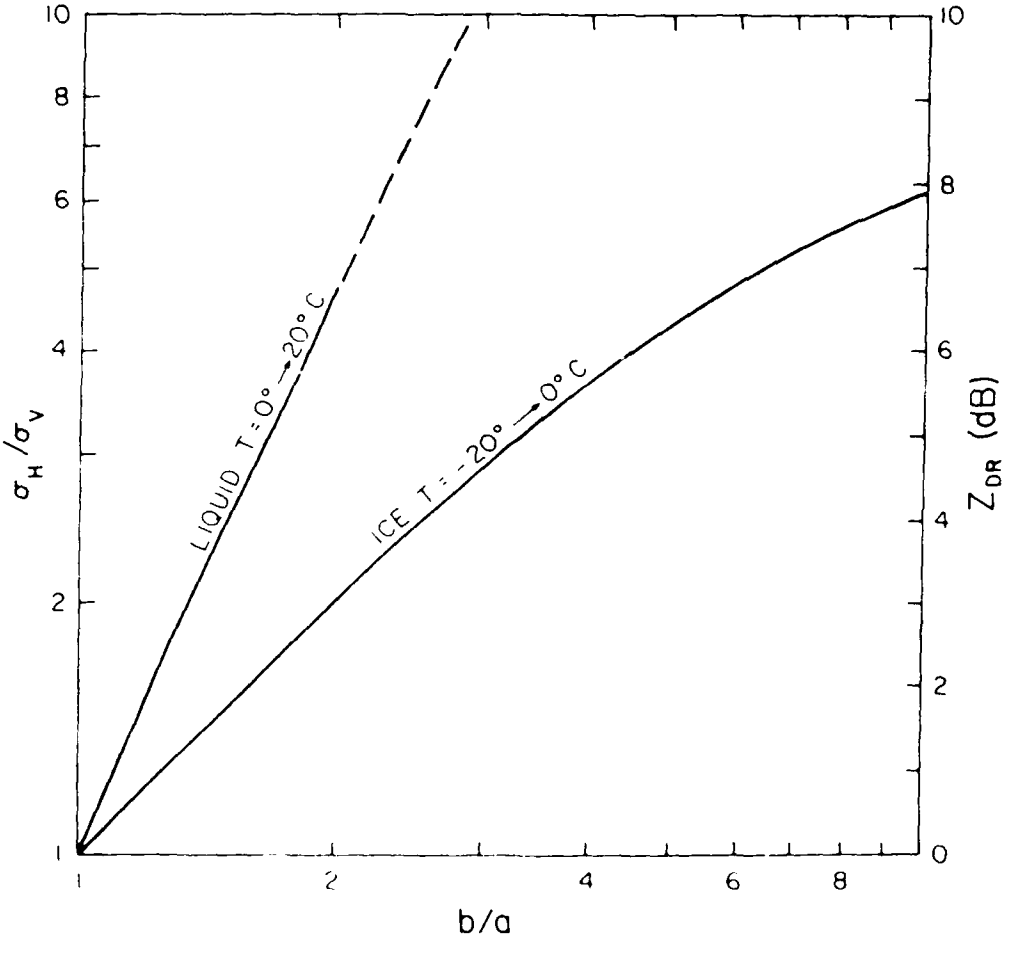

Figure H-1. The ratio of backscatter cross sections σ_H/σ_V for oblate spheroidal scatterer as a function of its axis ratio. (The dashed portion of the line for a liquid is at ratios where drops are unstable. However, it can be used for water-coated ice.) [13]

APPENDIX I

METHODS FOR FILTERING CLUTTER AS A RESULT OF ANOMALOUS PROPAGATION

I.1 INTRODUCTION - THE PROBLEM

Ground-based radars occasionally produce significant ground clutter returns from areas where there is usually little to no clutter and often from areas where the antenna beam should be well above the horizon. Anomalous propagation (AP), or ducting, results from the bending of the radio waves toward the earth due to a decreasing index of refraction with increasing altitude [8]. For the index of refraction to decrease with height, the temperature must increase with height (e.g., temperature inversion) or the water-vapor content must decrease with height, or both. Therefore, ducting occurs when the upper level air is exceptionally warm and dry in comparison with the air near the earth's surface [9]. Three typical meteorological conditions that cause ducting are described in the table below.

CONDITION	OCCURRENCE
Radiation of heat from the earth (land) on clear nights.	Summer when ground is moist, night-time.
Movement of warm dry air, from land, over cooler bodies of water (ocean).	Either night or day, mostly late afternoon and evening.
Diverging downdraft under a thunderstorm.	Short-lived (one hour).

Because water-vapor gradients are more likely to produce ducting than temperature gradients, ducting is generally more prominent over oceans in warm climates. However, since land tends to change temperature more rapidly than the ocean, there is more variability in over-land ducting, making its prediction (and compensation) more difficult. There are fewer cases of AP associated with thunderstorms because thunderstorms tend to "mix-up" the atmosphere, making conditions unfavorable for AP. Therefore, AP is not likely to occur during bad weather, but is most likely to occur during fair weather conditions, when weather channel information is not of critical importance for ATC. This allows some ability for the forecasting of AP and for operational suppression of the resulting echoes.

In Huntsville, the FAA has observed AP returns on the ASR-9's weather display during the night and early morning hours when there was no weather present. The current ground clutter suppression technique does not allow the weather channel to filter AP-based ground clutter returns. The weather channel uses a clear-air clutter map to determine, for each range-azimuth cell, which of four clutter filters to select (see Section 1.2). When there is no AP, the clutter map accurately represents the location and magnitude of the stationary clutter. However, when conditions are favorable for AP, the antenna beam is bent toward the earth, causing stationary surface clutter to be detected

by the radar. This AP surface clutter is strong because the radio waves bent by the inversion are attenuated much less than the free-space loss factor. The clutter map does not indicate the presence of the AP-based clutter and hence the weather processor chooses the all-pass filter, allowing the AP clutter to pass. Further, the smoothing stages of the weather processor tend to make the AP clutter appear as a valid weather echo. For example, Figure I-1 shows the ASR-9 weather channel output recorded on 18 August 1988 when there was actually no weather present in the radar's field of view.

Two methods are considered herein that deal with the AP problem, specifically for the ASR-9 weather channel. These methods, attempt to remove the AP, but require changes to the weather channel's processing algorithms.

I.2 CLUTTER IDENTIFICATION BASED ON SPATIAL CHARACTERISTICS

Goodchild (FAA) pointed out that AP clutter returns on the normal video PPI displayed a larger spatial variance than that of weather (see Figure I-2) He suggested that the existing weather channel's spatial smoothing parameters be adjusted to exploit this difference to filter AP. With this scheme, little or no hardware modification would be required.

To evaluate this approach, FL-3 fan beam data was used to emulate the ASR-9 weather output for both weather and AP events while varying the M of 16 and X of 9 spatial smoothing parameters [5]. The normal settings for M and X in the weather channel are 8 and 5, respectively. As these parameters are increased, echoes with large spatial variations will be suppressed relative to more homogeneous returns such as from weather. Consider setting M and X equal to 15 and 9 respectively. These settings require that 15 of 16 consecutive range cells and then 9 of 9 neighboring cells contain the same level in order to report a specific level. The ASR-9 weather channel reflectivity thresholds compensate for the biases introduced by spatial filters on the six-level reflectivity output. In terms of the weather channel, a bias is present when, given that the actual weather level is exactly between two adjacent reflectivity levels, there is not an equal (i.e., 50 %) probability for the weather channel to report either the higher or lower level. For example, if the average of the signal incident on the weather channel is exactly on the threshold between Levels 4 and 5, then it is desired that, after passing through the weather channel spatial filters, that there is equal probability of reporting a Level 4 or 5. To prevent the changed smoothing parameters from biasing weather intensity estimates, the weather level thresholds were adjusted downward.

Biases are introduced by the spatial filters because they are based on the median as opposed to the mean (average). If the probability distribution function of the signal was symmetrical about its mean (e.g., Gaussian), then the mean would be equal to the median value. However, the mean and median are not generally equal because the signals of interest tend not to have symmetrical probability distribution functions. For example, assuming a signal with a Rayleigh distribution function and a mean that is exactly at the threshold between two adjacent NWS levels is first input to the 8 of 16 median, then to the 5 of 9 spatial filter, there would be close to a zero percent probability that the level above the threshold would be reported and close to a 100 percent probability that the level below the threshold would be reported. i.e., there is a bias toward

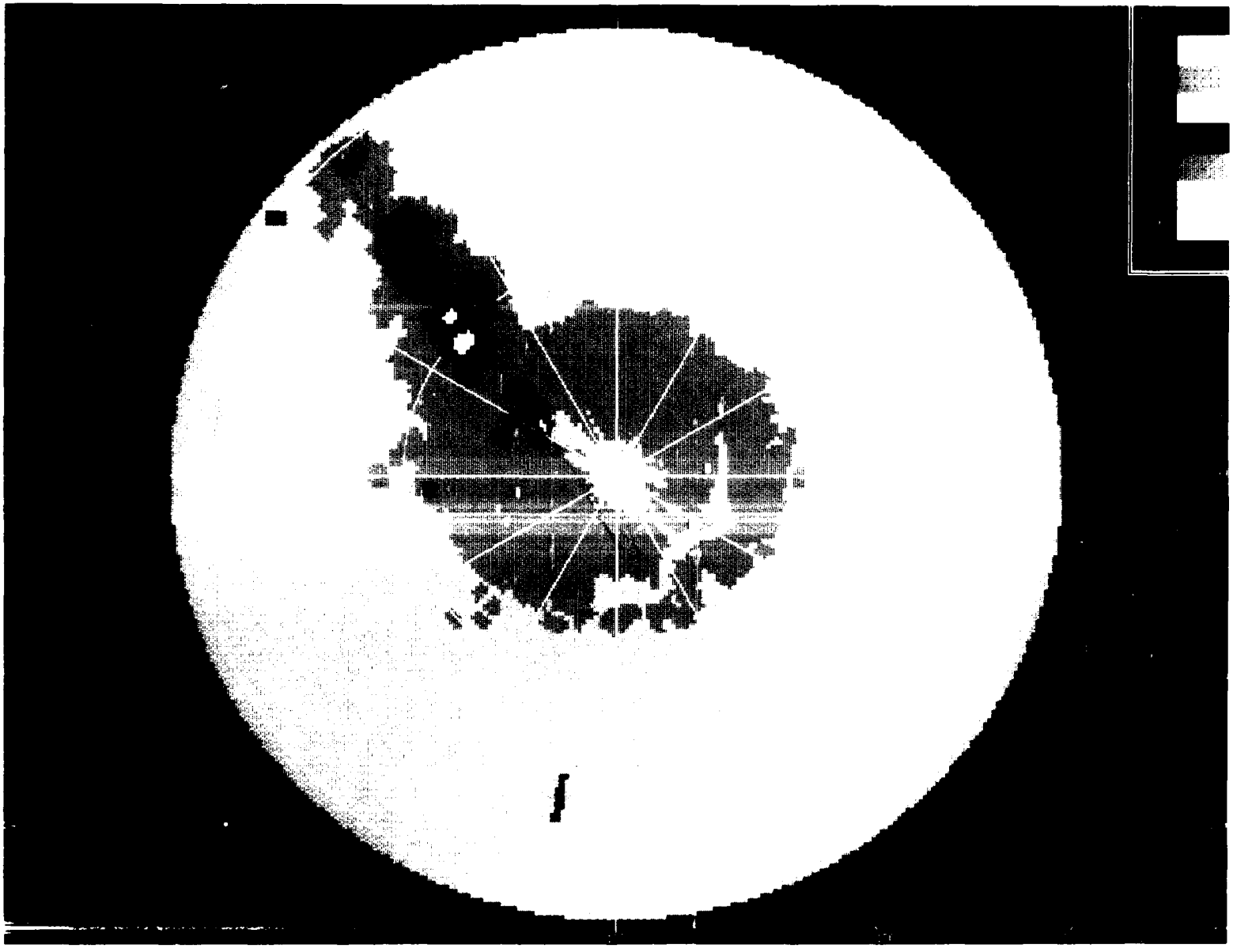

Figure I-1. ASR-9 weather channel six-level output recorded during anomalous propagation event on 18 August 1988.

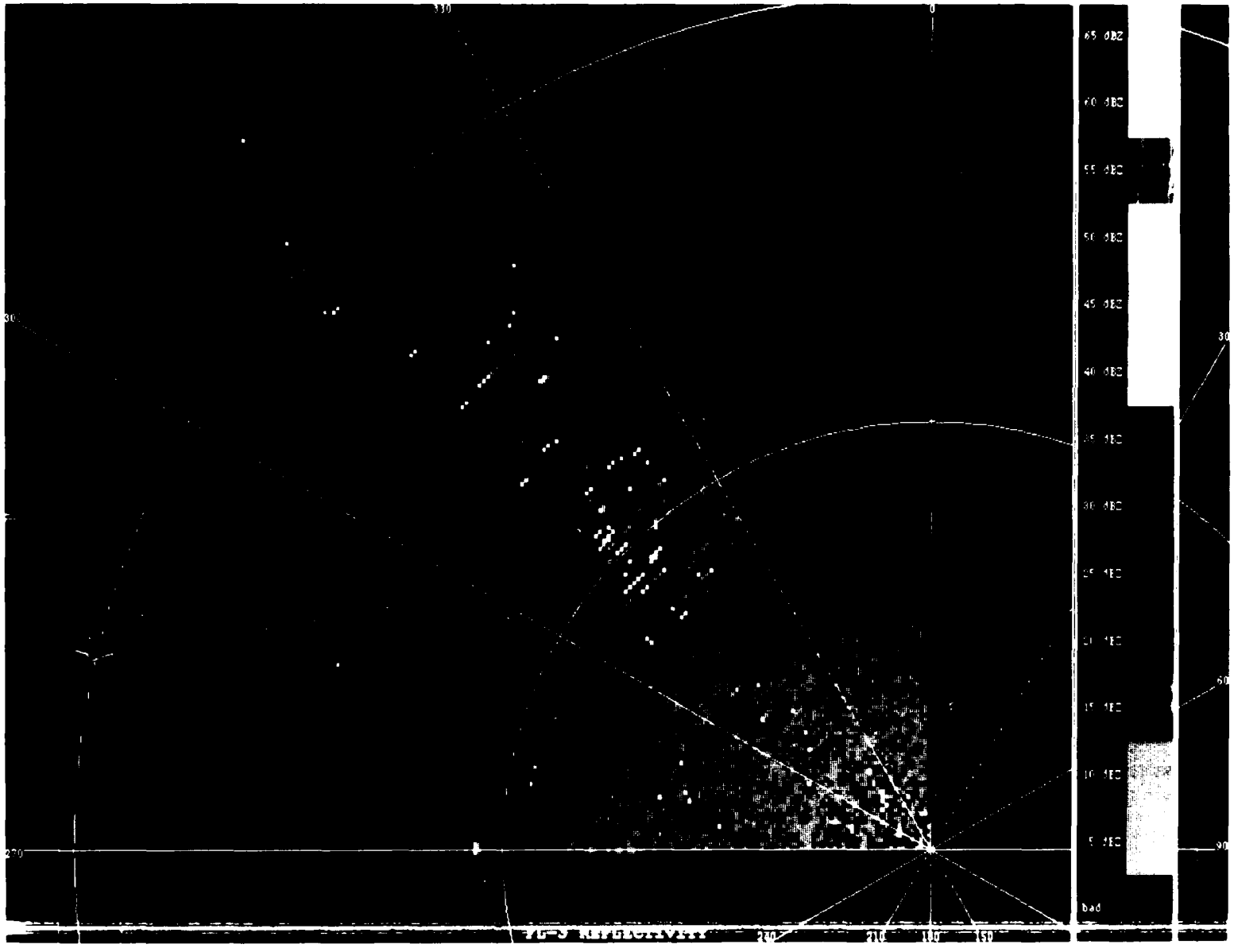

Figure 1.2 - 11.3 raw reflectivity output for same event as Figure 11.2 showing spatial variance of anomalous propagation

lower levels.

Table I-1 contains the adjustments (in dB) to the NWS thresholds that are required to result in the 50 percent probability criterion described above. They are tabulated as a function of M of 16 and X of 9. Note that, for nominal operation of the weather channel (i.e., 8 of 16 and 5 of 9), lowering the thresholds by about 2.1 dB is required. The threshold offsets provided in Table I-1 were used to offset emulation reflectivity data for a particular M and N chosen.

Effect on AP: Figure I-3a shows the ASR-9 weather channel emulation based on FL-3 data recorded during an AP event on 25 August, 1988. Note that the AP causes significant areas of false precipitation as high as Level 4. Figure I-3b shows the emulation output for the same AP event, but with M and X equal to 15 and 9 respectively. Clearly, the result is a significant reduction in the total area of AP, but some Level 2 and 3 remain.

Effect on weather: Figures I-3c and I-3d show the emulation output, based on FL-3 data recorded during the occurrence of weather, for normal spatial smoothing parameter settings and for values of M,X equal to 8,5 and 15,9 respectively. Note that there is a significant loss of Level 1 and Level 2 reflectivity. From Table I-1, it is clear that much of the apparent loss of AP is directly attributable to a loss in sensitivity associated with the adjustment made to the reflectivity thresholds, not so much due to the smoothing itself.

I.3 CLUTTER IDENTIFICATION BASED ON SPECTRAL CHARACTERISTICS

It was recognized that the Doppler spectrum of weather, as seen by an ASR, will normally be significantly different from that of clutter. Even though the mean velocity of weather and clutter can both be zero or near zero, the wide vertical beam of the ASR-9 antenna results in a spectrum width of weather greater than that of clutter. The existence of shear contributes to the widening of the spectrum width of weather observed by the ASR-9. Stationary ground clutter is illuminated by only the lower edge of the antenna beam and produces a spectrum width dependent on the antenna's azimuth beamwidth and scan rate. Figure I-4 shows examples of spectrum width for stationary (zero mean velocity) clutter, AP-caused stationary clutter, and stationary weather. The dashed-line spectrum is the theoretical spectrum width for stationary ground clutter assuming a Gaussian antenna beam and an antenna scan rate equal to that of the ASR-9 (12.5 rpm). Clearly, if one could measure the spectrum width on a cell-by-cell basis, one could distinguish between clutter and weather, and between AP and weather.

An attractive technique for the detection of signals with simultaneous low mean Doppler and low spectrum width makes use of the four existing clutter filters of the ASR-9 weather channel. These filters have maximum clutter attenuation factors between zero (all-pass) and 49 dB. The attenuation of a signal by a filter is a function of the filter impulse response, signal spectrum width, and mean velocity. Figure I-5 shows plots of the attenuation produced by the most severe filter as a function of mean velocity for various spectrum widths. Clearly, only low Doppler, low spectrum width signals are attenuated by large amounts. Thus, by simply thresholding the difference between the

TABLE I-1

ASR-9 REFLECTIVITY THRESHOLD ADJUSTMENTS AS A FUNCTION OF M AND X

M	X	ATTEN	1-CELL PROBAB.
3	1	3.369	0.1139
	2	2.830	0.1468
	3	2.460	0.1717
	4	2.143	0.1944
	5	1.843	0.2169
	6	1.534	0.2408
	7	1.191	0.2684
	8	0.763	0.3036
	9	0.089	0.3603
4	1	2.528	0.1670
	2	1.993	0.2055
	3	1.623	0.2338
	4	1.306	0.2590
	5	1.004	0.2837
	6	0.693	0.3095
	7	0.345	0.3387
	8	-0.088	0.3754
	9	-0.776	0.4333
5	1	1.774	0.2221
	2	1.233	0.2649
	3	0.858	0.2957
	4	0.535	0.3227
	5	0.226	0.3487
	6	-0.092	0.3757
	7	-0.448	0.4058
	8	-0.894	0.4431
	9	-1.604	0.5010
6	1	1.063	0.2787
	2	0.510	0.3248
	3	0.124	0.3574
	4	-0.209	0.3856
	5	-0.527	0.4124
	6	-0.856	0.4400
	7	-1.225	0.4704
	8	-1.688	0.5077
	9	-2.427	0.5645
7	1	0.369	0.3367
	2	-0.204	0.3851
	3	-0.604	0.4189
	4	-0.950	0.4477
	5	-1.281	0.4749
	6	-1.624	0.5026
	7	-2.010	0.5328
	8	-2.495	0.5695
	9	-3.272	0.6245
8	1	-0.330	0.3958
	2	-0.927	0.4459
	3	-1.346	0.4802
	4	-1.708	0.5093
	5	-2.056	0.5364
	6	-2.417	0.5637
	7	-2.824	0.5934
	8	-3.336	0.6289
	9	-4.160	0.6813
9	1	-1.051	0.4561
	2	-1.679	0.5070
	3	-2.121	0.5414
	4	-2.504	0.5702
	5	-2.873	0.5969
	6	-3.256	0.6235
	7	-3.689	0.6520
	8	-4.236	0.6859
	9	-5.118	0.7351
10	1	-1.813	0.5175
	2	-2.480	0.5684
	3	-2.951	0.6024
	4	-3.360	0.6305
	5	-3.756	0.6563
	6	-4.167	0.6818
	7	-4.633	0.7088
	8	-5.223	0.7405
	9	-6.179	0.7858
11	1	-2.640	0.5801
	2	-3.357	0.6302
	3	-3.865	0.6632
	4	-4.308	0.6902
	5	-4.737	0.7146
	6	-5.185	0.7386
	7	-5.693	0.7637
	8	-6.340	0.7927
	9	-7.392	0.8333
12	1	-3.565	0.6440
	2	-4.348	0.6925
	3	-4.905	0.7238
	4	-5.393	0.7491
	5	-5.867	0.7718
	6	-6.364	0.7937
	7	-6.929	0.8164
	8	-7.651	0.8422
	9	-8.834	0.8774
13	1	-4.643	0.7094
	2	-5.516	0.7552
	3	-6.142	0.7842
	4	-6.692	0.8072
	5	-7.229	0.8276
	6	-7.795	0.8469
	7	-8.442	0.8666
	8	-9.274	0.8885
	9	-10.647	0.9174
14	1	-5.974	0.7767
	2	-6.982	0.8185
	3	-7.712	0.8442
	4	-8.358	0.8642
	5	-8.993	0.8815
	6	-9.666	0.8976
	7	-10.441	0.9136
	8	-11.446	0.9308
	9	-13.125	0.9525
15	1	-7.791	0.8468
	2	-9.032	0.8825
	3	-9.944	0.9037
	4	-10.762	0.9195
	5	-11.574	0.9328
	6	-12.446	0.9446
	7	-13.461	0.9559
	8	-14.797	0.9674
	9	-17.075	0.9806
16	1	-10.898	0.9219
	2	-12.704	0.9478
	3	-14.079	0.9617
	4	-15.349	0.9712
	5	-16.643	0.9786
	6	-18.067	0.9845
	7	-19.773	0.9895
	8	-22.085	0.9938
	9	-26.186	0.9976

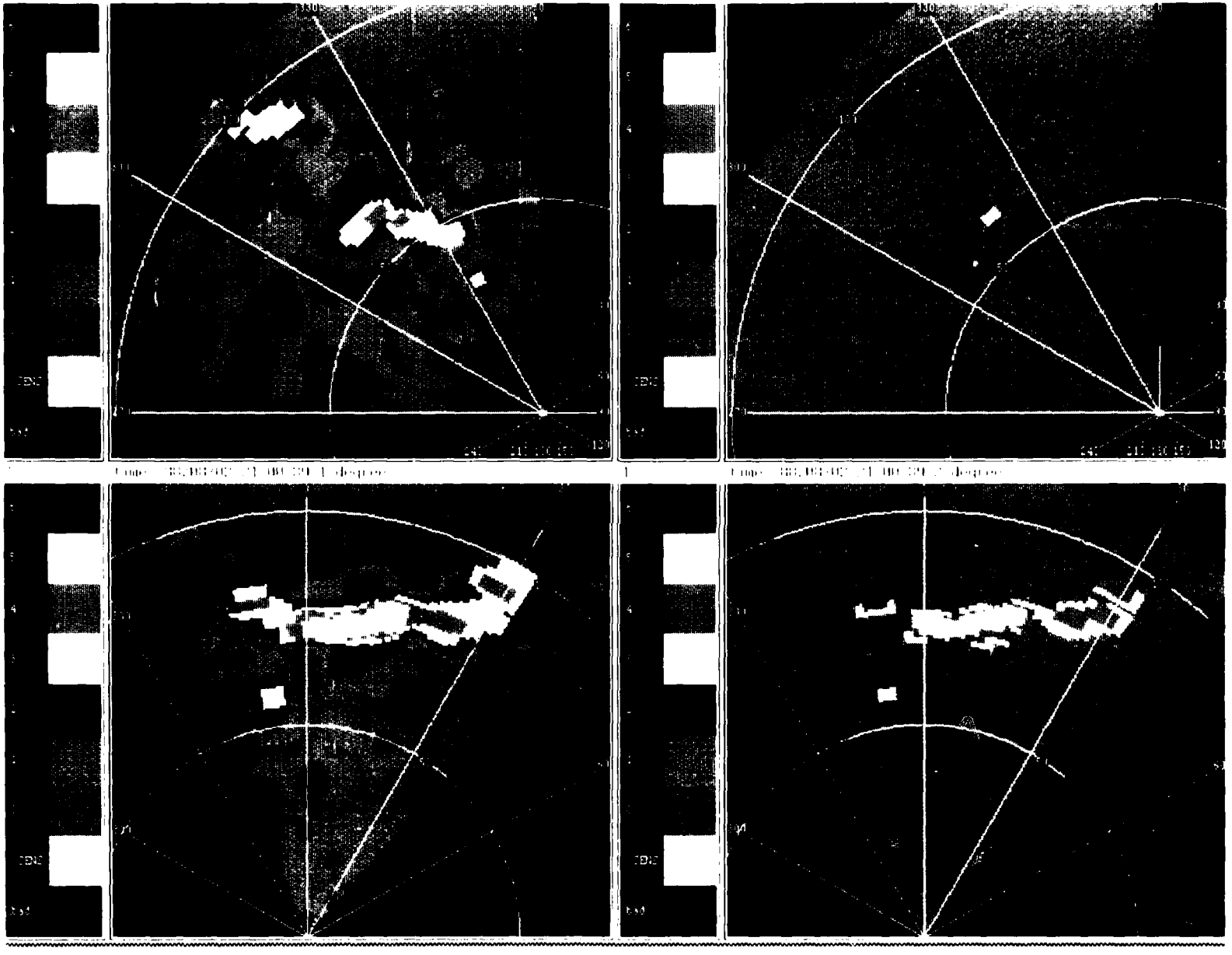

Figure 1-3. FL 3 based emulation of ASR 9, showing effect of varying smoothing parameters on both AP and weather. (a) AP, 8 of 16, 5 of 9 spatial filters. (b) AP, 15 of 16, 9 of 9 spatial filters. (c) Weather, 8 of 16, 5 of 9 spatial filters. (d) Weather, 15 of 16, 9 of 9 spatial filters.

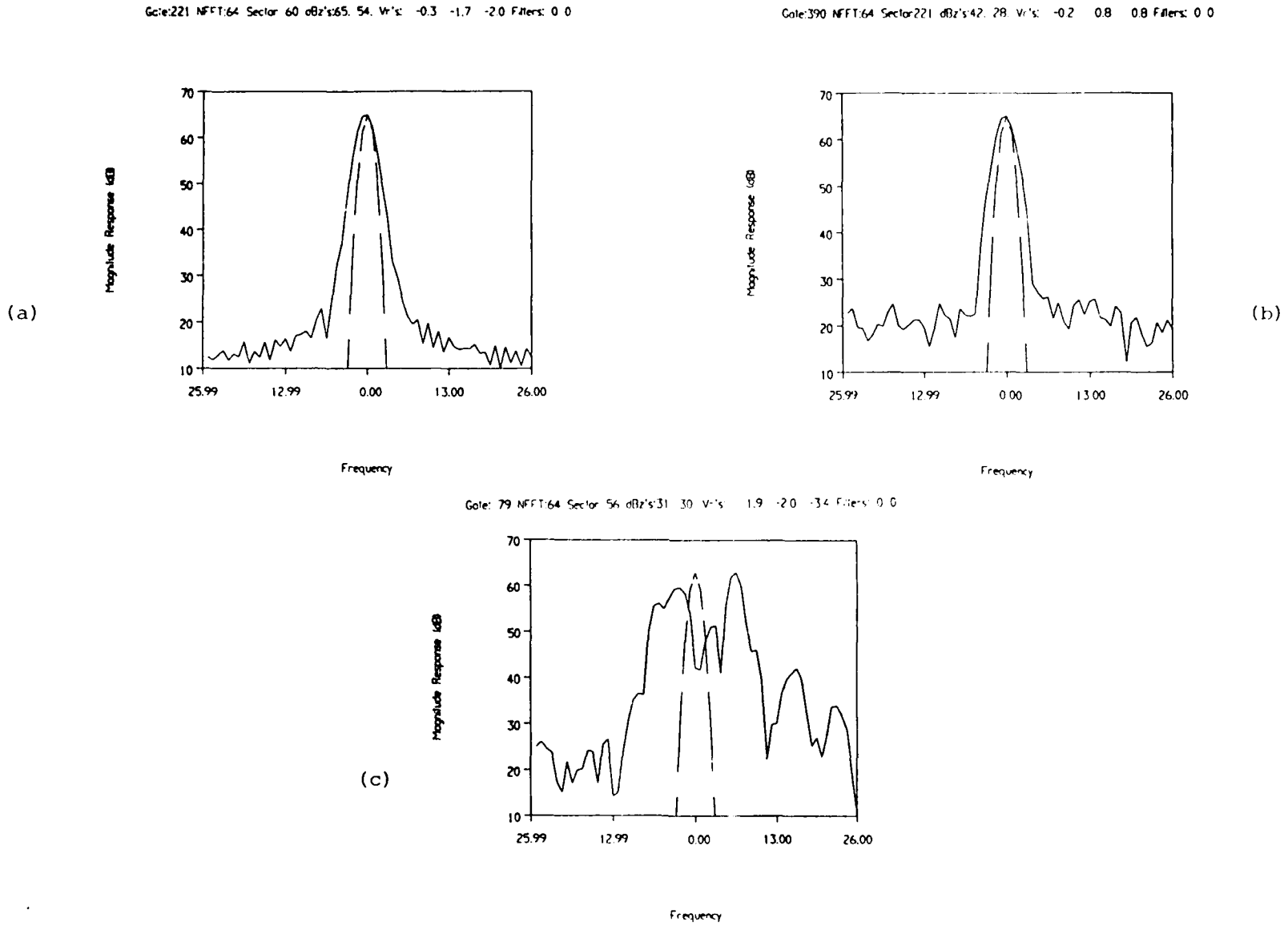

Figure I-4. Typical spectral characteristics of clutter, AP, and zero mean velocity weather; (a) Clutter spectrum, (b) AP spectrum, (c) Weather spectrum.

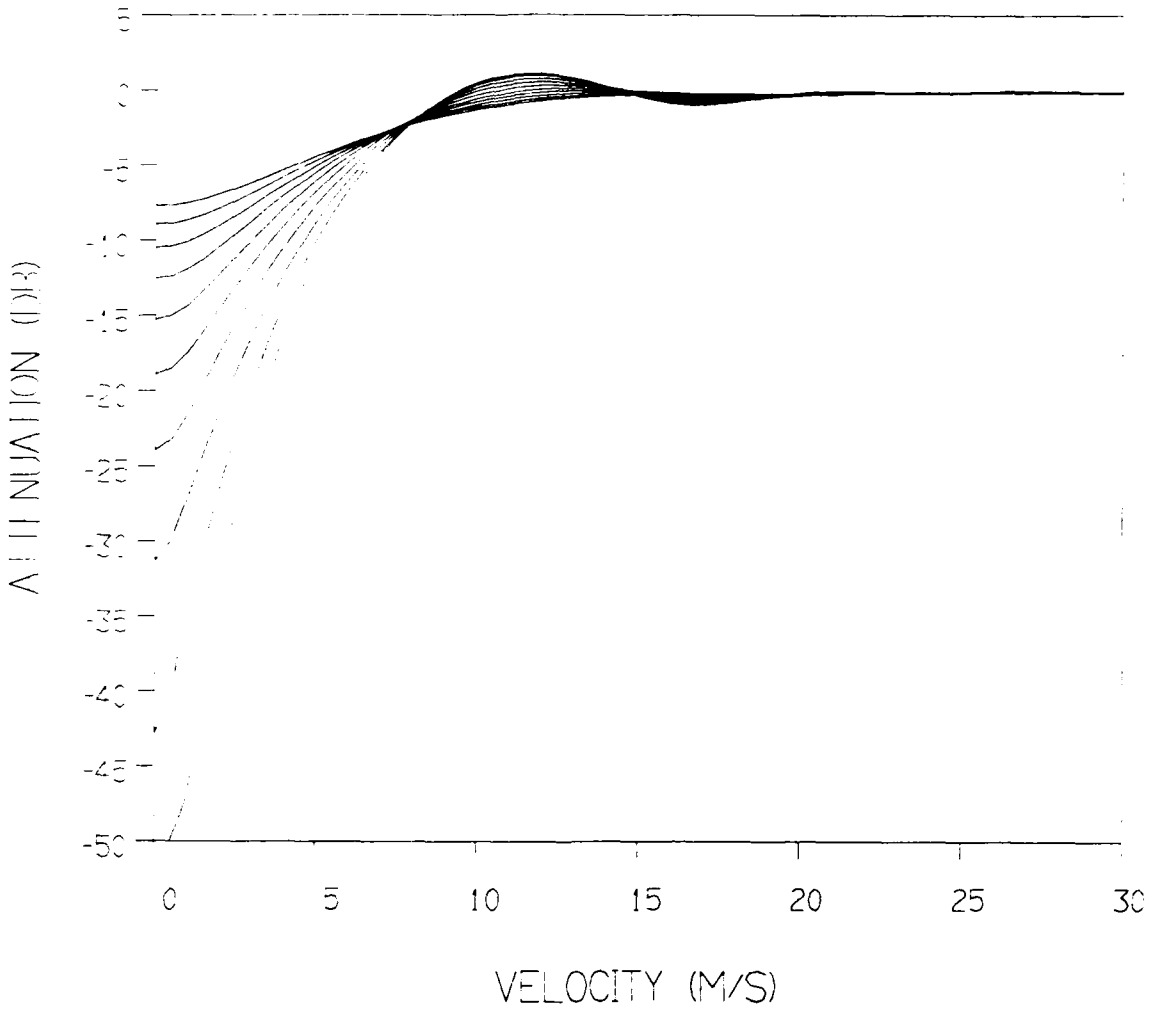

Figure I-5. Signal attenuation through the most attenuating ASR-9 clutter filter (No. 3) versus mean velocity for various spectrum widths.

all-pass filter and filter No. 3, one can detect and delete echoes with spectral characteristics indicative of ground clutter.

To test this technique, emulation software was used to generate products based on both weather and AP fan beam data. On a cell-by-cell basis, the output of the most attenuating clutter filter was compared to the output of the all-pass filter and the difference was then compared to a 29 dB fixed threshold. If:

(1) the difference was more than 29 dB and

(2) the clear day clutter map did not indicate that this cell normally contained ground clutter,

then weather threshold crossings in this cell were considered to be caused by AP. Weather detections for such cells were censored.

Effect on AP: Figure I-6a shows the ASR-9 weather channel emulation based on fan beam truth data recorded during an AP event on 25 August 1988 (same event as Figure I-3a) and Figure I-6b shows the result of AP filtering as described above. Note that the technique performs well in the deletion of AP, with only some residual Level 1 remaining.

Effect on weather: Figure I-6c shows the emulation output, based on input fan beam data recorded during the occurrence of weather, with the normal spatial smoothing parameter settings and for values of M and X equal to 8 and 5, respectively (same event as Figure I-3c). Figure I-6d shows the same emulation, but with AP censoring. Note that there is no significant loss of weather data due to this technique.

In all likelihood, no one AP deletion method will work unconditionally and without sometimes affecting the weather reports. However, Doppler spectrum based clutter identification and removal using the existing clutter filter outputs, for the events studied, works quite well without loss in sensitivity. Clearly, further study is needed before a technique is recommended for implementation and before ASR-9 weather channel modifications are made.

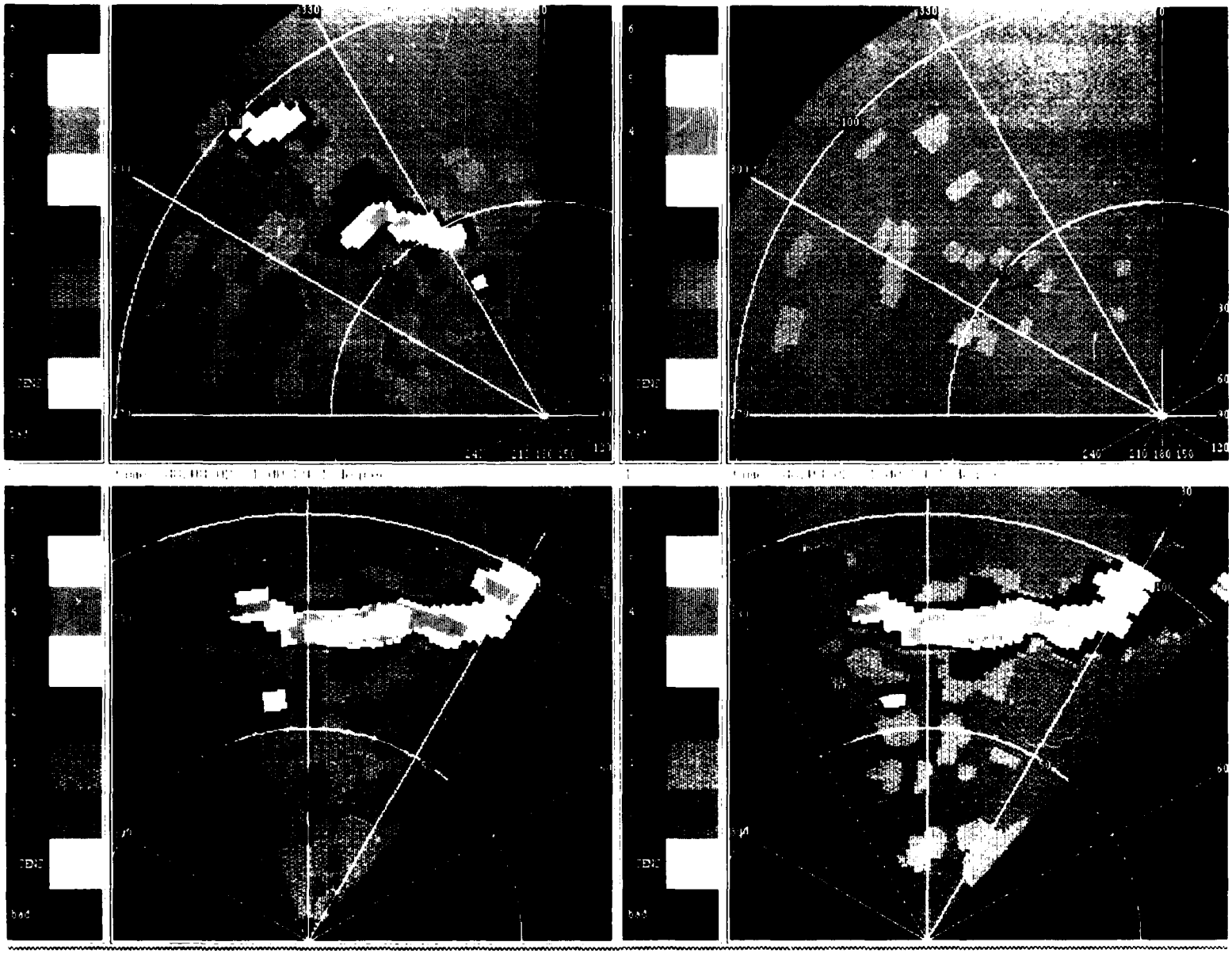

Figure I-6. FI-3 based emulation of ASR-9, showing effect of spectrum width based AP filter on both AP and weather. (a) AP, nominal spatial filter parameters, (b) AP, spectrum width based filter, (c) Weather, nominal spatial filter parameters, (d) Weather, spectrum width based filter. AP is predominantly reduced while weather is generally unaltered.

INDEX

END

FILMED

9-89

DTIC